THE
PHYSICAL REVIEW

A journal of experimental and theoretical physics established by E. L. Nichols in 1893

SECOND SERIES, VOL. 72, No. 3 AUGUST 1, 1947

Directional Properties of Fission Neutrons*

ROBERT R. WILSON**
Los Alamos Scientific Laboratory, Santa Fe, New Mexico
(Received April 2, 1947)

An experiment has been performed to measure the correlation between direction of neutron and fragment in the fission process. The results are consistent with the isotropic evaporation of neutrons from the moving fragments.

THE simplest picture of the emission process of fission neutrons is that these are evaporated from the moving fission fragments. If this is true, and if the evaporation velocity is comparable with that of the fragments, then one would expect the neutrons, when measured in the laboratory system, to be emitted predominantly in the direction of the fragments. The present experiment was designed to detect and measure the directional correlation of the fission fragments and the emitted neutrons.

Figures 1 and 2 show the experimental arrangement. The direction of the fission fragments was determined by the thin collimator placed over the U_{235} foil which was one mg/cm² thick. The collimator consisted of a grid of closely spaced $\frac{1}{16}$ in. holes drilled in a $\frac{1}{8}$ in. thick block of aluminum. The holes were drilled over a square area one inch to the side which corresponded to the area of the foil. The fission fragments penetrating the collimator were detected by the ionization chamber formed from the collimator and the ion collection plate $\frac{3}{8}$ in. away. It was possible to rotate this system with respect to a neutron counter which consisted of a bundle of ten proportional counters $1\frac{1}{2}$ inches long and

TABLE I. Counting rate of the numbers of neutrons emitted at angles 0 and $\pi/2$ in the laboratory system.

Angle	Time min.	Recoils / 64	Fissions / 1024	Coincidences / 4	Coincidences per $2.56\cdot10^4$ fissions	Accidental counts per $2.56\cdot10^4$ fissions	True coincidence counts per $2.56\cdot10^4$ fissions
0°	23	472	1941	41.0	2.11	0.29	1.82
$\pi/2$	14	273	1093	6.7	0.61	0.27	0.34
π	5	91	403	8.5	2.11	0.26	1.85
$3\pi/2$	6	108	573	3.5	0.61	0.25	0.36

Av. of number of neutrons emitted per fission at 0° and π; $n(0)=(1.83\pm7\%)/2.56\cdot10^4$.
Av. of number of neutrons emitted per fission at $\pi/2$ and $3\pi/2$; $n(\pi/2)=(0.34\pm16\%)/2.56\cdot10^4$
$n(\frac{1}{2}\pi)/n(0)=0.18\pm0.03$.

* This document is based on work performed in 1945 at Los Alamos Scientific Laboratory of the University of California under Contract No. W-7405-eng-36 for the Manhattan Project, and the information contained therein will appear in Division V of the Manhattan Project Technical Series as part of the contribution of the Los Alamos Laboratory.
** Now at Cornell University.

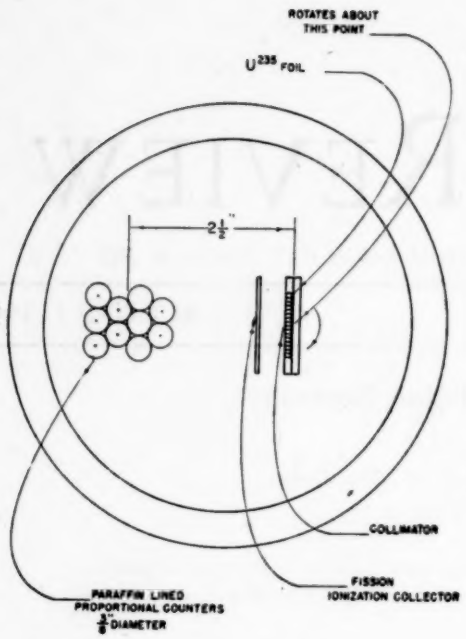

FIG. 1. Plan view of counter arrangement.

⅜ in. in diameter. The three-mil wires along the axis of all counters were connected in parallel to a fast amplifier (Model 500). The inside of each cylinder was coated with paraffin. The sensitive area of the counter was very nearly a square one-inch to the side. The front of the neutron counter was 1⅞ in. from the center of the U_{235} film. The geometry was such that if the neutrons were emitted exactly in the direction of the fission fragments, then no neutrons would be counted by the proportional counter at angles greater than 45° with respect to the direction of the fragments. Argon at 60 cm Hg plus CO_2 at one cm Hg was used to fill the chamber and was thus the counting gas for both the ionization chamber and the proportional counter. A negative potential of 1000 volts was applied to the collimator and the cylinders so that electrons were collected in each case. A typical number-bias curve for the proportional counter is shown in Fig. 3.

The fission pulses from the ionization collection plate and the neutron pulses from the wire were amplified separately and then led to a coincidence counter. The number of fissions, the number of neutrons, and the number of coincidences were all counted simultaneously when the foil was irradiated by the nearly pure thermal neutron flux of the water boiler. The resolving time of the coincidence system was 0.25μ sec. as determined by placing a strong source of fast neutrons at various distances from the proportional counter and then measuring the accidental counts.

The first run was made to determine the counting rate of the number of neutrons per fission in the direction of the fission fragments (0°), to the counting rate of neutrons per fission emitted perpendicular (in the laboratory system) to the fragment direction. The fission counter bias was set as low as possible so that all fragments were registered. Table I summarizes the data. The neutron counting rate observed perpendicular to the fragment direction was about one-fifth of that observed in the direction of the fragments.

The second run was made to try to determine the effect of the energy of the fission fragment counted both on the number of neutrons emitted in the direction of the fragment (0°) and the opposite direction (π). The energy of the fragment was varied by changing the fission counter bias. A typical number-bias curve is shown in Fig. 4. The gain of the amplifier was different

TABLE II. Influence of the fission fragment energy on the numbers of neutrons emitted at angles 0 and π.

Angle	Fission counter bias in volts	Time min.	Recoils / 64	Fissions / 1024	Coincidences / 4	Coincidences per $2.56\cdot10^4$ fissions	Accidental counts per $2.56\cdot10^4$ fissions	True coincidence counts per $2.56\cdot10^4$ fissions
0	0	10	250	796	15	1.88	0.35	1.53±0.20
0	0	10	240	742	12	1.62	0.34	1.28±0.24
0	40	10	239	356	7.75	2.18	0.34	1.84±0.33
0	50	10	238	106	2	1.9	0.34	1.6 ±0.6
π	0	10	218	682	10.5	1.55	0.30	1.55±0.24
	40	10	230	318	4.0	1.26	0.33	0.93×0.25
	50	10	239	55	0	0	0.35	−±100%

TABLE III. Angular distribution of the neutrons emitted from fission fragments.

Angle	Time min.	Recoils 64	Fissions 1024	Coincidences 4	Coincidences per $2.56 \cdot 10^4$ fissions	Accidental counts per $2.56 \cdot 10^4$ fissions	True coincidences counts per $2.56 \cdot 10^4$ fissions
0	10	331	729	16.25	2.23	0.47	1.76 ± 0.28
$\pi/16$	12	501	883	14	1.58	0.59	0.99 ± 0.21
$\pi/8$	12	417	868	7	0.81	0.49	0.32 ± 0.15
$3\pi/16$	11	450	780	6	0.77	0.57	0.20 ± 0.16
$\pi/4$	13	576	910	6.25	0.68	0.61	0.07 ± 0.13
$3\pi/8$	12	525	824	5	0.61	0.66	-0.05 ± 0.13
$7\pi/16$	13	595	905	9.75	1.07	0.64	0.43 ± 0.17
π	12	556	831	13	1.56	0.65	0.91 ± 0.22
π	10	487	775	11.75	1.51	0.68	0.83 ± 0.22
$3\pi/2$	10	439	809	5	0.62	0.62	0.00 ± 0.12
2π	12	518	779	12.25	1.58	0.60	0.98 ± 0.23

at that time. The data are summarized in Table II. The statistics are poor, as can be seen from the large standard errors given in the last column. The energy of the fragment has no evident effect on the number of neutrons per fission emitted in the forward direction. There is a slight indication that fewer neutrons are emitted from the low energy fragment because there seem to be fewer recoils in the backward direction at the higher biases. This effect may be instrumental.

A third run was made to obtain a curve of the numbers of neutrons emitted per fission at various angles. Table III shows the data, and the standard errors listed in the last column indicate that the results are too rough to plot. Furthermore, the sensitivity of the neutron counter seemed to change during the course of the run.

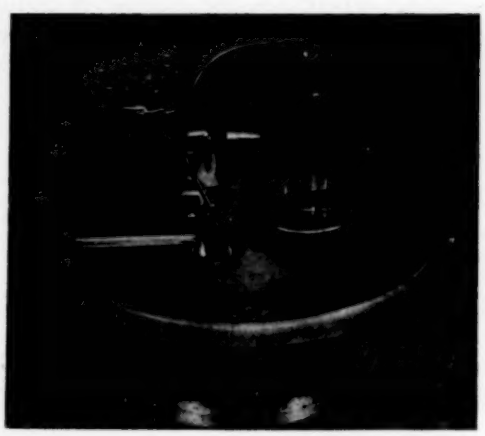

FIG. 2. View looking down on the chamber with enclosing shell removed. The rotating fission collimator and counter are to the right; the neutron counter is to the left; and the preamplifier is below.

However, anything really unusual might have been noticed even with such rough data.

The first run was made under good conditions, so let us see what conclusions can be drawn from it about the process of neutron emission. Assume the simplified picture that the fission fragments all have the same velocity and that the neutrons are evaporated isotropically with respect to the moving fragment and with a uniform velocity.

The ratio of the number of neutrons emitted in the forward direction to those emitted at 90° in the laboratory system can be calculated to be

$$N(\tfrac{1}{2}\pi)/N(0) = r(r^2-1)^{\frac{1}{2}}/(r+1)^2, \qquad (1)$$

where $r = v_n/v_f$, and v_n is the speed of the emitted neutron with respect to the fragment, and v_f is the speed of the fragments.

Now the proportional counter is sensitive to the energy of the neutrons. The speed of a neutron emitted at 0° is (v_n+v_f), while that of a neutron emitted at an angle $\pi/2$ is $(v_n^2+v_f^2)^{\frac{1}{2}}$.

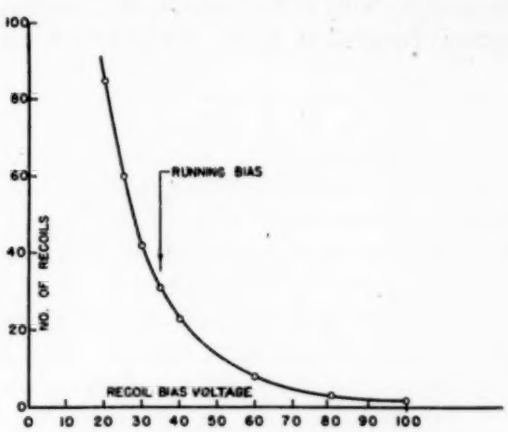

FIG. 3. A typical number-bias curve for the recoil proportional counter.

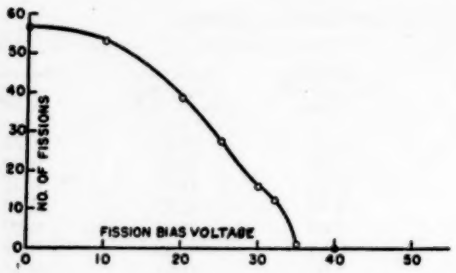

FIG. 4. A typical number-bias curve for the fission counter.

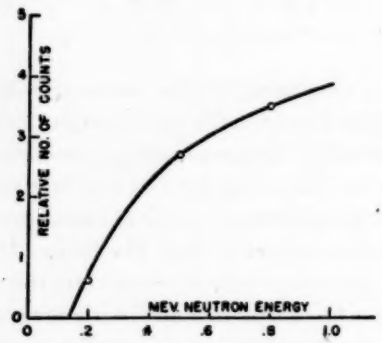

FIG. 5. Energy response of the recoil proportional counters.

The energy sensitivity of a neutron counter of the same dimensions and gas filling was taken at a different time, using the lithium (p, n) neutrons obtained from a Van de Graaff generator. The curve is shown in Fig. 5, and for our purpose the sensitivity can be approximated roughly by $K'(E_n)^{\frac{1}{2}}$. If we make this correction to Eq. (1) we get

$$n(\tfrac{1}{2}\pi)/n(0) = r(r-1)/(r+1)^2 \qquad (2)$$

where $n(\frac{1}{2}\pi)/n(0)$ is the ratio of the numbers of neutrons counted at angles $\pi/2$ and 0. In Fig. 6

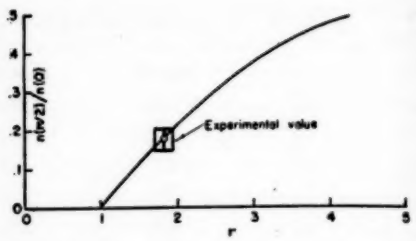

FIG. 6. Theoretical ratio of neutron counts at right angles to fission direction to neutron counts in the direction of the fission fragment as a function of r, the ratio of the speed of the emitted neutron with respect to the fragment to the speed of the fragment.

is plotted $n(\frac{1}{2}\pi)/n(0)$ as a function of r, and we can read a value of $r = 1.8 \pm 0.2$ corresponding to the experimental value $n(\frac{1}{2}\pi)/n(0) = 0.18 \pm 0.3$ If the average energy of a fission fragment is 70 Mev, and the average atomic weight is 100, the velocity v_f is the same as that of a neutron of 0.7 Mev; hence the energy of evaporation would be $0.7 \times (1.8)^2 \approx 2$ Mev. Had we assumed that the detector was insensitive to energy the evaporation energy would be about one Mev. The crudeness of the experiment and its interpretation are apparent.

I had hoped to split the neutron counter into two equal parts and count coincidences between these neutron counters when they were on opposite sides of a piece of uranium exposed to thermal neutrons and when the two counters were on the same side. This would give information about the mechanism of emission of fission neutrons as well as of the quantity $\langle \nu^2 \rangle_{Av} - \langle \nu \rangle_{Av}^2$, where ν is the number of neutrons per fission. However, the very brief time available for the experiment did not permit this extension.

A Thermal Neutron Velocity Selector and Its Application to the Measurement of the Cross Section of Boron

E. FERMI, J. MARSHALL, AND L. MARSHALL
Argonne National Laboratory, University of Chicago, Chicago,** Illinois*
(Received April 25, 1947)

A mechanical velocity selector for the study of monochromatic neutrons in the range of energies below 0.3 ev is described.

The instrument has been applied to the measurement of the cross section of boron, which is found to be 703×10^{-24} cm² for neutrons of 2200 meters per second velocity.

INTRODUCTION

SLOW neutrons emerging from various moderators with different geometries usually have average velocities comparable, but by no means equal, to the thermal agitation velocity. Large differences, both positive and negative, are observed depending on the nature and the geometry of the moderating substance. This phenomenon has been observed by various experimenters.[1–4]

In this paper we have collected some typical examples of the variations of average velocity of slow neutrons using different moderators as indicated by changes in the apparent cross section of boron. Since boron is often used as a standard substance in slow neutron measurements, its cross section has been determined also by use of monochromatic neutrons obtained with a velocity selector of new design operated in connection with the thermal column of the Argonne graphite pile.

The observed temperatures of the neutrons emitted from the various moderators and arrangements of moderators appear to be in accordance with the individual arrangements employed. Within the experimental errors of the method, the cross section of boron varies as the 1/v law, and the measured cross section is 703×10^{-24} cm² per atom per neutrons of velocity 2200 meters per second.

TEMPERATURES OF NEUTRONS FROM VARIOUS SOURCES

With the thermal purification column of the graphite pile at the Argonne Laboratory as a primary neutron source, a number of measurements were made of the cross section of boron. In all cases the detector was a proportional counter filled with BF_3 gas. By the use of cadmium diaphragms a neutron beam was obtained with small angular dispersion.

The absorber and detector in these experiments were both boron and consequently both obeyed the 1/v law of neutron absorption. It was possible, therefore, to use the correction method given by Bethe[5] to calculate the cross section of boron for mono-energic neutrons of energy kT where T is the absolute temperature of the Maxwellian distribution emitted from the source. Since the cross section of 2200 meters per second neutrons (kT at 293°K) is known, one can then determine the effective temperature of the neutron beam. It must be understood that these effective temperatures are based on the assumption that the neutron beam is Maxwellian in velocity distribution. This is certainly not strictly true for most sources employed.

The results of these experiments are given in Table I. It is quite clear from an inspection of the table that the effective temperature of the neutron beam depends strongly on the source of neutrons. During these experiments the temperature of the thermal column was in the neighborhood of 30°C or 303°K.

* The information contained in this document will appear in Division IV of the MPTS as part of the contribution of the Argonne National Laboratory.

** All three authors now at Institute for Nuclear Studies, University of Chicago.

[1] J. Rainwater and W. W. Havens, Jr., Phys. Rev. **70**, 136 (1946).

[2] W. W. Havens, Jr. and J. Rainwater, Phys. Rev. **70**, 154 (1946).

[3] J. H. Manley, L. J. Haworth, and E. A. Luebke, Phys. Rev. **69**, 405 (1946).

[4] R. F. Bacher, C. P. Baker, and B. D. McDaniel, Phys. Rev. **69**, 443 (1946).

[5] H. A. Bethe, Rev. Mod. Phys. **9**, 134 (1937).

TABLE I.

Source of neutrons	Absorber	Cross section for kT neutrons (cm^2)	Effective temp. (°K)
1. Beam from surface of thermal column	Gaseous BF_3	$\sigma_B = 855 \times 10^{-24}$	198
2. Beam passed through a 3.7-cm slab of paraffin	Gaseous BF_3	598×10^{-24}	408
3. Beam passed through 7.6c m. of heavy water at 33.7°C in a container 18-in. diam.	Gaseous BF_3	Corrected to 20.4°C $\sigma_B = 710 \times 10^{-24}$	288
4. Beam passed through a 22 cm. column of graphite 10 cm square	Pyrex plate calibrated in velocity selector	2800×10^{-24}	18.4
5. Beam from hole in thermal column 125 cm deep, 10 cm square	Gaseous BF_3	701×10^{-24}	293
6. Beam from a "black hole" in thermal column, a hole 10 cm×10 cm×22 cm high connected to surface of thermal column by a 42-cm tube of cadmium of internal diam. 2.5 cm	Gaseous BF_3	755×10^{-24}	255

The source arrangement given under case 1 produces low temperature neutrons because of the filtering action of the graphite in the pile and thermal column.[6] Very slow neutrons whose de Broglie wave-lengths are longer than periodicities encountered in the graphite crystals are scattered very little and can penetrate to the surface of the column more easily than the faster neutrons. In case 2 the slower neutrons are removed preferentially because both the absorption and scattering cross sections of hydrogen are larger and also because scattering in the forward direction is preferred at higher energy. Heavy water (case 3) acts somewhat in the same way because also for deuterium compounds the scattering cross section and the coherence of successive free paths vary with the energy in the same direction as for hydrogen compounds. Therefore, the effective temperature of the neutrons is raised from the initial 198°K to 288°K. The fact that this last temperature is quite close to the actual temperature of the heavy water probably is coincidental. In case 4 the filtering effect of the graphite is shown very strongly. Most neutrons that are scattered are removed from the beam and the graphite column is so long that almost none of the warm neutrons can travel the whole distance without being scattered. Case 5 gives a rather good approximation of the temperature of the source. The neutrons in the beam from the deep hole should be a fair sample of the neutrons present at the bottom of the hole. Essentially it is a case of blackbody radiation from a hole in the wall of a furnace. Case 6 was expected to give a good temperature value, but failed to do so, probably because the hole was not deep enough.

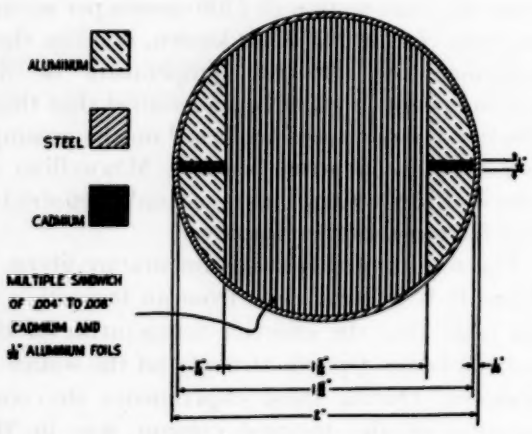

FIG. 1. Cross section of the shutter of the velocity selector.

VELOCITY SELECTOR

The velocity selector makes use of a rotating shutter to interrupt the beam of neutrons from the thermal column of the pile. The shutter was constructed by inserting a multiple sandwich of 0.004-inch to 0.008-inch cadmium foils and $\frac{1}{32}$-inch aluminum sheet tightly into a steel cylinder about $1\frac{1}{2}$ inch in diameter with walls $\frac{1}{32}$ inch thick. The shutter was mounted in ball bearings on a heavy steel base plate and was belt and pulley driven by a Dumore grinder motor. Maximum rotational speeds of 15,000 revolutions per minute were possible. It was constructed in the shops of the Metallurgical Laboratory under the direction of Mr. T. J. O'Donnell who is responsible for its mechanical design.

[6] H. L. Anderson, E. Fermi, and L. Marshall, Phys. Rev. 70, 815 (1946).

A cross section of the shutter is shown in Fig. 1. From the thickness of the aluminum spacers between the cadmium foils, and from the dimensions of the shutter, one would estimate that no neutrons from a parallel beam would be able to get through when the shutter was more than 1.2° from its full open position. In the experimental arrangement used, it was impossible to use a strictly parallel beam of neutrons. The collimators actually used allowed a maximum divergence of neutron direction in the beam of approximately 3°. Consequently, one would expect the shutter to be completely closed during each 180° of rotation except for an interval of $3°+2\times1.2°=5.4°$. Actually it was found that the counters indicated background intensity except when the shutter was in a 6° interval.

Through one end of the shutter was inserted a steel rod with its axis perpendicular to the axis of the shutter and with a minor surface ground and polished perpendicular to its axis at each end. Light from a projection lamp and lens system was reflected from these surfaces onto two photo-cells so placed that each photo-cell was illuminated twice during each revolution. One of the photo-cells was used with an amplifier and scaling circuit as a revolution counter. The other, adjustable and calibrated as to angulars position, was connected to an electronic switch circuit which allowed pulses from the proportional counter to be recorded only when the photo-cell was illuminated.

BF_3 filled proportional counters were used as the neutron detector. A nest of four was connected in parallel and mounted at a distance of 146 cm from the shutter. A thick shield of wood, iron, and paraffin was placed between the counters and the pile to compensate somewhat for the fact that the top shield of the graphite pile was not so thick as might be desired. A hole in this shield allowed neutrons from the shutter to reach the counters.

The neutron beam between the shutter and the counters was collimated to make sure that no slow neutrons from sources other than the shutter could enter the counters. Slow neutrons reflected from the walls and roof of the building were eliminated by protecting the sides and back of the counters with a $\frac{1}{2}$-inch thick layer of boron carbide.

The shutter and an improved velocity selector arrangement are to be more fully described in a paper by Brill and Lichtenberger.

DETERMINATION OF BORON CROSS SECTION FOR NEUTRONS OF KNOWN VELOCITY

The cross section of pure BF_3 at several different pressures was measured for neutrons from the thermal velocity selector for velocities ranging from 1700 to 5000 meters per second. Within the experimental accuracy of the method the cross section of boron varied according to the 1/v law. After corrections for scattering were made, the average cross section of boron for neutrons of 2200 meters per second velocity was 699×10^{-24} cm²/atom. 2200 m/sec. is the velocity of a neutron of energy kT where T is 293°K.

In order to verify this value a similar measurement was made with a different boron compound as absorber. $Na_2B_4O_7$ was ignited at about 400° and dissolved in heavy water. The solution was enclosed in a thin-walled aluminum cell, and a second cell of identical wall thickness, which contained an amount of heavy water equal to that in the solution, was prepared. The transmissions of these two absorbers for neutrons from the velocity selector were measured, and the value of the boron cross section for 2200 m/sec. neutrons was found to be 700×10^{-24} cm² corrected for scattering.

In good agreement with these values was the cross section as calculated from measurements at the indium resonance energy.[7] Transmission measurements were made using a collimated beam of neutrons from the interior of the graphite pile of the Argonne Laboratory. The indium foil detectors were protected from thermal neutron activation by thick cadmium covers. Background measurements were made

TABLE II.

	Measurement	$\sigma_{kT}(B)$ at 293°K
$Na_2B_4O_7-D_2O$	Velocity selector	700×10^{-24} cm²
BF_3	Velocity selector	699×10^{-24}
BF_3	In resonance	710×10^{-24}
	Average	703×10^{-24} cm²

[7] J. Marshall, Phys. Rev. **70**, 107 (1946).

by use of an indium filter. Thus the measurements were limited in more than one way to neutrons absorbed strongly by indium.

BF_3 gas in a steel cylinder was interposed in the collimated beam. The BF_3 was highly purified (the same gas as used in the thermal neutron transmission experiments described above). The transmission of the steel container filled with BF_4 at 44 and 68 lb/in.^{2} was compared with the transmission of the empty container. The density of gas used was determined by weighing the cylinder. The pressures used and the length of the cylinder (30 cm) were such that the transmissions were in an accurately determinable range (approximately a $\frac{2}{3}$ transmission for the 68-lb sample).

The total cross section of BF_3 for indium resonance neutrons was measured as 107.1×10^{-24} cm^2/atom. Assuming

$$\sigma_{\text{scattering}}(F) = 3.7 \times 10^{-24} \text{ cm}^2,$$
$$\sigma_{\text{scattering}}(B) = 2 \times 10^{-24} \text{ cm}^2,$$
$$\text{indium resonance energy} = 1.44 \text{ ev},$$

the boron absorption cross section for neutrons at velocity 2200 m/sec. is 710×10^{-24} cm^2/atom.

The results of the three measurements are given in Table II.

This report is based on work done at the Argonne National Laboratory, the University of Chicago, under the auspices of the Manhattan District, U.S. Corps of Engineers, War Department.

PHYSICAL REVIEW VOLUME 72, NUMBER 3 AUGUST 1, 1947

Scattering of Fast Neutrons by Helium*

T. A. HALL† AND P. G. KOONTZ‡
University of California, Los Alamos Scientific Laboratory, Santa Fe, New Mexico

(Received March 28, 1947)

Measurements have been made of the angular distribution of helium recoils for incident neutrons of energies from 0.6 to 1.6 Mev. The distribution curves also permit estimates of the total cross section in this energy range. The results confirm the existence of a cross-section peak of about 6.8×10^{-24} cm^2 around 1 Mev and indicate, under the assumption of *s*- and *p*-wave scattering only, that the peak is double. But preliminary attempts to fit the data to Bloch's detailed theory of *s*- and *p*-scattering with a split *p*-level have not been successful, and the sign of the postulated splitting is not established.

INTRODUCTION

A SCATTERING theory for helium must satisfy quantitatively two previous sets of data as well as that reported here. Barschall and Kanner[1] obtained recoil distribution curves at neutron energies of 2.5 and 3.1 Mev, and Staub and Tatel[2] obtained the backward scattering cross section as a function of energy around 1 Mev, finding a peak (possibly double). The Barschall-Kanner curves are strongly anisotropic with a preponderance of forward scattering. Wheeler and Barschall[3] have shown that the data at 2.5 Mev can be fitted by the assumption of strong spin-orbit coupling, a *p*-wave resonance around 2.5 Mev, and a weak addition of *d*-wave of a size not unreasonably large for 2.5 Mev. But this data at 2.5 and 3.1 Mev cannot be matched with a simple theory involving only resonances around 1 Mev: an *s*-wave resonance would be isotropic and higher resonances at 1 Mev must fall off to insignificance at 2.5 and 3.1 Mev. Thus the two sets of data provide essentially two different problems, at any rate for analysis in terms of resonances. The Bloch formula for

* This paper will appear in Division V of the Manhattan Project Technical Series as part of the contribution of the Los Alamos Laboratory of the University of California.
† Now at the University of Chicago, Chicago, Illinois.
‡ Now at Iowa State College, Ames, Iowa.
[1] H. H. Barschall and M. H. Kanner, Phys. Rev. **58**, 590 (1940).
[2] H. Staub and H. Tatel, Phys. Rev. **58**, 820 (1940).
[3] J. A. Wheeler and H. H. Barschall, Phys. Rev. **58**, 682 (1940).

resonant p-wave scattering[4] used below can satisfy only one set, and we only consider the fitting of this formula to the data near 1 Mev of Staub and Tatel and of this paper. The main contribution from this paper is a group of recoil energy distribution curves for neutron energies from 0.6 to 1.6 Mev. While the authors have had opportunity to make only a preliminary theoretical analysis, it has seemed worth while to present these new data.

Earlier observations of scattering near 1 Mev were made by Gaerttner, Pardue, and Streib,[5] who found a total cross-section peak around 0.8 Mev, and by Staub and Stephens,[6] who found a total cross-section peak near 1 Mev. Taken together, these studies indicated a double peak, but they were not sufficiently detailed to permit a quantitative check with theory on this score. The question of the double peak has been investigated in its theoretical aspects by Dancoff,[7] who concluded that a Thomas relativistic spin-orbit coupling should produce an inverted doublet (with size of splitting essentially unknown) while the tensor spin-orbit interaction of mesotron theory could be expected to produce a normal doublet with splitting of the order of 100 kev. None of the experimental data has determined whether the splitting is normal or inverted, nor is the size of the splitting established beyond the fact that it cannot be more than about 600 kev.

EXPERIMENTAL PROCEDURE

The measurements were made at the larger Van de Graaff generator loaned to the Los Alamos Laboratory by the University of Wisconsin. The lithium $p-n$ reaction provided the neutrons. A cylindrical proportional counter,[8] with guard rings at the end to define the counting volume, was filled with a helium-argon mixture and placed in the neutron flux; the helium recoil pulses were fed through a preamplifier and amplifier of rise-time $\frac{1}{2}$ microsecond and RC decay time 20 microseconds into a discriminator

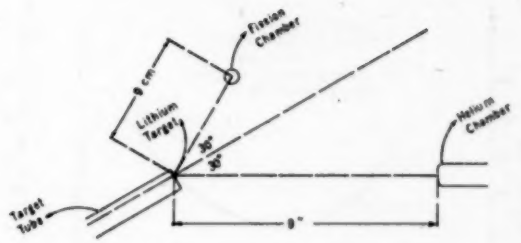

FIG. 1. Experimental arrangement for curves of energy distribution of recoils.

which counted simultaneously all pulses of a size above a set level ("integral count") and all pulses of a size within a set channel ("differential count"). Both settings were adjustable, and by moving the channel along the recoil energy scale while keeping its width constant, one obtained the energy distribution of the helium recoils. (The recoil energy was simply proportional to the pulse height.) Two kinds of data were taken: first, detailed curves of the energy distribution of the helium recoils for a given neutron energy (Figs. 2–6), and secondly, brief studies of the high energy end of these curves at successive neutron energies (Fig. 7). In each case, total counts above a certain recoil energy (determined by the need to eliminate γ-background) were recorded, and neutron flux was measured. Also proton current in the Van de Graaff generator was recorded during the runs.

In the case of the detailed curves the experimental arrangement was as follows: The scattering chamber was placed with its end about 9 inches from the lithium target, and its axis pointing to the target. (This puts the beginning of the counting volume about 11 in. from the

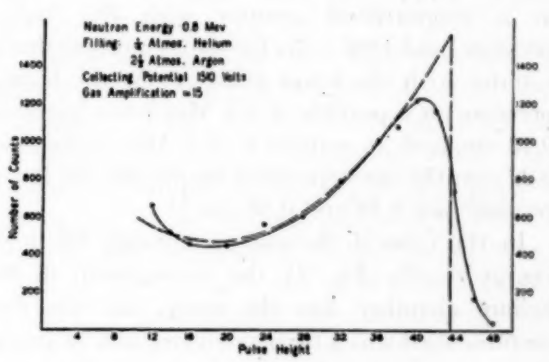

FIG. 2. Equation of parabolic fit: $y=1051-64.55x+1.800x^2$.

[4] F. Bloch, Phys. Rev. **58**, 829 (1940).
[5] E. R. Gaerttner, L. A. Pardue, and J. F. Streib, Phys. Rev. **56**, 856 (1939).
[6] H. Staub and W. E. Stephens, Phys. Rev. **55**, 131 (1939).
[7] S. M. Dancoff, Phys. Rev. **58**, 326 (1940).
[8] P. G. Koontz and T. A. Hall, Rev. Sci. Inst. (to be published).

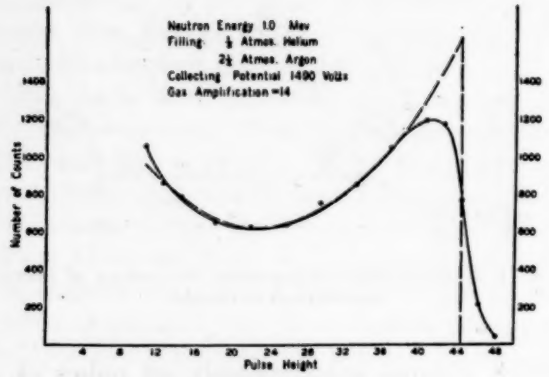

FIG. 3. Equation of parabolic fit: $y=1785-87.93x+1.660x^2$.

target.) The chamber axis made an angle of 30° with the target tube axis. Also off at an angle of 30°, and about 9 cm from the lithium target, was the flux monitor which was a U^{235} fission foil placed in an ionization chamber. This arrangement is sketched in Fig. 1. The Van de Graaff generator was then set to give the desired neutron energy at 30°. The distance of the chambers from the target remained about as given throughout the runs, but was measured after each run to secure accurate flux measurement.

Data were taken with two different gas fillings, and under operation both as an ion chamber and as a proportional counter with gas multiplication of about 14. The two fillings were ($\frac{1}{2}$ atmosphere of helium+$2\frac{1}{2}$ atmospheres of argon), and ($\frac{1}{2}$ atmosphere of helium+1 atmosphere of argon), the lower pressure being used to permit recording of slower recoils without interference from γ-background. The collecting potential was 1450 volts for use as an ion chamber and 2500 for use as a proportional counter with the higher pressure, and 1500 volts for use as a proportional counter with the lower pressure. At the higher pressure an α-particle of 0.5 Mev has a range of 0.13 cm, and an α-particle of 1 Mev a range of 0.22 cm; the corresponding figures for the lower pressure are 0.28 and 0.48 cm.

In the case of the curves covering the high energy recoils (Fig. 7), the arrangement of the helium chamber was the same, but the flux monitor used was a fission detector almost insensitive to energy, placed about 6 feet from the target.

EXPERIMENTAL RESULTS

The results are summarized in Figs. 2–6. In clarifying their meaning, the following facts should be noted:

The curves obtained are almost the same for ion chamber and proportional counter operation. This was also the case in previous testing of this counter using the nitrogen $n-p$ reaction. In the ion chamber case, because of the small rise and decay time of the amplifier and the low mobility of positive ions, the pulse is due mostly to the collection of the electrons, which travel over different distances from their point of origin to the central wire. Nevertheless, since ion chamber and proportional counter curves are quite similar, we may assume that the pulse is proportional to the energy of the recoil in each case[9] (except for wall effect, irregularity of multiplication, etc.). Hence the abscissas in Figs. 2–6 may also be considered to represent the recoil energy. Furthermore, writing

E = neutron energy
E_m = maximum energy of recoil
E_r = energy of recoil
ϕ = angle of recoil
} laboratory system

θ = scattering angle of neutron, center of gravity system

$d\omega = 2\pi \sin\theta d\theta$

$d\sigma/d\omega$ = cross section per unit solid angle in the center of gravity system,

we have

$$E_r = E_m \cos^2\phi, \quad \theta + 2\phi = \pi,$$

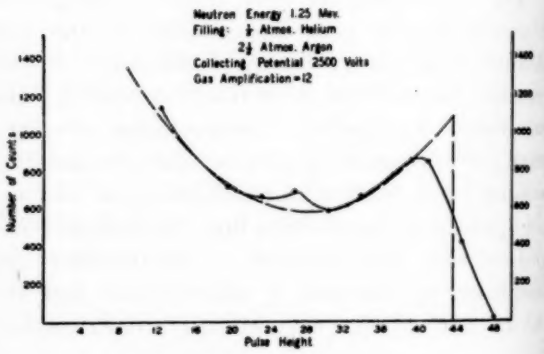

FIG. 4. Equation of parabolic fit: $y=2225-92.77x+1.312x^2$.

[9] The effect of "electron collection" is described briefly in reference 8. It is discussed in greater detail in the forthcoming "Los Alamos Encyclopedia" but the necessary analyses were developed before the Manhattan Project began.

and

$$E_m = 4M_\alpha M_n/(M_\alpha + M_n)^2,$$

from which it follows that the curve of recoil distribution *vs.* recoil energy has the same shape as the curve of $d\sigma/d\omega$ *vs.* $\cos\theta$, with $\theta = 0$, $\cos\theta = 1$ at zero recoil energy and $\theta = \pi$, $\cos\theta = -1$ at maximum recoil energy. Thus Figs. 2–6 give directly the differential cross section in the center of gravity system.

For each of these curves a check was made on γ-background, runs were made at different bias settings with a quartz shield blocking the lithium target from the proton beam. This procedure showed the effect of γ-rays from the bulk of the Van de Graaff generator, but eliminated γ-rays normally produced beyond the quartz shield in the target tube and lithium target. However, other measurements[10] have shown that at a distance of about 2 inches from the target, γ-rays from a target and γ-rays from the generator bulk are of about equal strength, and those from the target fall off as $1/r^2$ with distance from the target; so that the γ-effect cannot be significantly larger than that observed in the procedure above. All data plotted were taken at points where the background is negligibly small.

The theory indicates (see below) that the differential curves should be parabolas. Parabolas have been fitted and are drawn in Figs. 2–6. At the high energy end of the curves, the experimental curve is broadened and decreased in height by the width of the channel of the discriminator; the parabolic curve has been extended to a point where the area under it is about the same as that under the experimental curve. A further requirement was that the end point of the parabolic curve, corrected for channel width, should agree in height with the experimental peak. This requirement was met in each case to within 15 percent or better of the experimental peak height. In this way the abscissa of the high energy end can be determined to about 1 percent of the pulse height. The abscissa scale in Figs. 2–6 is arbitrary. The end of the parabola should be taken to correspond to the recoil of maximum energy, which is $[4M_nM_\alpha/(M_n+M_\alpha)^2] = 16/25$ of the energy of the incident neutron.

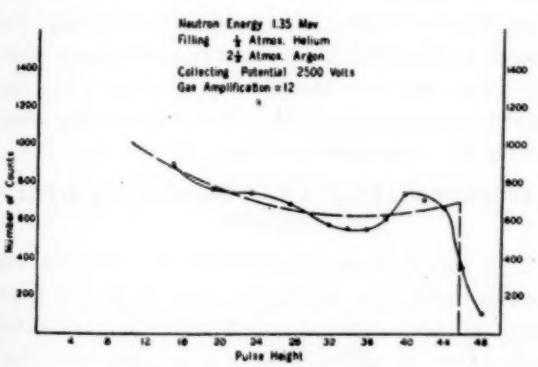

FIG. 5. Equation of parabolic fit: $y = 1406 - 48.43x + 74.44x^2$.

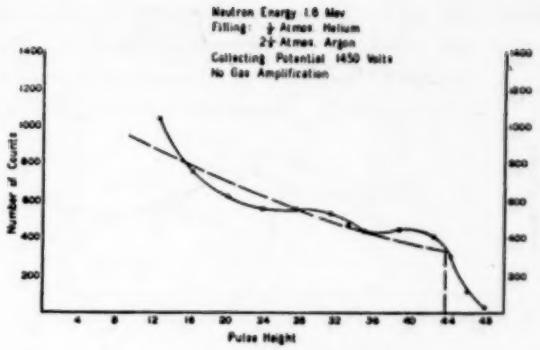

FIG. 6. Equation of parabolic fit: $y = 1206 - 26.26x + 0.1788x^2$.

The ordinate scale in Figs. 2–6 and Fig. 7 is also "arbitrary," being the actual number of counts observed. Most points represent the average of two points, so that twice as many counts are involved. When two or three runs were made on one point, repetition was on the whole well within statistical error. The "curve peaks" of Fig. 8 are also plotted on an arbitrary ordinate scale. These peaks are the same as those recorded in Fig. 7.

Figure 9 is a curve of the total scattering cross section *vs.* energy. The numbers plotted were obtained in two steps: (1) calculation of the cross section down to the integral bias, which depends solely on measured quantities, and (2) multiplication by a factor obtained by extrapolating the parabolic fit to zero recoil energy. (This factor is simply the ratio of areas under the full curve and under the curve down to the integral cut-off.)

The first step involved three quantities:

[10] These measurements were made by R. Taschek in connection with another experiment.

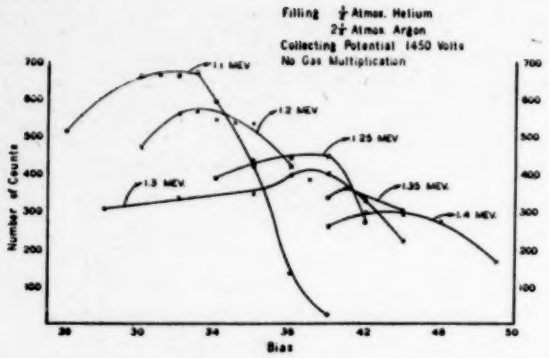

FIG. 7. Backward scattering differential curves.

neutron flux, number of helium atoms present, and integral count. The flux measurements have a probable error of about 5 percent, owing to the fact that only about 3000 fission monitor counts were obtained per run, and to uncertainties in relative distances of chamber and monitor from the target. The number of helium atoms present should be quite well known, the pressure having been measured by a mercury manometer, the temperature being known to a few degrees, and the active volume having been measured to about 3 percent. The error in the number of integral counts is negligible, as one obtains about 15,000 integral counts with each point on the curve. An associated error arises in the determination of the energy corresponding to the integral bias. This error is caused by the uncertainty in locating the exact position of the maximum recoil energy on the graph. This uncertainty amounts to about $1\frac{1}{2}$ percent in the total cross section. Thus the probable error with perfect extrapolation would be 6 percent.

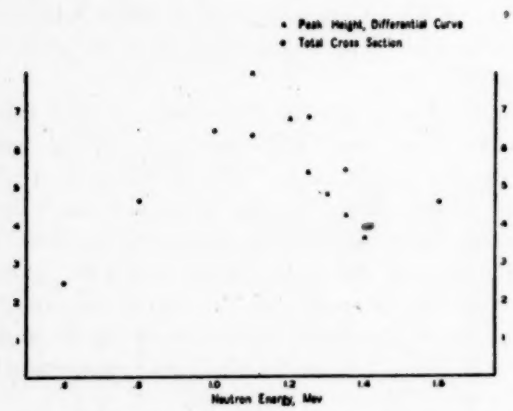

FIG. 8. Evidence of increased anisotropy at peak.

TABLE I. Total cross section *vs.* neutron energy.

E(Mev)	$\sigma(10^{-24}$ cm$^2)$
0.6	2.48
0.8	4.91, 4.63, 4.28
1.0	6.42, 6.75, 6.16
1.1	6.35
1.25	6.96, 6.70
1.35	5.66, 5.22
1.6	4.60

The extrapolation itself is uncertain. It is poorest at lower neutron energies, where the area under the extrapolated curve is a larger fraction of the total, and where the curve cannot be fitted so well because its shape is not so well determined. The integral bias is always set as low as possible without γ-background interference; at the higher gas pressures this permits settings at about 0.22-Mev recoil energy and at the lower gas pressure settings of about 0.13 Mev. Thus the integral bias energy ranges from about $\frac{1}{3}$ to $\frac{1}{5}$ of the maximum recoil energy in the curves presented. While it is not certain that the curves should be simply parabolic, it is very unlikely that they will deviate much from a parabolic shape. (This would require strong d-wave or higher order scattering, which is very unlikely for energies as low as 2 Mev where the neutron wave-length in the center of gravity system is more than 3×10^{-12} cm.) The extrapolated area is probably correct to 25 percent or better (as a guess), so that the errors arising from extrapolation might be expected to range from 4 to 8 percent. This leaves the final probable error on the cross sections around 10 percent. This figure seems reasonable considering the spread in Fig. 9 at those energies for which more than one run was taken. Fig. 9 then gives the energy dependence of the cross section. The same points are tabulated in Table I.

INTERPRETATION AND COMPARISON WITH THEORY

The Bloch theory is general, introducing few assumptions. The scattering near 1 Mev is built from s- and resonant p-waves. A spin-orbit interaction is allowed for; it is assumed that there are two resonant compound p-levels, of energies $E_{1/2}$ and $E_{3/2}$, $\frac{1}{2}$ and $\frac{3}{2}$ being the total angular momenta of the two levels. The only assumptions introduced are that all other levels

of the compound nucleus do not affect the scattering of the neutrons at the energies used, that the spin-orbit forces are small enough so that the phases of the scattered waves δ_l and the half-width Γ are about the same for the two levels, and that the phases δ_l, $l\neq 0$, for non-resonant components, are negligibly small.

The Bloch formula reads

$$\frac{d\sigma}{d\omega}=\lambda^2\left\{\left[\sin\delta_0+e^{-i\delta_0}\left(\frac{\Gamma}{E_{3/2}-E-i\frac{1}{2}\Gamma}+\frac{1}{2}\frac{\Gamma}{E_{1/2}-E-i\frac{1}{2}\Gamma}\right)\cos\theta\right]^2+\frac{\sin^2\theta}{4}\left[\frac{\Gamma}{E_{3/2}-E-i\frac{1}{2}\Gamma}-\frac{\Gamma}{E_{1/2}-E-i\frac{1}{2}\Gamma}\right]^2\right\},$$

where $d\sigma/d\omega$ is the cross section per unit solid angle in the center of gravity system, $\lambda=\lambda/2\pi$, λ is the neutron wave-length in the center of gravity system, δ_0 is the phase shift of the s-scattered wave, Γ is the half-width of the He^5 levels, E is the energy of the incident neutron, and θ is the neutron scattering angle in the center of gravity system. The quantities Γ and δ_0 are dependent on the incident neutron energy, the dependence of δ_0 not being well-known apart from the fact that it must be slowly varying. The quantities Γ, δ_0, $E_{3/2}$, and $E_{1/2}$ are the parameters left adjustable in fitting the data, for we have used the energy dependence[11]

$$\Gamma=3\Gamma_0E^{\frac{1}{2}}/(1+3.1/E),$$

with E in Mev and Γ_0 a constant.

According to the Bloch formula (or to any superposition of s- and p-waves alone), the differential cross section as a function of $\cos\theta$ is a parabola. Figures 2–6 are actually plots of $d\sigma/d\omega$ *vs.* $\cos\theta$, with $\theta=0$, $\cos\theta=1$ at the origin and $\theta=\pi$, $\cos\theta=-1$ at the maximum recoil energy. The parabolic fit is good from 0.6 to 1.1 Mev, and is not too bad from 1.1 to 1.6 Mev. Furthermore, one can fit *any one* of the curves by using parameters near those suggested by Staub and Tatel from their data: $\Gamma=0.4$ at 1 Mev, $E_{3/2}=1.45$ Mev, $E_{1/2}=1.05$ Mev, $\sigma_0=1.5$ barns, for example, yield a good fit at 1 Mev

$$(\sigma_0=4\pi\lambda^2\sin^2\delta_0).$$

Sets of parameters not very different from Staub and Tatel's may be found to fit any of the curves. Also, fits may be obtained both with the assumption of an inverted doublet ($E_{3/2}<E_{1/2}$) and with the assumption of a normal doublet ($E_{3/2}>E_{1/2}$). But as yet no set of parameters has been found which, with the energy dependence of Γ and δ_0 mentioned, has provided a reasonably good fit for all the curves from 0.8 to 1.6 Mev; those parameters which suit the lower energy curves fit badly at the higher, and *vice versa*. As long as a good fit is not found, nothing can be said from this data as to whether the doublet is normal or inverted, or even as to the fundamental nature of the scattering. In particular, in addition to resonant p-scattering which should have the form of the Bloch formula, there still may be a significant contribution from a fairly constant p-background of non-resonant nature, a possibility which is not studied in this paper.

The data of Staub and Tatel indicate that the p-splitting may be significant, giving a double peak. (It is possible to draw a smooth single-peak curve through their data going scarcely beyond experimental error, but the points themselves indicate a double peak.) Figure 9 also presents the appearance of a double peak, although the accuracy is not good enough to assure that it is real. But if one assumes the correctness of the Bloch formula, Figs. 2–6 furnish indirect evidence

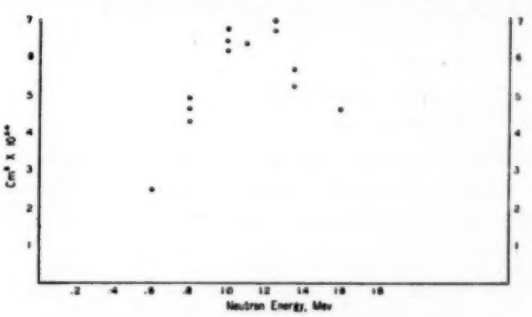

FIG. 9. Helium total scattering cross section.

[11] We are grateful to Professor V. F. Weisskopf for his unpublished derivation of this relation, based on the analyses of V. F. Weisskopf and D. H. Ewing, Phys. Rev. 57, 472 (1940).

that the peak is double. In the case of zero splitting and neutron energy equal to the resonant energy, the Bloch formula reduces to

$$d\sigma/d\omega = \lambda^2(\sin^2\delta_0 + 9\cos^2\theta + 6\cos\theta\sin^2\delta_0).$$

Then if we take the ratio of differential cross section at $\theta=\pi$ and at the minimum of the curve, we get

$$\frac{\sigma_\pi}{\sigma_{\min}} = \frac{9-5\sin^2\delta_0}{\sin^2\delta_0-\sin^4\delta_0}.$$

The value of $\sin^2\delta_0$ is probably about 0.3. (We have $\sigma_\pi = 4\pi\lambda^2\sin^2\delta_0$; σ_0 has been measured to be[12] 1.25×10^{-24} cm^2 at thermal energies and probably remains the same or decreases slowly as energy increases; $\lambda^2\sim1/E$.) But in any event the ratio $(9-5\sin^2\delta_0)/(\sin^2\delta_0-\sin^4\delta_0)$ cannot be less than 25, the minimum value reached at $\sin^2\delta_0=0.6$. The largest ratio $\sigma_\pi/\sigma_{\min}$ observed in the curves is only about 3, and the resonance cannot be so sharp that all the curves miss it badly. Therefore, on the assumption of the Bloch theory, it is necessary to have a splitting of the p-level in order to bring the theoretical ratio down.

There are two more points of interest in the data. The kinks in Figs. 4 and 5 were repeated too well to be caused by statistical fluctuation. They could be caused by d-waves except for the fact that the energy is still too low for strong d-scattering. There is no possibility of explaining them by simple s- and p-scattering. It is possible that such deviations from a smooth curve could be caused by the presence of a group of neutrons of lower energy, but other experiments have given no evidence for the existence of such a group.

A second point of interest is indicated in Fig. 8. The total cross sections are those of Fig. 9, averaged. The peak heights, taken from Fig. 7 but plotted on an arbitrary scale, indicate the variation in the backward scattering cross sections. The Bloch formula predicts that forward and backward scattering cross sections will rise faster than the total cross section as resonances are approached. (This will be so unless the $p-s$ interference term is too large, in which case either the forward or the backward cross section will rise slower than the total, while the other will rise still faster. It is unlikely that the interference term is this large.) In confirmation of the prediction, the peak heights of Fig. 8 rise faster than the integral counts.

[12] J. Schwinger, Phys. Rev. **58**, 1004 (1940).

CONCLUSION

The interpretation given above must be considered as preliminary comment on the theory; it remains to be seen whether or not a more systematic approach will yield a detailed check between theory and the experimental distribution curves. At present, the data have not determined the adequacy of s- and p-scattering with spin-orbit interaction in treating the 1-Mev helium resonances, but it does indicate, assuming this adequacy, that there is a splitting of the p-level.

ACKNOWLEDGMENTS

We wish to express our gratitude to Drs. V. F. Weisskopf, H. Staub, and N. H. Barschall for many helpful discussions, and to the members of the electrostatic generator crew who ran the generator during the experiments.

This paper is based on work performed under Contract No. W-7405-Eng-36 with the Manhattan Project at the Los Alamos Scientific Laboratory of the University of California.

Distribution of Neutrons in the Atmosphere

H. M. AGNEW,* W. C. BRIGHT, AND DAROL FROMAN
University of California, Los Alamos Scientific Laboratory, Los Alamos, New Mexico

(Received March 10, 1947)

Measurements on the distribution of neutrons in the atmosphere have been made to an altitude of 36,600 feet. Observations were made with counters filled with boron trifluoride containing 82 percent of B^{10}. Information concerning the spectral distribution of the neutrons was obtained by using the counters in various shielding geometries. Counters were used bare (no shielding), cadmium-covered, boron-covered, and surrounded with a layer of paraffin. The counting rates of all counters varied in the same way with altitude in the pressure range from 20 to 50 cm Hg. Within this pressure range the intensity I is given quite accurately by the relation $I=I_0e^{-0.083p}$, where p is expressed in cm of Hg. The counting equipment was carried in a B-29 type aircraft.

1. INTRODUCTION

SEVERAL previous experiments[1] have been performed to study the neutrons associated with the cosmic radiation, and some theoretical discussions[2] of their origin have been published. The purpose of the experiments described here was to observe the dependence upon altitude of the total neutron flux and of the general spectral distribution of these neutrons, in the range of altitudes easily accessible to the B-29 airplane in which the equipment was carried. Among other quantities, the "cadmium ratio" was measured at various altitudes. The cadmium ratio is the ratio of the neutron counting rate of a bare counter to that of the same counter, cadmium-shielded, under otherwise identical conditions. Thus, this ratio is a measure of the fraction of neutrons in the thermal region of energy.

2. APPARATUS AND EXPERIMENTAL METHOD

The neutron detectors were proportional counters, $1\frac{1}{2}$ inches in diameter and 11 inches in effective length, constructed with thin brass walls and a 0.0025-inch center wire. The counters were filled with BF_3 to a pressure of 20 cm of Hg. Some counters were filled with BF_3 enriched to 82 percent in the B^{10} isotope, while others were filled with gas containing boron of normal isotopic constitution.

All counters gave counting rates essentially independent of voltage when operated in the region of 1550 to 1650 volts and, since they contained equal quantities of boron, counting rates in a given flux of slow neutrons were in the ratio of the B^{10} contents. Those counters containing 82 percent of B^{10} had an efficiency of about 2 percent for thermal neutrons. Within the statistical counting errors in the experiments described here, all of the counters containing enriched boron showed equal efficiencies for the detection of slow neutrons in the laboratory. The counters containing ordinary BF_3 were used in the flights only to check the assumption that all counts above background were produced by neutrons and not by other cosmic-ray phenomena such as showers. It was assumed that the effects of processes other than neutron capture were negligible if counters in identical geometries gave counting rates proportional to their B^{10} contents at all altitudes.

* Now at the University of Chicago.

[1] L. H. Rumbaugh and G. L. Locher, Phys. Rev. **44**, 855 (1936); E. Schopper, Naturwiss. **25**, 557 (1937); E. Schopper and L. Schopper, Physik. Zeits. **40**, 22 (1939); W. Heitler, C. F. Powell, and G. E. F. Fertel, Nature **144**, 283 (1939); G. L. Locher, Phys. Rev. **44**, 774 (1933); **45**, 296 (1934); **50**, 394 (1936); J. Frank. Inst. **224**, 555 (1937); D. K. Froman and J. C. Stearns, Phys. Rev. **54**, 969 (1938); E. Fünfer, Naturwiss. **25**, 235 (1937); Zeits. f. Physik **111**, 351 (1938); C. G. Montgomery and D. D. Montgomery, Phys. Rev. **56**, 10 (1939); S. A. Korff, Phys. Rev. **56**, 210 (1939); Rev. Mod. Phys. **11**, 211 (1939); Proc. Am. Phil. Soc. **84**, 589 (1941); S. A. Korff and W. E. Danforth, Phys. Rev. **55**, 980 (1939); H. v. Halban, M. Magat, and L. Kowarski, Comptes rendus **208**, 572 (1939); S. A. Korff and E. T. Clarke, Phys. Rev. **61**, 422 (1942); S. A. Korff and M. Kupferberg, Phys. Rev. **65**, 253 (A) (1944); M. M. Shapiro, Rev. Mod. Phys. **13**, 58 (1941); M. Blau and H. Wambacher, Akad. Wiss. Wien **146**, 469 (1937); A. Filippov, A. Jdanov, and I. Gurevich, J. Phys. U.S.S.R. **1**, 51 (1939); W. Heitler, C. F. Powell, and H. Heitler, Nature **146**, 65 (1940); S. A. Korff and B. Hamermesh, Phys. Rev. **69**, 155 (1946).

[2] H. A. Bethe, S. A. Korff, and G. Placzek, Phys. Rev. **57**, 573 (1940); ibid., **69**, 158 (1946). E. Bragge, Ann. d. Physik **39**, 512 (1941).

Four counters were used in different geometries during each flight in order that a rough determination of the energy distribution of the neutrons might be made. One counter was used without shielding. Its response was expected to vary in the same way with neutron energy as the B^{10} capture cross section, i.e., the sensitivity was expected to be approximately inversely proportional to the velocity of the neutrons. Another counter was covered with 0.030-inch cadmium sheet. This shield absorbed neutrons with energies less than about 0.4 ev but had little effect on the response of the counter to neutrons of greater energy. A third counter was surrounded by a layer one inch thick of B_4C (normal boron) packed to a specific gravity of 1.3. Because this shield exhibits an absorption inversely proportional to neutron velocity, the enclosed counter was effectively protected against neutrons of energies less than several tens of electron volts. The fourth counter was enclosed in a cadmium-covered cylindrical shield of paraffin with 2-inch wall thickness. This counter was primarily a fast neutron detector since its sensitivity was roughly independent of neutron energy in the range from a few electron volts to about a million electron volts.

Precautions were taken to insure that the counters were influenced as little as possible by their surroundings in the airplane. The bare, cadmium-shielded and boron-shielded counters were placed in the pressurized tail gunner's compartment of the B-29. All gunnery equipment and hydrogenous material were removed from this section, and the armor glass of the observation ports was replaced by Duralumin and steel. The effects of the counters on each other were minimized by spacing them about 2 feet apart. A small high voltage battery and preamplifiers for the counter signals were the only other pieces of apparatus in the tail compartment. Removal of the kapok insulating layer from the tail resulted in rather low temperatures in this section of the plane during flight. In order to insure that the counter voltage remained constant, the battery was enclosed in a steel box lined with hair felt and heated electrically from the plane's 28-volt line. The counters themselves were checked in the laboratory and found to be insensitive to temperature in the range from −55°C to 25°C.

The paraffin-covered counter could not be placed near any of the others during the experiment because of the effect of the paraffin on

TABLE I. Neutron counting rates observed during flights.

Date of flight	Atmospheric condition	Altitude (ft.)	Pressure (cm Hg)	Counts per minute corrected for background $A(E)$	$Cd(E)$	$B_4C(E)$	$A(N)$	$B_4C(N)$	$P(E)$	Enriched to normal ratio $A(E)/A(N)$	Cadmium ratio $A(E)/Cd(E)$
5/8/46	Clear	36,650	16.6	25.37	—		—	—	332	—	
		34,700	18.1	21.57	—		5.06	—	301	4.30	
		29,700	22.9	15.37	—		3.86		216	3.98	
		*24,850	28.4	9.67	—		2.56	—	150	3.78	
		20,100	34.8	5.45	—		−0.95	—	82	—	
										$B_4C(E)/B_4C(N)$	
5/21/46	Clear	33,630	19.1	18.47	9.14	6.45		1.59	322	4.06	2.02
		*29,770	22.9	15.53	6.74	4.35		1.23	217.3	3.54	2.31
		24,830	28.3	11.25	4.84	2.39		0.46	159	5.18	2.32
		*19,940	35.0	6.32	2.84	1.59		0.39	87	4.07	2.22
		*15,000	43.0	2.97	1.13	0.72		0.32	—	2.25	2.63
		14,840	43.2	2.54	1.02	−0.005		0.01	42.6	—	2.49
		*9,980	52.5	0.57	0.7	0.05		−0.37	16	—	0.81
4/11/46	Clear	29,900	22.8	17.67	7.93				250		2.22
		*26,900	26.0	12.47	5.96				184		2.09
		24,780	28.5	9.97	4.79				154		2.08
		*22,000	32.0	7.41	3.65				113		2.03
		19,800	35.2	6.25	2.45				85.8		2.55
		*17,000	39.7	4.01	1.93				59.2		2.08
		*12,000	48.4	1.34	0.77				26.2		1.74
3/20/46	Clouds at 22,000	29,800	22.8	16.97	8.84	3.74			252		1.92
		24,930	28.3	12.67	6.21	2.74			164		2.04
		14,930	43.2	4.74	2.05	1.02			45		2.31
4/5/46	Cloud up to 25,000 ft., flying 200 ft. under toward hole	10,000		10.07	6.91	7.08			20.6		1.45
		10,300		3.37	1.97	1.92			25.6		1.71
		10,300		4.57	1.77	1.92			24.0		2.58
		10,380		2.97	0.97	1.52			24.0		3.06
		10,420		2.27	1.17	1.52			19.2		1.90

*Coming down.

Note: Counter filling indicated by
(E) = enriched boron
(N) = normal boron

Counter shielding indicated by
A = bare (no shield)
Cd = cadmium shield
B_4C = boron carbide shield
P = paraffin shield

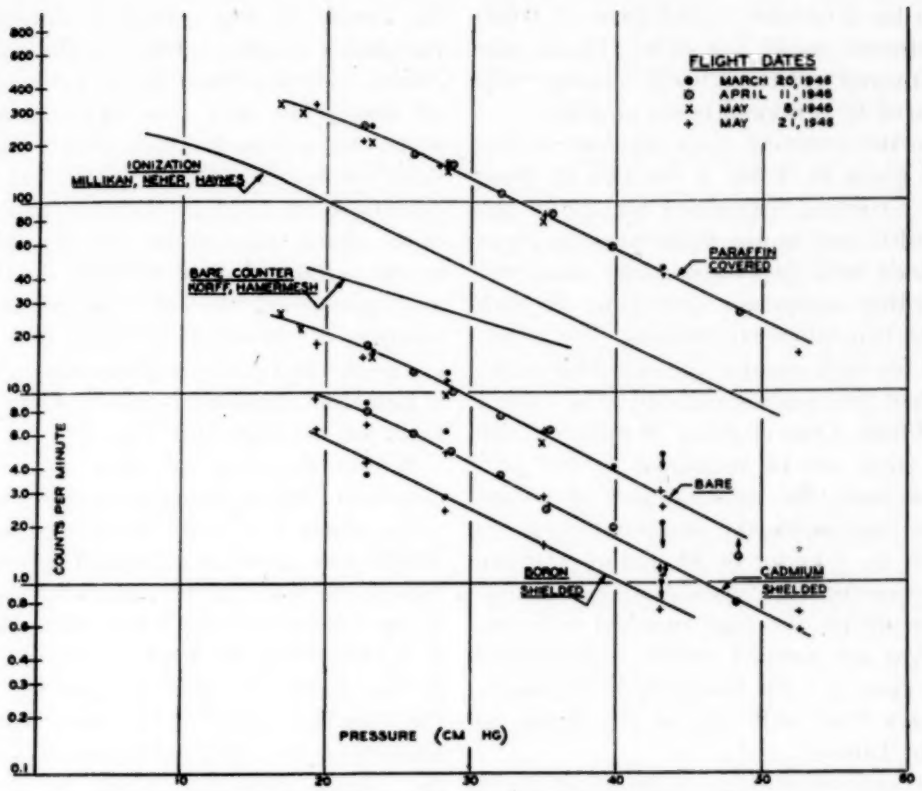

FIG. 1. Neutron distribution in the atmosphere.

their counting rates. Thus, this counter was suspended from the ceiling of the radar room near hydrogeneous material whose geometry did not remain constant during a run. However, the 0.030-inch cadmium cover surrounding the paraffin shield rendered this counter insensitive to neutrons thermalized in the vicinity. Initially it was feared that the gasoline carried by the plane (some 6500 gallons) would affect the counting rates. However, measurements taken at the same altitude at the start and at the end of a flight, after the gas load was some 3,500 gallons less, gave the same results even for the paraffin-shielded counter in the radar room. The radar room is much nearer the gasoline tanks than is the tail compartment. Consequently, it is believed that the counters in the tail compartment can be considered to be in free space, except for the dural tail structure.

The recording equipment consisted of preamplifiers placed near their respective counters and linear amplifiers, scalers, and mechanical registers. The filament supply lines for the preamplifiers and the co-axial signal leads were strung from the tail compartment to the recording equipment which was placed in the radar room. Only four sets of recording equipment were used, so that it was not possible to use both the enriched and normal counters with all types of shielding simultaneously. The normal boron counters were used only in replacement for the enriched bare counter and the enriched boron-shielded counter.

3. RESULTS AND CONCLUSIONS

The ratio of the slow neutron efficiencies of the enriched and normal boron counters was measured in the laboratory. This ratio was compared with that obtained at various altitudes for both the bare and the boron-shielded counters and was found to remain constant within the statistical counting errors. This meant that the counters were counting neutrons plus natural background at all times, and that the effects of showers were negligible. It is clear that, if one-inch thickness of B_4C did not produce enough

showers to be detectable, a thickness of 0.030 inch of cadmium would not either. Hence, the cadmium-covered enriched boron counter was never replaced by a normal boron counter.

The observed counting rates obtained in five flights are given in Table I. In two of these flights the recording equipment for one of the counters failed, and in one flight counting rates were obtained with five counters by using the same recording equipment part time at each altitude for two different counters. The geometries used for each counter are indicated in the table. Each of the counting rates given in Table I is obtained from a run of about 30 minutes. The statistical error can be estimated in any particular case from the total number of counts obtained by multiplying the counting rates given in the table by a factor of 30. Figure 1 shows curves of counting rate plotted against atmospheric pressure for the four enriched counters. These curves are parallel within experimental error. The curve for the boron-shielded counter includes data from only two of the flights as indicated in Table I.

The two curves with titles to the left in Fig. 1 are included for comparison and are plotted to an arbitrary scale. The upper curve for ionization caused by cosmic rays[3] is parallel to the curves obtained in these experiments. The lower of these two curves represents recent data obtained by Korff and Hamermesh[1] by means of an unshielded BF_3 counter carried by an unmanned balloon. The difference in slope between this curve and the others shown may arise from the relatively poor statistical accuracy, especially at the lower altitudes, which is attained in balloon flights.

One flight was made during cloudy weather, and the condition of the aircraft kept it below the clouds. It was extremely difficult to note the plane's position relative to the main body of clouds, as it was about 200 feet beneath them at all times. The only data obtained were taken under an extremely thick cloud. Observations were continued while the plane flew toward an opening in the overcast. Directly under the body of the cloud, the counting rate was high, except in the paraffin-covered monitor. As the opening was approached, the counting rate in the other counters decreased. It is hoped that this effect can be checked in later experiments incorporating a humidity measuring device. Data from this flight are not plotted in Fig. 1.

Within the error of these experiments the cadmium ratio is found to be constant, with a value about 2.2, at all altitudes from 7000 to 34,000 feet above sea level. The value of the ratio at the lower of these altitudes was obtained in the laboratory and is not shown in Table I. It is clear from the slopes of the graphs shown in Fig. 1 that the neutron counting rate of all the counters varied in the same way with the altitude as does the total ionization produced by the cosmic radiation. Thus, no variation of spectral distribution with altitude was observed, although it is evident that the experiment was not designed to detect variations in the neutron energy distribution in the region above 100 ev or so. In the pressure range 20 to 50 cm of Hg the neutron flux, I, observed with all counters is quite accurately given by $I = I_0 e^{-0.083p}$, where p is the pressure expressed in cm of Hg.

The authors wish to express their appreciation to the officers and men of the 428th A.A.F. Base Unit (Special) who were so efficient and cooperative in flying a B-29 for this work.

This paper is based on work performed under Contract No. W-7405-eng-36 with the Manhattan District at the Los Alamos Scientific Laboratory of the University of California.

[3] R. A. Millikan, H. V. Neher, and S. K. Haynes, Phys. Rev. **50**, 992 (1936).

Collision Cross Sections of Carbon and Hydrogen for Fast Neutrons

WILLIAM SLEATOR, JR.*
Department of Physics, University of Michigan, Ann Arbor, Michigan
(Received March 17, 1947)

Experiments are described by means of which the collision cross sections of carbon and hydrogen were determined for neutrons of nine different energies between 6 Mev and 22 Mev. The experimental method was such that data could be taken on groups of neutrons having energies within an interval small compared to the neutron energy, and at any energy produced by an energy heterogeneous source. The results are consistent with those of other observers at the four neutron energies in this range which have been previously investigated. A comparison with various theories shows that at high energies the observed hydrogen cross sections are about 10 percent larger than pure S-wave cross sections computed on the basis of a square well interaction between neutron and proton, and that they agree very well with the "symmetrical" theory of Rarita and Schwinger.

1. INTRODUCTION

NEUTRON sources in the 5- to 25-Mev energy range available up to 1943, when the present experiments were carried out, produced neutrons distributed continuously in energy. Therefore, in order to measure cross sections for neutrons in energy intervals small compared to the neutron energy, it was necessary to use a detecting system which could discriminate against neutrons outside of a particular interval. The first method which accomplished this made use of a nuclear reaction with a definite energy threshold as neutron detector. In this case, the most energetic neutrons produced by the source must be a reasonable interval above the detector threshold, and the method is limited to those energies at which there are suitable threshold reactions. It has been used at 7 Mev by Grahame and Seaborg[1] with $Fe^{56}(n, p)Mn^{56}$, at 12 Mev by Salant and Ramsey[2] with $Cu^{63}(n, 2n)Cu^{62}$, and at 21 Mev by Sherr[3] with $C^{12}(n, 2n)C^{11}$.

Aside from the present results, the only other total cross-section data known to the writer on neutrons above 6 Mev are those of Ageno, Amaldi, Bocciarelli, and Trabacchi.[4] They measured the cross sections of hydrogen, deuterium, and carbon at 4.1, 12.5, and 13.5 Mev with neutrons from Be, B, and Li targets, respectively, bombarded with 1-Mev deuterons. Their detecting method was similar in principle to that of the present experiments. However, since only 1-Mev deuterons were available, they were restricted to energies near those released in the nuclear reactions.

A very complete study of the cross sections of carbon, hydrogen, deuterium, and oxygen between 0.35 Mev and 6.0 Mev has been made by Bailey *et al.*[5] Above 2 Mev, these workers also used a heterogeneous neutron source and a differential method, somewhat different from that described below, to observe the effects of the neutrons in small energy intervals.

The results obtained by these observers on carbon and hydrogen for neutron energies greater than 5 Mev are shown in Figs. 3 and 4, along with the results of the present experiments. Theoretical work relating data of this sort to the problem of nuclear forces will be referred to, and the experimental results compared with those of various theories, in the last section of the paper.

2. EXPERIMENTAL METHOD AND APPARATUS

The fast neutron collision cross section of a nucleus can be determined most easily by means of a transmission experiment, that is, one in which the fraction of a neutron beam is measured

* Now at the University of Minnesota.
[1] D. C. Grahame and G. T. Seaborg, Phys. Rev. **53**, 795 (1938).
[2] E. O. Salant and N. F. Ramsey, Phys. Rev. **57**, 1075A (1940).
[3] R. Sherr, Phys. Rev. **68**, 240 (1945).
[4] M. Ageno, E. Amaldi, D. Bocciarelli, and G. C. Trabacchi, Naturwiss. **31**, 231 (1943); Phys. Rev. **71**, 20 (1947).
[5] Carl L. Bailey, W. E. Bennett, Thor Bergstrahl, R. G. Nuckolls, H. T. Richards, and J. H. Williams, Phys. Rev. **70**, 583 (1946); **70**, 805 (1946).

which a known amount of the element transmits unaltered in direction and in energy. In general, cross sections obtained in this way will be the sum of cross sections for three different processes: elastic scattering, inelastic scattering, and radiative capture. However, the capture cross sections of both hydrogen and carbon for neutrons of the energies dealt with in the present experiment are negligible.[6] In the case of hydrogen, moreover, inelastic scattering does not take place, so that a transmission measurement will give just the total scattering cross section appropriate for comparison with theory. The result of this kind of experiment will not make possible the separate evaluation of the two cross sections for carbon unless some other information can also be used. (This question is discussed below in Section 4.) Transmission measurements are particularly advantageous when the source is such that the detector must define the energy interval, since in a transmission experiment the detector need not be altered in any way between the beam strength measurements to be compared, and its energy response will necessarily be the same. Thus the method is free of the source of error which has been most serious for angular distribution measurements.**

Neutrons for the present experiments were obtained by bombarding beryllium and lithium with 10-Mev deuterons produced by the Michigan cyclotron. In the first case the reaction is $Be^9+D^2\rightarrow B^{10}+n^1$, and the most energetic neutrons had about 14-Mev energy. Neutrons from this reaction were used to study three energy intervals between 6 and 11 Mev. They were not used at higher energies because of the relatively small number near the upper energy limit. The lithium reaction, $Li^7+D^2\rightarrow Be^4+n^1$, produced neutrons having energies up to about 25 Mev, with which 7 energy intervals between 10 and 23 Mev were investigated.

The detecting method used was one which will determine the number of neutrons in an energy interval of almost arbitrary size at any energy. The essence of the method is this: the protons in any energy interval, which are knocked out of a thin paraffin layer at a particular angle, are all due to neutrons in a corresponding but slightly larger energy interval. (The neutron energy interval is larger by a small factor depending on the scattering angle and also by an additive amount equal to the energy which a proton can lose in going through the paraffin layer.) The intensity of the neutron beam is measured, in units of unknown but constant absolute magnitude, by counting these recoil protons. To determine the neutron intensity in a particular energy interval it is necessary to take the difference between two sets of counts during which the same number of neutrons, distributed in the same way with respect to energy, are produced by the source. This can be approximated by keeping conditions at the source constant, and then measuring while two equal charges of deuterons fall on the cyclotron target. Between the paraffin layer and the ionization chamber are placed aluminum absorbers such that one of these sets of counts measures the total number of neutrons having energies above the lower limit of the interval, while the other measures the number which have energies above the upper limit of the interval.

The efficiency of this system is necessarily low because only a very small fraction of the neutrons will collide with protons in a layer of paraffin thin enough so that there will be a relatively small energy difference between protons produced on the two sides of the layer by neutrons of the same energy. Also, unless the angles subtended by the detector at the paraffin layer and by the paraffin layer at the detector are small, a large energy spread will be introduced by the collisions which occur at widely different angles. Thus the number of protons observed is small, and it is important to have as large a ratio as possible between the pairs of counts whose difference is to be taken. When the Li target was

[6] H. A. Bethe, Rev. Mod. Phys. **9**, 160 (1937).

** For example, in the latter experiments on hydrogen (references 7 and 8), the recoil proton intensity is measured at two different angles with respect to the neutron beam, and the angular distribution is then inferred from a comparison of these two intensities. If the comparison is to be significant, the neutron energy intervals used at the two angles must be exactly the same because the neutron intensity in the interval depends very strongly on where the interval is cut off at the low energy end. This means that the proton cut-off energy will have to be different at the two angles by exactly the right amount. This adjustment can cause serious errors because, for example, it depends quantitatively on the somewhat uncertain range-energy relation of protons in aluminum.

[7] Howard Tatel, Phys. Rev. **61**, 450 (1942).

[8] E. Amaldi, D. Bocciarelli, B. Ferretti, and G. C. Trabacchi, Naturwiss. **30**, 582 (1942).

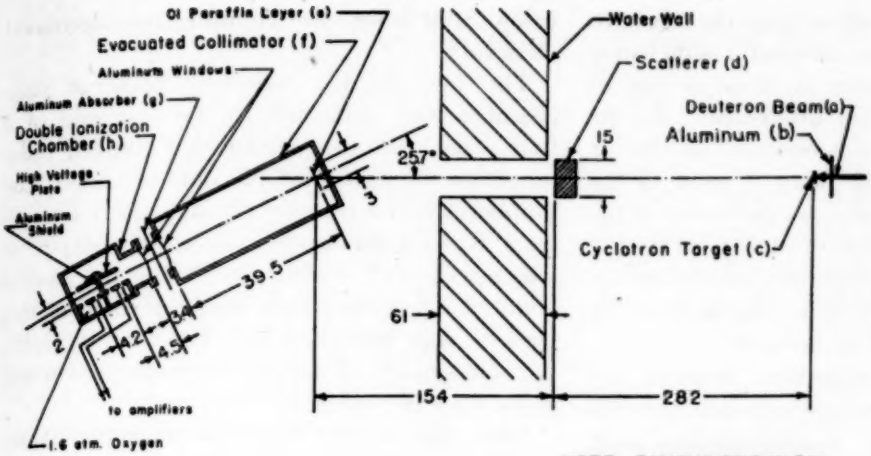

FIG. 1. Arrangement of apparatus, Be target in cyclotron. When the Li target was used, the angle between neutron and proton paths was 31.4°, the paraffin layer was 0.028 cm thick and 32.7 cm from the ionization chamber, and the collimator was not used.

used, the largest values of this ratio occurred when the upper limit of the interval was somewhere near the energy of the most energetic neutrons produced by the source. In general, therefore, enough Al was put in front of the Li target in the cyclotron to bring about an approximate coincidence of these two energies. Under these conditions, a thick paraffin layer would do as well as a thin one, since only those protons losing very little energy in the paraffin would be able to get through the Al absorbers.

However, with neutrons from the Be target the best values of this ratio occurred when the upper limit of the energy interval was several Mev below the peak energy of the source. Also, in order to work on the 9–13-Mev region with the more abundant Li neutrons, it was necessary to cut off the energy interval below the peak energy of the source, which could not be made as low as the 14 Mev released in the reaction. Therefore a thin paraffin layer (one in which the protons lost on the average about ½ Mev) was used, making it possible for the detector to put an upper as well as a lower limit on the working energy interval.

The arrangement of the apparatus is shown schematically in Fig. 1 for the low energy runs in which beryllium was used as the cyclotron target. The set-up used at high energies with the lithium target differed from this only in the respects noted below. The following lettered remarks correspond to the letters in the figure.

(a) The arrow represents the deuteron beam produced by the cyclotron, with energy about 10 Mev and intensity 8–15 microamperes.

(b) This line represents the aluminum absorbers of various thicknesses which were put in front of the target during most of the runs with Li to slow down the deuterons.

(c) The cyclotron target was a piece of beryllium or lithium about 3.0 cm. wide, 2.0 cm high, and 0.4 cm thick, screwed tightly to the water-cooled brass target cup. The dimensions of the effective neutron source, i.e., the part of the target receiving most of the deuteron beam, were about 2.0 cm horizontally and 0.4 cm vertically.

(d) The scatterers were blocks of graphite or paraffin about 15 cm square, set up 282 cm from the cyclotron target and 154 cm from the paraffin layer. Various thicknesses were used. The determination of their composition and density will be described in the next section.

(e) The paraffin layer from which protons were knocked by a small fraction of the neutrons was, for the runs with the Be target 9 cm high, 3 cm wide (perpendicular to the recoil protons), and 0.01 cm thick. When Li was used as the cyclotron target, the layer was 12 cm high, 2 cm wide, and 0.028 cm thick.

(f) At low energies an evacuated box, labeled "collimator," with an aluminum window to let the protons out, contained the paraffin layer and extended nearly to the ionization chamber. Its angle and length were such as to put the ionization chamber outside of the direct neutron beam (in order to cut down the number of recoiling

nuclei in the chamber), and to cause the sensitive region of the chambers to subtend a sufficiently small angle at the paraffin layer so as not to widen the energy interval intolerably. At the higher energies this box was omitted, and an air space of 32.7 cm took the place of some of the aluminum absorber. In this case the center of the proton beam made an angle of 31.4° with that of the neutron beam. The minimum proton energy necessary to cause a coincidence is computed for the two cases in Table I of Section 3.

(g) The aluminum absorbers defining the limits of the energy intervals were put into the proton path at this line. The thicknesses used, and the resulting proton and neutron energies, are shown in Table II of Section 3.

(h) The double ionization chamber and circuits arranged to record only coincidences were necessary because in a single chamber the background count in the cyclotron room was much too high. The chamber and circuits will now be described.

The coincidence ionization chamber was built and used by H. Tatel to measure the angular distribution of protons scattered by 11-Mev neutrons. Its construction has been described in Tatel's article,[7] so that for our purposes a statement of the critical dimensions and the conditions under which it was used in the present experiments will be sufficient. The general shape and most of the dimensions can be seen in Fig. 3.

Each of the two sensitive regions is 4 cm high, 2 cm wide in the direction of the electric field, and 2.3 cm deep along the proton path. Corresponding points in the two chambers are 4.2 cm apart along the proton path. Between them, perpendicular to the proton path, is a thin aluminum shield. The protons entered the chamber through an aluminum window (1 mil thick for the low energy runs and 2 mils thick for those at high energy), and then had to travel 4.5 cm before reaching the sensitive region of the first chamber. Throughout the present experiments the chambers were filled with oxygen at 1.6-atmospheres pressure, and the ion collecting potential was about 5700 volts. A test of the dependence of the counting rate on the collecting voltage showed that with the electrical sensitivity at its standard value, and an oxygen pressure of 1.6 atmos., the voltage had to drop below 5100 before the counting rate decreased observably.

The low voltage collecting plate of each chamber was connected to the first grid of a four stage resistance-capacitance coupled pulse amplifier, the gain of which could be varied. The amplifiers were connected through discriminators to a Rossi coincidence circuit, the output of which went to a scaling circuit and mechanical counter. The coincidence resolving time of this system was measured by Tatel with alpha-particle sources of various strengths and found to be 1.2×10^{-4} seconds.

Since the method used to determine transmission fractions required that all protons which passed through the chambers be counted, it was necessary to measure the over-all sensitivity of the counting systems to discover what proton energies were allowable. Accurately reproducible settings of the electrical sensitivity, which depended on the relation between amplifier gain and discriminator bias, were made by means of an 1000-cycle oscillator in the manner described by Tatel. The operating value was taken to be the most sensitive setting at which no noise pulses were counted (this test was made with the cyclotron running). Then the over-all sensitivity of each counting system, i.e., the minimum energy loss a particle must have in the sensitive region of the chamber in order to produce a countable pulse, was determined by tests made at reduced pressure with polonium alpha-particles. The first chamber and its circuits were found to be such that under operating conditions (electrical sensitivity as above, 1.6 atmos. O_2, and 5700 volts) a particle would be counted if it lost more than 78 kev/cm in the sensitive region. This is equivalent to 44 kev/cm in standard air, so that the most energetic protons which the first chamber could count were those which had about 11.6 Mev as they entered the sensitive region. (For alpha-particles the range-energy relation given by Holloway and Livingston[9] was used, and for protons that of Livingston and Bethe.[10]) To be detected by the second chamber and its circuits, a particle had to lose 73 kev/cm

[9] M. G. Holloway and M. S. Livingston, Phys. Rev. **54**, 31 (1938).

[10] M. S. Livingston and H. A. Bethe, Rev. Mod. Phys. **9**, 268 (1937).

or 168 kev in the 2.3 cm long sensitive region. This is the energy loss of a proton in the last 0.24 air cm of its range, so that the least energetic protons which could cause coincidences were those whose paths ended about 0.24 air cm inside the sensitive region of the second chamber. These protons had about 2.5 Mev as they entered the sensitive region of the first chamber.

Thus the system as it was used would count any protons which, as they entered the sensitive region of chamber 1, had energies between 2.5 Mev and 11.6 Mev. Because of the curvature of the range-energy relation, this will correspond to a smaller energy difference in the protons before they have passed through the Al absorbers. However, the initial energy range of the protons which the chambers could count was ample even for those cases in which a working interval was used, the upper limit of which was several Mev below the energy of the fastest neutrons produced by the source.

3. MEASUREMENTS

The composition of the paraffin scatterers was determined by means of melting point measurements. Two samples of the paraffin changed from completely liquid to completely solid between 60° and 56°C. This implies an average chain length of 26.6 carbons, and gives for the ratio, f, of the number of H atoms to the number of C atoms, $f=2.075\pm0.2$ percent. The scatterers used were two blocks of this paraffin about 6 inches square and $1\frac{1}{2}$ inches thick. The surfaces through which the neutrons were to pass were scraped flat and parallel (to ±0.001 inch) with a steel straight edge. Measurements of size and mass gave the mass per unit area to within 0.1 percent. For one block this was 3.163 g/cm², and for the other, 3.139 g/cm². The graphite used for the carbon scatterers was obtained from the National Carbon Company of Cleveland, and according to their analysis contained less than 0.1 percent of substances other than carbon. It was in the form of pieces $\frac{1}{2}$ inch thick and 6 inches square whose surfaces had been machined flat and parallel, and the mass per unit area of each was determined as above.

The calculation and final values of the neutron energy intervals used are shown in Tables I and II. These may be made clearer by the following remarks.

The difference between two counts will give the number of recoil protons in an energy interval $(E_{p0}-E_{p1})$ which has been sharply cut off at both ends by the aluminum absorbers. The lower and upper limits, E_0 and E_4, of the neutron energy interval to which this corresponds are given by the expressions

$$E_0=E_{p0}/\cos^2\theta_0, \quad E_4=(E_{p1}+\Delta E_p)/\cos^2\theta_2.$$

Here θ_0 is the minimum angle, and θ_2 the maximum angle, between the paths of neutron and proton at which the proton can reach the ionization chamber, and ΔE_p is the energy a proton loses in going all the way through the paraffin layer. The probability that a neutron of a particular energy will produce a proton in the interval $E_{p0}-E_{p1}$, i.e., the efficiency of the neutron detector, is not the same for all neutron energies between E_0 and E_4, but behaves somewhat like the solid curve in Fig. 2. The dotted curve shows how it would look if $\theta_2=\theta_0$ and $\Delta E_p=0$. Here $E_1=E_{p1}/\cos^2\theta_0$.

The actual effective energy distribution of the neutrons in an interval is the product of this detector efficiency and the distribution function of the neutrons produced by the source. Since this function was always greater at the low energy end of the interval, the effective neutron energy is lower than the center of the efficiency curve. The available information about the neutron distribution was sufficient to justify a guess at the effective neutron energy for each interval (last column of Table II) but not to locate it exactly.

At each new energy interval, various Al thicknesses were tried in the target cup, and sometimes the absorbers in front of the chamber were also changed, until what appeared to be the optimum combination was discovered. The criterion used in making this adjustment was not the relative position of the upper limit of the interval and the peak energy of the source (though in the runs on lithium these probably coincided fairly closely) but the ratio of the number of neutrons (per deuteron) in the interval to the number above it.

When this adjustment was such as to produce an adequate ratio for an appropriate energy

interval, the fraction of the neutrons transmitted in this interval by a particular scatterer could be determined. In the discussion of this process the word "count" will mean a determination of the number of coincidences which occur while a definite number of deuterons, measured in arbitrary but constant integrator units, fall on the cyclotron target, for a particular configuration of scatterer and absorbers (e.g., scatterer in the beam and upper limit absorber in front of chamber). A "run" is a determination of the transmission fraction of a particular scatterer for the neutrons in a particular interval, and always consists of several of each of four different kinds of counts. The scatterer-absorber arrangements for these counts are (a) lower limit absorber in front of chamber and scatterer not in beam, (b) upper limit absorber in front of chamber and scatterer not in beam, (c) and (d), similar to (a) and (b), respectively, but with the scatterer in the beam. Let A be the total number of coincidences observed, and N_A the total number of integrator units of deuterons striking the cyclotron target during all the counts of type (a) in a run, and let B, N_B, C, N_C, D, and N_D be the corresponding quantities for counts of the other three types. Then the observed fraction T_{obs} of the neutrons in the working interval transmitted by the scatterer is given by

$$T_{obs}=\frac{C/N_C-D/N_D}{A/N_A-B/N_B}.$$

It would have been desirable, of course, to measure the length of a count in terms of the number of neutrons in the working energy interval produced by the source, but this would have required essentially another complete detecting system. Instead, the length of a count was measured in terms of the charge of deuterons falling on the cyclotron target by means of a current integrator attached to the latter. The number of "integrator units" of deuterons was proportional to the number of neutrons produced as long as cyclotron operating conditions were kept absolutely constant. The two factors which were observed to have the greatest effect on this ratio were (1) the strength of the magnetic field, which affected the energy of the deuterons, and (2) the pressure in the cyclotron tank on which the energy distribution of the deuterons depended. Numerous tests showed that by careful adjustment and operation of the cyclotron these things could be kept effectively constant during times the order of 30 minutes, but seldom for as much as an hour. Therefore, it was desirable to take at least one of each of the 4 kinds of counts about every half hour. Since the number of coincidences occurring in a count of 5 to 10 minutes was in general not nearly large enough to produce a sufficiently accurate value of the transmission fraction, at least 5, and usually 8 or 10, counts of each kind were taken during each run. The value of T_{obs} from each run is given in Tables III and IV, Section 4. The relative standard deviation in T_{obs}, ΔT, given in these tables was computed on the assumptions that the standard deviation in each of the numbers A and B was equal to its square root, that the uncertainty in N_A and N_B was negligible, and that $N_B=N_A$ and $N_D=N_C$. (This latter condition was nearly always and always nearly fulfilled.) The ex-

TABLE I. Range of countable protons of least energy.

	Be target (as in Fig. 1)	Li target
Aluminum window, collimator:	0.001 inch or 7.35 mgm/cm²	0 mgm/cm²
Aluminum window, detector:	0.001 inch or 7.35 mgm/cm²	13.6 mgm/cm²
Aluminum internal shield detector:	0.0007 inch or 4.30 mgm/cm²	4.3 mgm/cm²
Total aluminum	19.00 mgm/cm² or 12.5 air cm.	11.8 air cm
Correction for Al	0.1 air cm	0.1 air cm
Air distance, collimator to detector	3.5 air cm	
Equivalent range, paraffin layer to detector 32.7 cm×741/760 (distance×mean air press. in atmos.)		31.9 air cm
Equivalent range in 1st chamber: 8.7 cm×1.6×1.1 (distance×O_2 press.×O_2 st. power)	15.3 air cm	15.3 air cm
Equiv. range to register in 2nd chamber:	0.2 air cm	0.2 air cm
Total: Minimum range necessary to cause coincidence:	31.6 air cm	59.3 air cm
Corresponding proton energy:	4.80 Mev	6.88 Mev

TABLE II. Calculation of neutron energies. $E_0=E_{p0}/\cos^2\theta_0$, $E_4=(E_{p1}+\Delta E_p)/\cos^2\theta_2$.

Run numbers	Cyclotron target	Al thickness, target (mils)	Al thickness, chamber (mils)	Proton energy (Mev) Min. E_{p0}	Max. E_{p1}	Loss in paraffin ΔE_p	Neutron energy (Mev) Min. E_0 ($\theta_0=23°$)	Max. E_4 ($\theta_2=28.5°$)	Effective value E
7, 10, 13	Be	0, 6	0–3	4.80	5.91	0.40	5.68	8.16	6.5
8, 9	Be	0	3–6	5.91	6.96	0.34	6.99	9.44	7.8
11, 12, 14, 15	Be	0	6–12	6.96	8.73	0.29	8.24	11.70	9.3
							($\theta_0=28.7°$)	($\theta_2=34.1°$)	
1, 16	Li	13	0–6	6.88	8.62	0.90	8.94	13.9	10.6
17	Li	13	6–12	8.62	10.16	0.78	11.2	15.9	12.8
2, 26	Li	12.5	6–13	8.62	10.40	0.78	11.2	16.3	12.9
3, 18	Li	11	12–19	10.16	11.74	0.70	13.2	18.1	14.8
4, 19	Li	8.5	18–25	11.53	12.86	0.63	15.0	19.6	16.5
5	Li	6	24–30	12.68	13.8	0.56	16.5	20.9	18.0
20, 23	Li	6	24–31	12.68	14.0	0.56	16.5	21.2	18.1
6, 25, 21	Li	3	30–38	13.8	15.2	0.50	17.9	22.9	19.6
22, 24	Li	0	36–46	14.9	16.4	0.45	19.4	24.6	21.1

pression for ΔT then becomes

$$\Delta T=[(C+D)/(C-D)^2+(A+B)/(A-B)^2]^{\frac{1}{2}}.$$

4. CORRECTIONS AND FINAL RESULTS

The procedure outlined above either eliminates or takes account of all significant random or accidental errors involved in the determination of the transmission fraction. Evidence for this is the fact that the differences in values of a cross section at a particular energy, obtained from runs on different days, and with different scatterer thicknesses, are in general not greater than the assigned standard deviations of these values (see Table III).

The method is subject to other errors the presence of which cannot be discovered by repeating measurements if, as was the case, the same geometry is used on all the occasions. The following four kinds of systematic errors may occur.

(a) Neutrons which leave the source in such a direction as not to hit the scatterers may be scattered into the detector by nearby objects such as the cyclotron magnet or the water wall. Though the water wall could be expected to absorb most of these neutrons, a test of the magnitude of this effect was made by putting 75 cm of paraffin between the neutron source and the detector. (Judging by the measurements on paraffin scatterers this reduced the number of neutrons in the beam by a factor of more than 300.) Counts were then taken at several different energy intervals, and at none of them was there a significant difference between the number of coincidences observed with the lower limit absorber in place and that with the upper.

(b) Since the scatterer and the detector are not of negligible size compared to their distances from the source and from each other, some neutrons scattered by the scatterer will reach the detector. The magnitude of this effect was calculated as described below, and found to be such that the observed values of T are the order of 1 percent too large.

(c) The scatterer will also scatter into the detector a fraction of those neutrons which have already been scattered once by some object nearer the source. However, the intensity at the scatterer of such neutrons was much less than that of the direct beam from the source, because on only one side of the source-scatterer line was there anything sufficiently close and massive to scatter neutrons appreciably (a vertical section of the magnet yoke). Since this iron certainly had no focusing effect, the "apparent source" in it was much weaker than the actual source. Since the direct neutrons which the scatterer scattered into the detector made only about a 1 percent change in T, the effect of this sub-

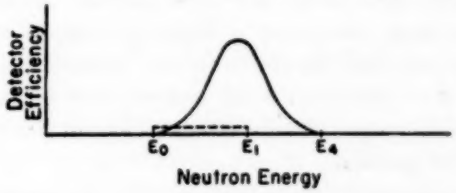

FIG. 2. Schematic diagram of detector efficiency as a function of neutron energy.

TABLE III. Calculation of total cross sections for carbon.

$\bar{\sigma}(C)$ = final value of total neutron-carbon cross section (elastic and inelastic scattering).
$\overline{\Delta\sigma}(C)$ = standard deviation in $\bar{\sigma}(C)$.
T = transmission fraction corrected for scattering into detector.

Run number	Mean neutron energy (Mev)	Scatterer thickness (xd) (g/cm²)	T_{obs}	T	ΔT (percent)	$\sigma(C)$ (10^{-24} cm²)	$\Delta\sigma(C)$ (percent)	$\bar{\sigma}(C)$ (10^{-24} cm²)	$\overline{\Delta\sigma}(C)$ (percent)
7	6.5	6.562	0.634	0.630	9.7	1.40	21		
10	6.5	10.936	0.432	0.428	9.6	1.54	11	1.51	10
8	7.8	6.562	0.596	0.592	10.4	1.59	19		
9	7.8	10.936	0.455	0.450	18	1.45	22	1.51	14
11	9.3	6.562	0.639	0.635	9.2	1.38	21		
12	9.3	10.936	0.450	0.446	10.1	1.47	12	1.45	10
1	10.6	13.123	0.395	0.390	9.5			1.43	10
2	12.9	10.936	0.499	0.494	10.9	1.28	15		
26	12.9	13.123	0.484	0.478	9.3	1.12	13	1.18	10
3	14.8	10.936	0.512	0.507	8.6			1.24	13
4	16.5	10.936	0.497	0.492	9.9			1.29	14
5	18.0	8.749	0.614	0.609	9.9			1.13	20
6	19.6	8.749	0.561	0.556	8.3	1.34	14		
25	19.6	15.311	0.376	0.370	9.8	1.30	10	1.31	8
24	21.1	13.123	0.468	0.462	7.4			1.17	10

stantially smaller number of indirect neutrons may be safely ignored.

(d) In those cases in which the upper limit of the energy interval was several Mev below the energy of the fastest neutrons produced by the source, the question arose whether some high energy neutrons might be scattered inelastically into the detector with an energy loss which would bring them into the working energy interval. Three major factors control the magnitude of this effect. In the first place, the total number of neutrons above the working interval was always smaller than the number in the interval, and most of these were within a few Mev of the upper limit of the interval. Secondly, Weisskopf[11] has shown that the mean energy after impact of neutrons in the 10–20-Mev range which suffer inelastic collisions is the order of one-third of their initial energy, so that only a small fraction lose less than 3 Mev. And finally, even if the angular distribution of the inelastically scattered neutrons had a pronounced maximum in the forward direction, the calculations described below show that only a small fraction of them would actually hit the detector. Thus it is clear that the contribution of inelastically scattered neutrons to the observed transmission fractions may be ignored.

To calculate the effect on the transmission fractions of the neutrons scattered into the detector by the scatterer, it is necessary to know something about the angular distribution of the scattered neutrons, at least at small angles. For carbon (and larger) nuclei enough is known about this to make a calculation worth while. Placzek and Bethe[12] have suggested that the elastic scattering of fast neutrons by compound nuclei may be regarded as essentially a diffraction of the neutron beam by the nuclei, which correspond to absorbing disks or spheres in a beam of light. On this assumption the angular distribution of the elastically scattered neutrons is given by

$$K(\theta) = R^2[J_1(kR\theta)/\theta]^2,$$

where $K(\theta)$ is the scattering cross section per unit solid angle at the angle θ, J_1 is a Bessel function of the first kind, k is the wave number of the incident neutrons, and R is the nuclear radius. The experimental results of Kikuchi, Aoki, and Wakatuki,[13] who observed the angular distribution of 15-Mev neutrons scattered by various elements, agree very well with this expression (except for their measurements at 14°, the smallest angle at which they could work, which are probably in error).

[11] V. F. Weisskopf, Phys. Rev. **52**, 295 (1937).

[12] G. Placzek and H. A Bethe, Phys. Rev. **57**, 1075A (1940).

[13] S. Kikuchi, H. Aoki, and T. Wakatuki, Proc. Phys. Math. Soc. Japan **21**, 410 (1939); **22**, 430 (1940).

TABLE IV. Calculation of total cross sections for protons.

$\bar{\sigma}(H)$ = final value of total neutron-proton scattering cross section.
$\overline{\nabla\sigma}(H)$ = standard deviation in $\bar{\sigma}(H)$.
T = transmission fraction corrected for scattering into detector.

Run number	Mean neutron energy (Mev)	Scatterer thickness (xd) (g/cm²)	T_{obs}	T	ΔT (percent)	$\sigma(C)$ from Fig. 3 (10^{-24} cm²)	$\sigma(H)$ (10^{-24} cm²)	$\Delta\sigma(H)$ (percent)	$\bar{\sigma}(H)$ (10^{-24} cm²)	$\overline{\Delta\sigma}(H)$ (percent)
13	6.5	6.302	0.302	0.300	6.3	1.56			1.40	8
14	9.3	6.302	0.414	0.410	5.2	1.44	0.90	10		
15	9.3	3.139	0.628	0.625	4.7	1.44	0.99	18	0.92	9
16	10.6	6.302	0.447	0.443	4.8	1.39			0.78	11
17	12.8	6.302	0.444	0.440	4.9	1.34			0.83	11
18	14.8	6.302	0.507	0.502	5.2	1.29			0.61	15
19	16.5	6.302	0.494	0.489	5.2	1.28			0.66	15
20	18.1	6.302	0.516	0.511	5.0	1.26	0.59	16		
23	18.1	3.163	0.746	0.743	4.5	1.26	0.45	33	0.55	14
21	19.6	6.302	0.539	0.533	5.3	1.25			0.52	18
22	21.1	6.302	0.576	0.569	5.0	1.25			0.41	21

The value of R to be used in the expression is related to the cross section σ_e for this elastic scattering by $\sigma_e=\pi R^2$. Since inelastic collisions also occur, σ_e is less than the total collision cross section, σ, calculable from the observed transmission fractions of the carbon scatterers. Sherr[3] has compared the results of his experiments at 24 Mev, in which he also measured total cross sections, with those of Grahame and Seaborg[1] whose method was such that they measured cross sections for inelastic scattering only. Sherr finds strikingly good agreement between the results of the two kinds of experiments if he assumes $\sigma_e=\sigma_i=\frac{1}{2}\sigma$. It is reasonable from the point of view of the optical analogy, also, that the cross section for the diffraction process should be equal to the actual area of the disk.

On the basis of these assumptions the transmitted intensity was calculated (neutrons scattered once and twice by the scatterer were taken into account). The resulting expression for the observed transmission fraction is

$$T_{obs}=e^{-N\sigma x}\left[1+\frac{A_s(l+h)^2}{l^2h^2}\left(N\sigma_e x\frac{\bar{K}(\theta)}{\sigma_e}+\frac{(N\sigma_e x)^2}{2}\frac{\bar{L}(\theta)}{\sigma_e^2}+\cdots\right)\right].$$

Here σ is the total and σ_e the elastic scattering cross section of carbon, Nx the number of atoms per cm² of scatterer, A_s the scatterer area (perpendicular to the beam), l and h the distances from source to scatterer and from scatterer to detector, $\bar{K}(\theta)$ the average value of $K(\theta)$ as θ goes from 0° to 6° (6° is the largest value θ can have for particles which reach the detector, and $K(\theta)$ is nearly constant in this region), and $\bar{L}(\theta)$ the corresponding average value of the function $L(\theta)$ which gives the angular distribution of neutrons which have been scattered exactly twice.

For the three inch thick carbon scatterer and a neutron energy of 21 Mev, the second term in the bracket is 1.2 percent of the first term and the third is 0.17 percent of the first. Thus even at high energies, where the anisotropy of the scattering is greatest, this correction is small compared to the statistical fluctuations. However, since it changes all the cross sections in the same sense, it was computed roughly for each of the energies and scatterer thicknesses used, and applied to T_{obs} to get T as shown in Table III. The corrections to the paraffin transmission fractions indicated in Table IV were made in the same way with the additional assumption that scattering by the protons is isotropic in the center of gravity system. (Though this is very likely contrary to fact, there does not seem to be information now available which would make any other specific assumption more probable.)

The sixth column of Table III gives ΔT, the relative standard deviation in T, computed as described above from the observed numbers of counts. The column headed $\bar{\sigma}(C)$ gives the total collision cross section for carbon at each different

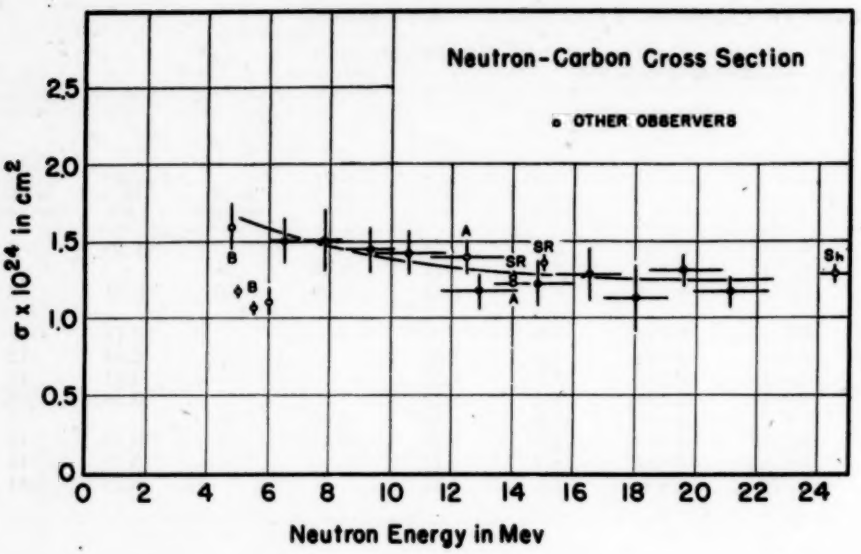

FIG. 3. Total neutron-carbon collision cross section as a function of energy. The length of the vertical line at each point is twice the standard deviation. The horizontal line indicates an energy range which contains about 0.8 of the neutrons in the interval. "*B*" represents Bailey *et al.*,[5] "*A*" Ageno *et al.*,[4] "*SR*" Salant and Ramsey,[2] and "*Sh*" Sherr.[3]

energy. The only significant contribution to $\overline{\Delta\sigma}(C)$, the relative standard deviation of $\bar{\sigma}(C)$, came from ΔT, since the standard deviation in Nx was less than 0.5 percent. In those cases in which two runs were made with the same energy interval, the columns headed $\sigma(C)$ and $\Delta\sigma(C)$ give the values for each run. $\bar{\sigma}(C)$ is the average of the two $\sigma(C)$s, weighted according to their reliability.

The final values of the neutron-carbon collision cross sections, represented by solid dots, are plotted against energy in Fig. 3. The open circles show the results of other observers. (All available data above 5 Mev are plotted.) The total length of the vertical line is twice the standard deviation (resulting from statistical fluctuations) as computed above, in the case of the present experiments. For the other observers it is twice the stated uncertainty. The length of the horizontal line represents half of the total energy interval (in those cases where the information was available), and it is centered approximately at the effective value of the neutron energy. This part of the interval contained at least 0.8 of the total number of neutrons in the whole interval. Points marked "*B*" in Fig. 4 were obtained by Bailey *et al.*,[5] those marked "*A*" by Ageno *et al*,[4] those marked "*SR*" by Salant and Ramsey,[2] and that marked "*Sh*" by Sherr.[3]

A value of $\sigma(C)$ for each energy interval must be used in the calculation of the proton cross section $\sigma(H)$ from measurements with paraffin scatterers, and the question arises whether the best value at any energy is the actual result of the measurement at that energy, or the value lying on a smooth curve determined by all the points. The results of Bailey *et al.*[5] suggest that the spacing of the virtual levels of the compound nucleus (about 0.3 Mev between maximum and minimum) is such that they would not be separated by the present experiments because of the large energy intervals which were used. Moreover, as the energy increases, one would expect the width of these levels to become greater compared to their separation in energy. Thus it is probable that the apparent fluctuations in $\sigma(C)$ are mainly due to the uncertainties in the measurement of the transmission fractions, and the value of $\sigma(C)$ used in the calculations of $\sigma(H)$ below were obtained from the smooth curve shown in Fig. 3.

For the paraffin scatterers the relation connecting the cross section with the corrected transmission fractions is

$$[\sigma(C)+f\sigma(H)]N_C x=\log(1/T),$$

where f is the ratio of H atoms to C atoms (as evaluated in the previous section) and $N_C x$ is the number of C atoms per unit area of scatterer. The values of $\sigma(C)$ used at each energy are given in Table IV as well as the final values of the proton cross sections $\bar{\sigma}(H)$. In estimating the standard deviation in $\bar{\sigma}(H)$, the contributions of f and $N_C x$ have been ignored, and the standard

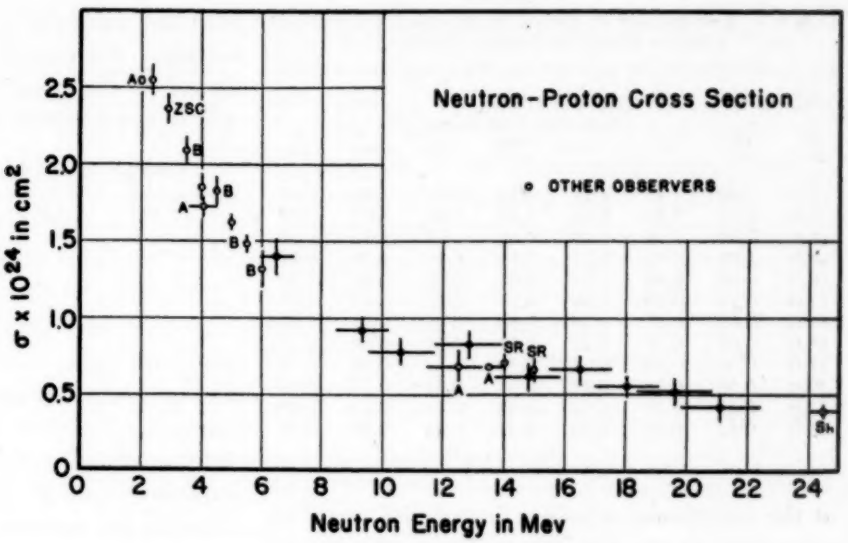

FIG. 4. Total neutron-proton collision cross section as a function of energy. Meaning of symbols as in Fig. 3. "*Ao*" represents Aoki[14] and "*ZSC*" Zinn, Seely, and Cohen.[15]

deviation in the values of $\sigma(C)$ read from the curve was assumed to be about 5 percent. In Fig. 4 the final values of $\bar{\sigma}(H)$ and also the results of other observers (complete above 3 Mev) are plotted against energy. The symbols here, including the initials representing other observers, have the same meanings as in Fig. 4. "*Ao*" and "*ZSC*" (which did not appear before) indicate, respectively, Aoki[14] and Zinn, Seely, and Cohen,[15] who both used D−D neutrons of sharply defined energy.

5. DISCUSSION

Because of the uncertain state of theories of nuclear radii, a comparison with them of measured cross sections of a single nucleus is of little significance. For this purpose measurements at a single energy on several nuclei differing widely in mass, such as those carried out by Sherr,[3] are much more useful. Thus the actual values of the carbon cross sections resulting from the present experiments are of interest principally because of the comparisons they allow, at those energies which have been previously used, with the experimental results obtained by other observers using different methods. As can be seen from Fig. 3, in which all the available data above 5 Mev have been plotted, the results of the present experiments agree with those of other observers above 6 Mev within experimental error.

In the previous section a theory was mentioned according to which the elastic scattering of fast neutrons by compound nuclei may be regarded as essentially a diffraction of the neutron beam by the nuclei. This picture should begin to be valid at energies such that the wavelength of the neutron beam is small compared to nuclear dimensions. At 15 Mev, for example, $\lambda=1.2\times10^{-13}$ cm, and $R=4.5\times10^{-13}$ cm. R is the "geometrical radius" of a carbon nucleus computed on the assumption discussed above, that the cross sections for elastic and inelastic scattering are equal so that $\sigma(C)=2\pi R^2$. Under these conditions, resonances will have a relatively small effect on the total cross section and one would expect the latter to be essentially independent of energy. This expectation is borne out by the experimental results shown in Fig. 3, which indicate that the average cross section over 2-Mev intervals changes very little between 15 and 25 Mev.

The experimental results for the total neutron-proton cross section, and also the predictions of several theories, are summarized in Table V in such a way as to facilitate comparisons.

Column 1 of Table V indicates the energies at which the cross sections have been evaluated. Column 2 contains values of σ_{exp} read from a smooth monotonically decreasing curve through the center of the region covered by the experimental points shown in Fig. 4. All the available data above 2 Mev have been considered. None

[14] H. Aoki, Phys. Rev. **55**, 795 (1939).
[15] W. H. Zinn, S. Seely, and V. W. Cohen, Phys. Rev. **56**, 260 (1939).

TABLE V. Comparison of measured proton cross sections with the results of various theories.

(1)	(2)	(3)	(4)	(5)	(6)	(7)	(8)
		Theoretical cross sections (10^{-24} cm^2)					
E (Mev)	σ_{exp} (10^{-24} cm^2)	σ_W	σ_{Wa}	σ_{KB} (s wave)	σ_{RSI}	σ_{RSII}	σ_{RSIII}
2.5	2.60	2.13	2.57	2.74	2.69	2.69	2.69
4.0	1.91	1.56	1.94	2.02	2.05	2.05	2.05
6.0	1.39	1.18	1.49	1.48	1.52	1.52	1.55
8.0	1.08	0.95	1.22	1.16	1.19	1.20	1.32
10.0	0.90	0.80	1.03	0.94	0.96	0.98	1.18
12.0	0.78	0.69	0.89	0.77	0.80	0.83	1.08
14.0	0.69	0.61	0.79	0.66	0.68	0.72	1.01
16.0	0.61	0.55	0.71	0.57	0.59	0.64	0.97
18.0	0.55	0.49	0.64	0.50	0.53	0.58	0.94
20.0	0.50	0.45	0.59	0.44	0.48	0.53	0.92
22.0	0.45	0.41	0.54	0.40	0.44	0.48	0.91
24.0	0.41	0.38	0.50	0.37	0.41	0.45	0.91

of the experimental points lies off the curve by more than 11 percent of its ordinate. In general, it would be safer to compare each of the theoretical curves directly with the data. However, since all the theoretical curves have the same character as the one drawn through the data, and since it is not necessary to distinguish between two theoretical curves which fit well over the whole range, the present method of comparison is probably adequate.

In column 3 of Table V are given values of the cross section computed from the Wigner formula

$$\sigma_W=\frac{\pi\hbar^2}{M}\left[\frac{3}{\frac{1}{2}E+|\epsilon|}+\frac{1}{\frac{1}{2}E+|\epsilon'|}\right]. \qquad (1)$$

The energies taken for the triplet and singlet levels of the neutron-proton system are $\epsilon=2.18$ Mev, $\epsilon'=0.072$ Mev. The value of ϵ' was computed by substituting into Eq. (1) the experimental value of σ for very slow neutrons (1–10 ev) obtained by Hanstein,[16] i.e., $\sigma_0=20\times10^{-24}$ cm^2. The values of σ predicted by Eq. (1) are too small throughout the energy range. However, beyond 4 Mev they come closer to the experimental values with increasing energy, and at the high energy end agree within 7 percent. There may be some significance in the fact that above 18 Mev this expression, based on the simple assumption that the range of the forces is zero, fits the data better than any of the other theories except the "symmetrical" one of Rarita and Schwinger (column 6). Column 4 of Table V contains values of σ obtained from the Wigner formula, modified by the inclusion of the first power of the range a of the forces. The value which was assumed here is $a=2.0\times10^{-13}$ cm.

$$\sigma_{Wa}=\frac{\pi\hbar^2}{M}\left[\frac{3(1+a(M|\epsilon|)^{\frac{1}{2}}/\hbar)}{\frac{1}{2}E+|\epsilon|}+\frac{1-a(M|\epsilon'|)^{\frac{1}{2}}/\hbar}{\frac{1}{2}E+|\epsilon'|}\right]. \qquad (2)$$

This expression, and the experimental value of σ for very slow neutrons given in the previous paragraph, lead to a value of 0.069 Mev for ϵ'. The resulting values of σ_{Wa} agree well with experiment up to about 6 Mev, but at higher energies the agreement is not so good as that of the simple Eq. (1). If in the above formula, a is set equal to 2.8×10^{-13} cm, the range of force suggested by proton-proton scattering, the resulting values of σ are about 10 percent larger than those in column 4, and differ from the data correspondingly more.

The results of Kittel and Breit[17] are given in column 5 of Table V. These authors assumed a square potential well of radius $a=2.8\times10^{-13}$ cm, and, retaining the first four powers of this radius, obtained expressions for the total S-wave scattering cross section. These values are in fairly good agreement with the experimental results in the low and middle energy range, but above 14 Mev are too small. On the assumption that the S-wave potential well is independent of energy, this difference gives an indication of the magnitude of the P-wave scattering cross section, i.e., about 0.03×10^{-24} cm^2 at 16 Mev, and 0.04×10^{-24} cm^2 at 24 Mev.

Kittel and Breit have calculated the P-wave cross section on the basis of Bethe's neutral form of meson theory and obtain $\sigma_{P\text{ wave}}=0.12\times10^{-24}$ cm^2 for a meson mass $\mu=177m$, and 0.01×10^{-24} cm^2 for $\mu=330m$, as suggested by proton-proton scattering. The magnitude of the P-scattering has also been calculated by Smorodinsky[18] from the angular distribution data of Amaldi and associates[8] by a direct method involving no meson theory and no assumption about the shape of the interaction potential. For a neutron

[16] H. B. Hanstein, Phys. Rev. **57**, 1045 (1940).

[17] C. Kittel and G. Breit, Phys. Rev. **56**, 744 (1939).

[18] J. Smorodinsky, J. Phys. U.S.S.R. **8**, 219 (1944).

energy of 16 Mev he obtains $\sigma_{P\ \text{wave}}=0.01\times10^{-24}$ cm², in fair agreement with the observed value assuming Kittel and Breit's S-wave cross section.

The last three columns of Table V contain estimates accurate to about 1 percent of the total cross sections predicted by the three theories of Rarita and Schwinger[19] (I "symmetrical," II "charged," and III "neutral"). The tabulated values in each column were read from a smooth curve drawn through five computed values (at 2.8, 6, 10, 15.3, and 25 Mev) of the cross section predicted by the corresponding theory.[20] The experimental values agree fairly well with the results of the "symmetrical" theory throughout the energy range, and very well above 12 Mev. Of the theories considered, this one gives the best over-all fit. The "neutral" theory, on the other hand, fits so poorly as to be unequivocally eliminated by the data. The "charged" theory differs consistently and significantly from the experimental results, and is at best an unlikely possibility.

The author wishes to express his gratitude to Professors H. R. Crane and G. E. Uhlenbeck for their interest and advice throughout the course of this work, and to Professor J. M. Cork, whose direction of the Michigan Cyclotron Laboratory made these experiments possible. He is also indebted to Mr. Wayne Middleton and to the other members of the cyclotron crew for their unfailing cooperation. The cyclotron operating expenses were met by a grant from the Horace H. Rackham Fund.

[19] W. Rarita and J. Schwinger, Phys. Rev. **59**, 556 (1941).
[20] The author is indebted to Dr. C. L. Critchfield for suggestions concerning these calculations.

PHYSICAL REVIEW VOLUME 72, NUMBER 3 AUGUST 1, 1947

The Vector Mesotron

JAMES H. BARTLETT
Department of Physics, University of Illinois, Urbana, Illinois
(Received April 15, 1947)

The wave equations of Proca for a vector mesotron (spin 1) are specialized first to the case in which there is no magnetic field, and then to that in which the field is central. The wave functions satisfy fourth-order homogeneous differential equations. For the states $l=j\pm1$, it is simpler to consider two simultaneous second-order differential equations in two unknowns (see Eqs. (19) and (21) of this article). For a coulomb field, the form of the radial functions at $r=0$ is established as $u=\exp[-aL/r^{\frac{1}{2}}]r^{\beta}f$, where $a=2(z\alpha)^{\frac{1}{2}}[j(j+1)]^{\frac{1}{4}}$, $L^2=\hbar/Mc$, $M=$rest mass of mesotron, f is an ascending power series in r, ze is the charge on the coulomb source, α is the fine-structure constant $e^2/\hbar c$, and β is a constant which can be determined.

INTRODUCTION

CORBEN and Schwinger[1] and, independently, Tamm[2,3] have discussed the stationary states of a vector mesotron in a coulomb field. Corben and Schwinger have written down the explicit radial equations when $l=j\pm1$, and Tamm[2] has indicated the general nature of the solution. It is the purpose of the present article to give further details of the solution, together with its derivation. The notation of Corben and Schwinger will be adopted.

WAVE EQUATION

The wave equations of Proca[4] for a vector mesotron in an external field with a four-potential A_α

[1] H. C. Corben and J. Schwinger, Phys. Rev. **58**, 953 (1940).
[2] I. Tamm, Phys. Rev. **58**, 952 (1940).
[3] I. Tamm, Comptes Rendus U.S.S.R. **29**, 551 (1940).
[4] See N. Kemmer, Proc. Roy. Soc. **A166**, 133 (1938).

$$\left(\frac{\partial}{\partial x_\alpha}-\frac{ie}{\hbar c}A_\alpha\right)\varphi_\beta-\left(\frac{\partial}{\partial x_\beta}-\frac{ie}{\hbar c}A_\beta\right)\varphi_\alpha=\kappa\chi_{\alpha\beta}, \tag{1}$$

$$\left(\frac{\partial}{\partial x_\alpha}-\frac{ie}{\hbar c}A_\alpha\right)\chi^{\alpha\beta}=\kappa\varphi^\beta, \tag{2}$$

($x_0=ct$, $a_0=-a^0$, $a_i=a^i$ ($i=1, 2, 3$), Greek suffixes run from 0 to 3, and Latin suffixes from 1 to 3. Unless they are summation variables, i, k, and l will denote 1, 2, and 3 in cyclic permutation.)

Here $\kappa=Mc/\hbar$, where M is the rest mass of the mesotron.

If we deal with stationary states, then $W\varphi=-i\hbar\partial\varphi/\partial t$. Let us write $(W+eA_0)/\hbar c=k$, and assume that $A_1=A_2=A_3=0$. Then (1) and (2) become, if Φ denotes the vector with components $(\varphi_1, \varphi_2, \varphi_3)$ and $\mathbf{g}$ that with components $g_l=\chi_{ik}$,

$$-ik\Phi-\nabla\varphi_0=\kappa\chi_0, \tag{3}$$

$$ik\chi_0-\operatorname{curl}\mathbf{g}=\kappa\Phi, \tag{4}$$

$$\operatorname{curl}\Phi=\kappa\mathbf{g}, \tag{5}$$

$$\operatorname{div}\chi_0=-\kappa\varphi_0. \tag{6}$$

Combining (4) with (5) and (3), and (3) with (6),

$$\operatorname{curl}\operatorname{curl}\Phi=ik\kappa\chi_0-\kappa^2\Phi,$$

$$=k^2\Phi-\kappa^2\Phi-ik\nabla\varphi_0, \tag{7}$$

$$\nabla^2\varphi_0+\operatorname{div}(ik\Phi)=\kappa^2\varphi_0. \tag{8}$$

If, now, we set $i\varphi_0=\varphi$, the equations become

$$\operatorname{curl}\operatorname{curl}\Phi-k^2\Phi+\kappa^2\Phi=-k\nabla\varphi, \tag{7a}$$

or

$$\operatorname{curl}\operatorname{curl}\Phi+\kappa^2\Phi=k(k\Phi-\nabla\varphi), \tag{7b}$$

$$\nabla^2\varphi-\kappa^2\varphi=\operatorname{div}k\Phi, \tag{8a}$$

or

$$-\kappa^2\varphi=\operatorname{div}(k\Phi-\nabla\varphi). \tag{8b}$$

Taking the divergence of Eq. (7a), we have

$$\kappa^2\operatorname{div}\Phi=k\operatorname{div}(k\Phi-\nabla\varphi)+(k\Phi-\nabla\varphi)\cdot\nabla k$$

$$=-\kappa^2k\varphi+(k\Phi-\nabla\varphi)\cdot\nabla k,$$

or

$$\operatorname{div}\Phi+k\varphi=(1/\kappa^2)(k\Phi-\nabla\varphi)\cdot\nabla k. \tag{9}$$

Then Eq. (8a) takes the form

$$\nabla^2\varphi-\kappa^2\varphi=k\operatorname{div}\Phi+\Phi\cdot\nabla k$$

$$=-k^2\varphi+(1/\kappa^2)k(k\Phi-\nabla\varphi)\cdot\nabla k+\Phi\cdot\nabla k \tag{10}$$

and Eq. (7a) can be transformed, by the use of (9), into

$$\nabla^2\Phi+k^2\Phi-\kappa^2\Phi=\nabla\operatorname{div}\Phi+k\nabla\varphi$$

$$=-\varphi\nabla k+(1/\kappa^2)\nabla[(k\Phi-\nabla\varphi)\cdot\nabla k]. \tag{11}$$

In the case that the field is central, Eqs. (9), (10), and (11) specialize to Eqs. (38), (37b), and (37a) of Corben and Schwinger. Eq. (9) [Eq. (38) of reference 1] is not a supplementary condition, but follows directly from the generalized Maxwell equations (3) to (6).

It is possible to eliminate φ and thus to obtain an equation which Φ satisfies. Let $O\Phi=\text{curl curl}\Phi-k^2\Phi+\kappa^2\Phi$. Then

$$\text{div}[(1/k)O\Phi]=-\nabla^2\varphi=-\kappa^2\varphi-\text{div}(k\Phi), \quad \text{curl}(1/k)O\Phi=0,$$

$$\nabla^2[(1/k)O\Phi]=\nabla\,\text{div}[(1/k)O\Phi]=-\kappa^2\nabla\varphi-\nabla\,\text{div}(k\Phi)=(\kappa^2/k)O\Phi-\nabla\,\text{div}(k\Phi),$$

or

$$(\nabla^2-\kappa^2)[(1/k)O\Phi]=-\nabla\,\text{div}(k\Phi). \tag{12}$$

Equation (12) is a fourth-order homogeneous equation for Φ. We shall determine the nature of the four solutions near $r=0$.

According to Corben and Schwinger, particles with $l=j\pm1$ have wave functions

$$\Phi=\{\mathbf{r}_1F_1(r)+i[\mathbf{r}_1\times\mathbf{L}]F_2(r)\}P_j^m, \quad \varphi=G(r)P_j^m, \tag{13}$$

where

$$F_2''+(2/r)F_2'-[j(j+1)/r^2]F_2+(k^2-\kappa^2)F_2$$
$$=(2/r^2)F_1-(1/r)\{F_1'+(2/r)F_1+[j(j+1)/r]F_2+kG\}. \tag{14}$$

This follows from Eqs. (41b) and (41d) of reference 1. It may be rewritten as

$$(1/r)(rF_2)''+(1/r)F_1'+(k^2-\kappa^2)F_2=-kG/r. \tag{15}$$

Now let

$$u_2=rF_2 \quad \text{and} \quad u_1=F_1+u_2'. \tag{16}$$

Then

$$u_1'+(k^2-\kappa^2)u_2=-kG. \tag{17}$$

Equation (44a) of reference 1 takes the form

$$-kG'=(-k^2+\kappa^2)F_1+[j(j+1)/r^2]u_1, \tag{18}$$

or

$$-k(G'-kF_1)=\kappa^2F_1+[j(j+1)/r^2]u_1. \tag{18a}$$

Differentiating (17), we obtain

$$u_1''+(k^2-\kappa^2)u_2'+2kk'u_2=-kG'-k'G$$
$$=(k^2-\kappa^2)(u_2'-u_1)+[j(j+1)/r^2]u_1+(k'/k)[u_1'+(k^2-\kappa^2)u_2].$$

Hence

$$u_1''-(k'/k)u_1'+\{k^2-\kappa^2-[j(j+1)/r^2]\}u_1=-(k'/k)(k^2+\kappa^2)u_2. \tag{19}$$

Combining Eqs. (41d) and (43) of reference 1, and using (18a)

$$F_1'+(2/r)F_1+[j(j+1)/r]F_2+kG=-(k'/\kappa^2)(G'-kF_1)=(k'/k\kappa^2)\{\kappa^2F_1+[j(j+1)/r^2]u_1\}. \tag{20}$$

If we now use Eqs. (16) and (17) and rearrange Eq. (20), we have

$$u_2''+\left(\frac{2}{r}-\frac{k'}{k}\right)u_2'+\{k^2-\kappa^2-[j(j+1)/r^2]\}u_2=\left(\frac{2}{r}-\frac{k'}{k}-\frac{j(j+1)k'}{\kappa^2r^2k}\right)u_1. \tag{21}$$

Equations (19) and (21), being two simultaneous equations of the second order, would yield a single differential equation of the fourth order if either u_1 or u_2 were eliminated.

By definition, $k=(W+eV)/\hbar c$. If the field is coulombian, $V=ze/r$, where ze is the charge on the source particle. Let $W=wMc^2$. Then, if $r_0=e^2/Mc^2$,

$$k=w(Mc/\hbar)+(ze^2/\hbar cr)=(ze^2/\hbar cr)\{1+(wr/zr_0)\}, \tag{22}$$

$$k'=-ze^2/\hbar cr^2; \quad k'/k=-(1/r)[1+(wr/zr_0)]^{-1}. \tag{23}$$

Solution Near the Origin

The origin is an irregular singular point, which necessitates the introduction of an exponential factor in the formal solution. This factor may be found by the procedure indicated by Ince,[5] which will always give a formal series in terms of the variable $r^{1/N}$, where N is the order of the differential equation. Application of this method leads to the factor $\exp[-aL/r^{\frac{1}{2}}]$, where $L^2=\kappa^{-1}$ and a is to be determined.[6]

Let
$$u_1=\varphi_1\exp[-aL/r^{\frac{1}{2}}] \quad \text{and} \quad u_2=\varphi_2\exp[-aL/r^{\frac{1}{2}}]. \tag{24}$$

Then
$$u'=\left(\varphi'+\frac{La}{2r^{\frac{1}{2}}}\varphi\right)\exp[-aL/r^{\frac{1}{2}}], \tag{25a}$$

$$u''=\left(\varphi''+\frac{aL}{r^{\frac{1}{2}}}\varphi'-\frac{3}{4}\frac{aL}{r^{\frac{3}{2}}}\varphi+\frac{a^2L^2}{4r^3}\varphi\right)\exp[-aL/r^{\frac{1}{2}}]. \tag{25b}$$

Now let
$$q_1=aL/r^{\frac{1}{2}}-(k'/k), \tag{26a}$$

$$q_2=-\frac{3}{4}\frac{aL}{r^{5/2}}+\frac{a^2L^2}{4r^3}+k^2-L^{-4}-\frac{j(j+1)}{r^2}-\frac{k'}{k}\frac{aL}{2r^{\frac{1}{2}}}. \tag{26b}$$

Then, from (19), (21), (25), and (26)
$$\varphi_1''+q_1\varphi_1'+q_2\varphi_1=-(k'/k)(k^2+L^{-4})\varphi_2, \tag{27a}$$

$$\varphi_2''+\left(q_1+\frac{2}{r}\right)\varphi_2'+\left(q_2+\frac{aL}{r^{5/2}}\right)\varphi_2=\left[\frac{2}{r}-\frac{k'}{k}-\frac{j(j+1)L^4k'}{r^2k}\right]\varphi_1. \tag{27b}$$

The formalism is simplified by the substitution $r=s^2$. The differentials transform as follows: $D_r=(1/2s)D_s$ and $D_r^2=(1/4s^2)[D_s^2-(1/s)D_s]$.

If $\omega=w/nr_0$, then $(k'/k)=-(1/r)(1+\omega r)^{-1}$. Expanding,
$$k'/k=-s^{-2}(1-\omega s^2+\omega^2s^4+\cdots) \tag{28}$$

Eqs. (27) become, if primes now denote differentiation with respect to s,
$$\varphi_1''-s^{-1}\varphi_1'+2s(aLs^{-3}+s^{-2}-\omega+\cdots)\varphi_1'+4s^2q_2\varphi_1=4(k^2+L^{-4})(1+\omega s^2)^{-1}\varphi_2, \tag{29a}$$

$$\varphi_2''-s^{-1}\varphi_2'+2s(aLs^{-3}+3s^{-2}-\omega+\cdots)\varphi_2'+4s^2(q_2+aLs^{-5})\varphi_2$$
$$=4s^2[3s^{-2}-\omega+\cdots+j(j+1)L^4s^{-6}(1-\omega s^2+\omega^2s^4-\cdots)]\varphi_1. \tag{29b}$$

These are of the form
$$\varphi_1''+P_1\varphi_1'+P_2\varphi_1=R_1\varphi_2, \tag{30a}$$

$$\varphi_2''+Q_1\varphi_2'+Q_2\varphi_2=R_2\varphi_1, \tag{30b}$$

where
$$\begin{aligned}
&P_1=2aLs^{-2}+s^{-1}-2\omega s+2\omega^2s^3+\cdots,\\
&P_2=a^2L^2s^{-4}-aLs^{-3}+4s^{-2}[n^2\alpha^2-j(j+1)]+\cdots,\\
&Q_1=P_1+(4/s);\quad Q_2=P_2+(4aL/s^3),\\
&R_1=4z^2\alpha^2s^{-4}+4z^2\alpha^2\omega s^{-2}+4L^{-4}(1-\omega s^2+\omega^2s^4-\ \ ),\\
&R_2=(4/s^4)j(j+1)L^4(1-\omega s^2+\omega^2s^4-\cdots)+12-4\omega s^2+\cdots.
\end{aligned} \tag{31}$$

[5] E. L. Ince, *Ordinary Differential Equations* (Longmans Green and Company, London, 1927) pp. 424–428.
[6] The scalar quantity L here and below is not to be confused with the angular momentum vector $\mathbf{L}$ in Eq. (13).

Now write

$$P_1=\sum_{n=0}^{\infty}P_{1,n}s^{n-2},\quad P_2=\sum_{n=0}^{\infty}P_{2,n}s^{n-4},$$
$$Q_1=\sum_{n=0}^{\infty}Q_{1,n}s^{n-2},\quad Q_2=\sum_{n=0}^{\infty}Q_{2,n}s^{n-4},$$
$$R_1=\sum_{n=0}^{\infty}R_{1,n}s^{n-4},\quad R_2=\sum_{n=0}^{\infty}R_{2,n}s^{n-4},\tag{32}$$
$$\varphi_1=\sum_{n=0}^{\infty}\varphi_{1,n}s^{n+\alpha_1},\quad\text{and}\quad\varphi_2=\sum_{n=0}^{\infty}\varphi_{2,n}s^{n+\alpha_2}.$$

For Eqs. (30a) and (30b) to be mutually consistent, since P_2 and R_1 (also Q_2 and R_2) are of the same order in s, we must have $\alpha_1=\alpha_2$. The recursion formulas are then

$$(\alpha_1+n+2)(\alpha_1+n+1)\varphi_{1,n+2}+\textstyle\sum_m P_{1,m}\varphi_{1,n-m+3}(\alpha_1+n-m+3)$$
$$+\textstyle\sum_m P_{2,m}\varphi_{1,n-m+4}=\sum_m R_{1,m}\varphi_{2,n-m+4},\tag{33a}$$
$$(\alpha_1+n+2)(\alpha_1+n+1)\varphi_{2,n+2}+\textstyle\sum_m Q_{1,m}\varphi_{2,n-m+3}(\alpha_1+n-m+3)$$
$$+\textstyle\sum_m Q_{2,m}\varphi_{2,n-m+4}=\sum_m R_{2,m}\varphi_{1,n-m+4}.\tag{33b}$$

The values of the first coefficients are

$$P_{10}=2aL,\quad P_{11}=1,\quad P_{12}=0;\quad P_{20}=a^2L^2,\quad P_{21}=-aL,\quad P_{22}=4[z^2\alpha^2-j(j+1)]=-4\rho^2;$$
$$Q_{1m}=P_{1m},\ m\neq1\quad\text{and}\quad Q_{11}=5;\quad Q_{2m}=P_{2m},\ m\neq1\quad\text{and}\quad Q_{21}=3aL;$$
$$R_{10}=4z^2\alpha^2,\quad R_{12}=4z^2\alpha^2\omega,\quad R_{14}=4L^{-4};\quad R_{20}=4j(j+1)L^4,\quad R_{22}=-4j(j+1)L^4\omega,$$
$$R_{24}=4j(j+1)L^4\omega^2+12.$$

If $n=-4$,

$$P_{20}\varphi_{1,0}=R_{10}\varphi_{20},\quad\text{and}\quad Q_{20}\varphi_{20}=R_{20}\varphi_{10},\tag{34}$$
$$P_{20}Q_{20}=R_{10}R_{20},\tag{35}$$
$$a^4=16z^2\alpha^2j(j+1).\tag{36}$$

If (33a) is multiplied by R_{20}, (33b) by P_{20}, and the two added, the terms in $\varphi_{1,n+4}$ and $\varphi_{2,n+4}$ will cancel out because of (35). We thus obtain, noting that $Q_{11}=P_{11}+4$ and $Q_{21}=P_{21}+4aL$,

$$(\alpha_1+n+2)(\alpha_1+n+1)[R_{20}\varphi_{1,n+2}+P_{20}\varphi_{2,n+2}]+\sum_{m=0}(\alpha_1+n-m+3)(R_{20}\varphi_{1,n-m+3}+P_{20}\varphi_{2,n-m+3})P_{1m}$$
$$+\sum_{m=1}\{(R_{20}\varphi_{1,n-m+4}+P_{20}\varphi_{2,n-m+4})P_{2m}-R_{20}R_{1m}\varphi_{2,n-m+4}-P_{20}R_{2m}\varphi_{1,n-m+4}\}$$
$$+4(\alpha_1+n+2)P_{20}\varphi_{2,n+2}+4cLP_{20}\varphi_{2,n+3}=0.$$

The second and third lines combine to give

$$\sum_{m=0}\varphi_{1,n-m+3}[(\alpha_1+n-m+3)R_{20}P_{1m}+R_{20}P_{2,n+1}-P_{20}R_{2,m+1}]$$
$$+\sum_{m=0}\varphi_{2,n-m+3}[(\alpha_1+n-m+3)P_{20}P_{1m}+P_{20}P_{2,m+1}-R_{20}R_{1,m+1}]$$
$$=[(\alpha_1+n+3)P_{10}+P_{21}][\varphi_{1,n+3}R_{20}+\varphi_{2,n+3}P_{20}]$$
$$+\sum_{m=1}[(\alpha_1+n-m+3)P_{1m}+P_{2,m+1}][\varphi_{1,n-m+3}R_{20}+\varphi_{2,n-m+3}P_{20}]$$
$$-\sum_{m=1}(P_{20}R_{2,m+1}\varphi_{1,n-m+3}+R_{20}R_{1,m+1}\varphi_{2,n-m+3}).$$

If $n=-3$, then with (34) we find

$$4aLP_{20}\varphi_{20}+2P_{20}\varphi_{20}[\alpha_1 P_{10}+P_{21}]=0, \quad \text{or} \quad \alpha_1=-\tfrac{1}{2}.$$

If $n=-2$,

$$\tfrac{3}{4}(R_{20}\varphi_{10}+P_{20}\varphi_{20})-2P_{20}\varphi_{20}+4aLP_{20}\varphi_{21}+2[-\tfrac{1}{2}P_{11}+P_{22}]\varphi_{20}P_{20}-P_{20}R_{22}\varphi_{10}-R_{20}R_{12}\varphi_{20}=0. \quad (37)$$

But $R_{22}=-\omega R_{20}$, $R_{12}=\omega R_{10}$, $R_{22}P_{20}\varphi_{10}=R_{22}R_{10}\varphi_{20}=-\omega R_{20}R_{10}\varphi_{20}$ and so the sum of the last two terms in (37) equals zero.

Consequently

$$\varphi_{21}/\varphi_{20}=\tfrac{1}{2}-2[-\tfrac{1}{2}P_{11}+P_{22}]=(1/4aL)(8\rho^2+\tfrac{3}{2}). \quad (38)$$

If $n=-1$,

$$-\tfrac{1}{2}P_{10}\varphi_{10}+P_{20}\varphi_{11}+P_{21}\varphi_{10}=R_{10}\varphi_{21}=R_{10}\varphi_{20}-(1/4aL)(8\rho^2+\tfrac{3}{2}),$$

$$\frac{\varphi_{11}}{\varphi_{10}}=\frac{1}{4aL}(8\rho^2+\tfrac{3}{2})+\frac{\tfrac{1}{2}P_{10}-P_{21}}{P_{20}}=\frac{1}{4aL}(8\rho^2+\tfrac{3}{2})+\frac{2}{aL}. \quad (39)$$

One can thus obtain all the φ_{2m} and φ_{1m} in terms of φ_{20} (or φ_{10}).

Summarizing,

$$\varphi_1=s^{\frac{1}{2}}\varphi_{10}\left\{1+\left[\frac{1}{4aL}(8\rho^2+\tfrac{3}{2})+\frac{2}{cL}\right]s+\cdots\right\}, \quad (40a)$$

$$\varphi_2=s^{\frac{1}{2}}\varphi_{20}\left\{1+\frac{1}{4aL}(8\rho^2+\tfrac{3}{2})s+\cdots\right\}, \quad (40b)$$

$\varphi_{20}=(a^2L^2/4z^2\alpha^2)\varphi_{10}$, where a is given by (36).

From (16) and (24)

$$F_2=(1/s^2)e^{-aL/s}s^{\frac{1}{2}}\{\varphi_{20}+\varphi_{21}s+\cdots\}, \quad (41)$$

$$F_1=u_1-\frac{1}{2s}\frac{du_2}{ds}=\frac{1}{s^2}e^{-aL/s}s^{\frac{1}{2}}\{\varphi_{10}+\varphi_{11}s+\cdots\}-\frac{1}{2s}\Big[aLs^{-\frac{1}{2}}e^{-aL/s}\{\varphi_{20}+\varphi_{21}s+\cdots\}$$
$$+e^{-aL/s}s^{-\frac{1}{2}}\{\tfrac{1}{2}\varphi_{20}+\tfrac{3}{2}\varphi_{21}s+\cdots\}\Big]. \quad (42)$$

That is, F_2 is of order $r^{-3/4}\exp(-aL/r^{\frac{1}{2}})$ and F_1 of order $r^{-5/4}\exp(-aL/r^{\frac{1}{2}})$ at the origin.[7]

The wave equation then has solutions of the form displayed in Eqs. (13), where F_1 and F_2 are given by Eqs. (42) and (41), respectively, and $s=r^{\frac{1}{2}}$. Equation (17) may be used to compute G.

For the more general case where the field is non-coulombian, one must solve Eqs. (19) and (21), using the appropriate dependence of k on the radius. The procedure is as given in Ince[5] if $k=O(1/r^i)$ as $r\to 0$, where i is an integer, and should not be particularly difficult even if this is not so.

The solutions which we have found above are expressed as power series near the origin, and it is not to be expected that convergence is rapid away from the origin. For practical computations, a knowledge of the solutions for all values of r is desirable. It seems that this is to be attained only with a machine such as the ENIAC or EDVAC, at least if one is concerned with the scattering problem,[8] which usually requires phase shifts to be found for many values of j.

[7] The exponential factor agrees with that found by Tamm, references (2) and (3).

[8] The scattering problem will have a solution if, at large r, one can find a stationary state which is a sum of a plane wave plus an outgoing wave. This question needs further study.

Effect of Pais' "f-Field" on the Symmetry of the Meson Field Part of Nuclear Hamiltonian

P. R. ZILSEL AND J. S. BLAIR
Yale University, New Haven, Connecticut*

AND

J. L. POWELL
University of Wisconsin, Madison Wisconsin*

(Received April 18, 1947)

If an "*f*-interaction" is introduced into the Hamiltonian for two protons, the square well of width e^2/mc^2 representing the specific nuclear proton-proton interaction at low energies must be modified to compensate for the effect of the "*f*-interaction." It is found that the experimental dependence of phase shift on energy for low energy proton-proton *S*-scattering would require the assumption of different well depths for different energies of the incident protons. The necessary changes in the potential would be sufficiently large to destroy the symmetry between the specific nuclear proton-proton and proton-neutron ^1S interactions.

1. INTRODUCTION

THE "*f*-interaction" proposed by Pais[1] in order to overcome some of the divergence difficulties of quantum electrodynamics would add to the coulomb interaction potential between two protons, a term V_f giving:

$$V_{\text{coulomb}}+V_f=(e^2/r)[1-2\exp(-\kappa r/r_0)], \quad (1)$$

where $r_0=e^2/mc^2$, and the range $1/\kappa$ must be about 2 to account for the mass difference between neutron and proton. A more exact evaluation gives[2] $1/\kappa=1.82$.

It has been shown by Breit and collaborators[3–5] that the experimental phase shift *vs.* energy curve for proton-proton scattering at energies between 0.2 and 2.6 Mev is best accounted for by taking the specifically nuclear interaction potential, which must be added to the coulomb repulsion as a square well of width r_0 and depth $D^e=11.35$ Mev, and that this corresponds almost exactly to the square well potential for the ^1S proton-neutron interaction in the same energy range. A preliminary estimate by Breit[2] indicated that the change δD^f in the well depth necessary to compensate for the effect of the "*f*-interaction" on the proton-proton *S*-wave phase shift at low energies would be sufficiently large to destroy the symmetry between the specifically nuclear proton-proton and proton-neutron ^1S interactions. The present work investigates the magnitude of δD^f as a function of E and $1/\kappa$ for $0.2\text{ Mev}\leqq E\leqq 2.6\text{ Mev}$, and $1\leqq 1/\kappa\leqq 3.5$.

2. PROCEDURE AND RESULTS

(a) First-Order Perturbation Estimate of δD^f

A first order perturbation calculation for the phase shift K_0 produced by a perturbing central field potential δV on a radial wave function of relative motion F_0/r gives[6]

$$K_0\cong-\int_0^\infty(\delta V/E')F_0^2d\rho, \quad (2)$$

where E' = energy of relative motion; $\rho=2\pi r/\Lambda$; Λ = wave-length of relative motion. To the approximation of Eq. (2) the phase shift produced by a square well perturbation of a given width is proportional to the depth δD_0 of the perturbation.

For proton energies up to $\sim$3 Mev the effect on the phase shift produced by the omission of the coulomb potential at distances smaller than r_0 can be compensated[2] by changing the well depth by $\delta D^e=-0.83$ Mev. Hence the first-order

* Assisted by Contract N6ori-97, Task I and Contract N6ori-44 Task XVI of the Office of Naval Research.

[1] A. Pais, Phys. Rev. **68**, 227 (1945).

[2] Unpublished calculation by G. Breit.

[3] G. Breit, H. M. Thaxton, and L. Eisenbud, Phys. Rev. **55**, 1018 (1939). Referred to as BTE in the text.

[4] G. Breit, E. U. Condon, and R. D. Present, Phys. Rev. **50**, 825 (1936).

[5] G. Breit and J. R. Stehn, Phys. Rev. **52**, 396 (1937).

[6] H. M. Taylor, Proc. Roy. Soc. **A134**, 103 (1931).

TABLE I. Values of δD_0^f in Mev.

$1/\kappa$	$E=0.2$ Mev	$E=1.4$ Mev	$E=2.6$ Mev
1.0	-1.70 ± 0.1	-1.51 ± 0.02	-1.46 ± 0.01
1.5	$-2.7\ \pm0.3$	$-2.1\ \pm0.1$	$-2.0\ \pm0.1$
2.0	$-3.4\ \pm0.3$	$-2.6\ \pm0.2$	$-2.4\ \pm0.2$
2.5	$-4.0\ \pm0.4$	$-3.0\ \pm0.2$	$-2.7\ \pm0.2$
3.0	$-4.6\ \pm0.3$	$-3.2\ \pm0.2$	$-2.9\ \pm0.2$

estimate δD_0^f of δD^f is

$$\delta D_0^f=-0.83\left[\int_0^\infty 2F_0^2\exp(-\kappa r/r_0)dr/r\right]\Big/\left[\int_0^{r_0}F_0^2dr/r\right]. \quad (3)$$

Here F_0/r is the regular S-wave function for the unperturbed potential

$$V_0(r)=-[D^e+\delta D^e]\cong-10.5\text{ Mev};\quad r<r_0$$
$$=e^2/r;\quad r>r_0.$$

For $r<r_0$, F_0 is a sine wave. For $r>r_0$ two approximations,

$$F_0\sim a+b\rho, \quad (\alpha)$$

$$F_0\sim A\sin(\rho+\delta), \quad (\beta)$$

were used in the evaluation of (3). Except for $E\ll1$ Mev, when $d^2F_0/dr^2>0$ over a considerable region of $r>r_0$, the actual value of F_0 (coulomb function) lies between (α) and (β), which thus give an upper and lower bound for δD_0^f. For low energies (α), and for high energies (β) is the better approximation. Because of the rapid decrease of $\exp(-\kappa r/r_0)$ with r for $r>r_0$, at least for small $1/\kappa$, the inaccuracy introduced by the use of (α) and (β) is small compared with the inaccuracy of the perturbation method itself. Equation (3) gives the following values of δD_0^f: The uncertainties indicated in the table arise because of the use of approximations (α) and (β) instead of the exact coulomb function at $r>r_0$ (cf. appendix).

(b) Phase Shift Calculation for $V=(e^2/r)[1-2\exp(-\kappa r/r_0)]-D^{f+c}{}_{\text{approx}}$ and Improved Estimate of δD^f

In order to improve the estimate of δD^f obtained in (a) for $1/\kappa=2$, the most likely value, phase shifts caused by δV were calculated for the regular solutions of the equation

$$d^2\mathfrak{F}/dr^2+(M/\hbar^2)[E'-e^2/r-\delta V]\mathfrak{F}=0, \quad (4)$$

with

$$\delta V=-2\exp(-2r/r_0)-D^{f+c}{}_{\text{approx}}, \quad (4')$$

for $E=0.4$ and 2.0 Mev. The well $D^{f+c}{}_{\text{approx}}$ is supposed to represent approximately the specific nuclear potential which must be added to the coulomb and "f-interactions" to give the experimental proton-proton scattering phase shifts. It was chosen as

$$D^{f+c}{}_{\text{approx}}=7.8\text{ Mev};\quad r<r_0$$
$$=0;\quad r>r_0.$$

This corresponds to an assumed value of $\delta D^f=7.8-11.35=-3.55$ Mev, which is larger than the values given in Table I, since δD_0^f will, in general, underestimate δD^f in the present case.

The values of $\mathfrak{F}$ were obtained by numerical integration up to $r=3e^2/mc^2$, at which point the phase shifts $K_0(r=3e^2/mc^2)$ were calculated from Eq. (7.8) of Breit, Condon, and Present,[4] the values of the coulomb functions occurring in this equation having been obtained from a table in BTE.[3]

At $r=3e^2/mc^2$ the values of $\mathfrak{F}$ were normalized to $F_0\cos K_0+G_0\sin K_0$ (F_0, G_0=regular and irregular coulomb function, respectively), and the small additional phase shifts δK_0 which were due to the "tail" of the f-field potential beyond $r=3e^2/mc^2$ were estimated by Eq. (2) with $F_0=\mathfrak{F}$, $\delta V=-(2e^2/r)\exp(-2r/r_0)$, the integral having been taken from $r=3e^2/mc^2$ to ∞; two approximations were used for $\mathfrak{F}$, giving upper and lower bounds for δK_0. The perturbation method was used because the quantities entering into the exact equation for the phase shift are not readily available for $r>3e^2/mc^2$. Its use is justified by the smallness of the values of δK_0 obtained (cf. appendix). The additional corrections δD in the well depth required to bring the phase shift calculated by this procedure into agreement with the experimental values were estimated by the first order perturbation formula:

$$K_0(\text{calc.})-K_0(\text{exp})\cong-\int_0^{r_0}(\delta D/E')\mathfrak{F}^2d\rho. \quad (5)$$

One thus obtains corrected values for the well

depth, $D^{f+c}=D^{f+c}_{\text{approx}}+\delta D$, and for $\delta D^f=D^{f+c}-D^c$. The results are summarized in Table II.

(c) Phase Shift Calculation for $V=(e^2/r)[1-2\exp(-\kappa r/r_0)]$ Without Square Well

The results so far obtained show that within the range of values for $1/\kappa$ considered physically admissible, the contribution to the phase shift caused by the "f-interaction" becomes comparable for low energies to the total observed phase shift because of a near resonance of the "f-field" wave functions for large $1/\kappa$. A rough estimate of the value of $1/\kappa$ which at a low energy would give the total observed phase shift from the "f-interaction" alone, without any square well, can be obtained by putting $F_0\cong C_0\rho$ (C_0=normalization constant for regular coulomb function) and then estimating the phase shift, K_0', due to the "f-interaction" by use of Eq. (2), with $\delta V=-2\exp(-\kappa r/r_0)$. For $E=0.2$ Mev, $C_0^2=0.271$, and one has, carrying out the integration,

$$K_0'\cong 0.00735\kappa^{-2}.$$

A factor 4/3 approximately corrects for the fact that the normalization constant C_0 is too low, since the attractive "f-field" potential increases the wave function at small ρ. For $E=0.2$ Mev the experimental value of the phase shift is $K_0=6.8°\cong 0.12$ radians, so that one has finally

$$\kappa^{-2}\cong(0.12/0.00735)(3/4);\quad 1/\kappa\cong 3.5.$$

Calculation, by the method of section (a), of the phase shifts produced by an "f-field" potential with $1/\kappa=3.5$ alone superimposed on the proton-proton coulomb potential for $E=0.2$ Mev and $E=2.0$ Mev gives:

$$1/\kappa=3.5\begin{cases}K_0'=0.1225\pm 0.0065\\ \quad=7.02°\pm 0.37°;\quad E=0.2\text{ Mev}\\ K_0'=0.2790\pm 0.0003\\ \quad=14.82°\pm 0.01°;\quad E=2.0\text{ Mev.}\end{cases}\qquad(6)$$

The indicated uncertainties are again due to the use of approximations for $\mathfrak{F}$ at $r>3e^2/mc^2$. (cf appendix). The experimental values are:

$$K_0\cong 6.8°;\quad E=0.2\text{ Mev}$$
$$K_0\cong 45°;\quad E=2.0\text{ Mev.}$$

TABLE II. Phase shifts and corrected well depths for $1/\kappa=2$.

E (Mev)	K_0*	K_0, experimental (from BTE)	δD (Mev)	D^{f+c} (Mev)	δD^f (Mev)
0.4	0.275 ± 0.001 $\cong 15.8°$	15.2°	−0.17	7.63	−3.72
2.0	0.638 ± 0.000 $\cong 36.55°$	45°	1.12	8.92	−2.43

* Calculated for the solutions of Eq. (4).

3. INTERPRETATION OF THE RESULTS AND CONCLUSIONS

The results show that the phase shift contribution caused by the "f-field" increases much more slowly with energy than the observed proton-proton scattering phase shifts at low energies. For $1/\kappa=3.5$ the total observed phase shift at $E=0.2$ Mev is accounted for by the "f-field," but at $E=2.0$ Mev only 1/3 of the observed phase shift can be attributed to it as is seen from Eq. (6).

If the "f-field" with the lower value of $1/\kappa=2$ is combined with a square well of width e^2/mc^2, the well depth must be reduced from the usual value $D^c=11.35$ Mev by several Mev and must be made velocity dependent to account for the observed phase shifts (Table II). The first-order estimates of δD^f (Table I) are approximately correct for $1/\kappa\leqq 2$, but they fail to show the large increase of the "f-field" phase shift at low energies for larger $1/\kappa$, which is due to a near resonance of the "f-field" wave function. Even for $1/\kappa\leqq 2$ the first-order perturbation values underestimate the "f-field" contribution to the phase shift at low energies. This is due to the fact that Eq. (3) underestimates the contribution of the "tail" of the "f-field" beyond r_0, since the unperturbed wave functions F_0 are concentrated at small ρ because of the large depth of the unperturbed well, $D^c=11.35$ Mev. This "tail" is important at low energies.

In summary, the calculations show that the "f-field" potential would have to be combined with a velocity dependent square well of width e^2/mc^2 to account for the observed proton-proton scattering. The variation of well depth with energy might be avoided by reducing the range of the well and correspondingly increasing its depth. In either case, the symmetry between the specific nuclear proton-proton and proton-

neutron ^1S potentials would have to be abandoned if an "f-interaction" were introduced into the proton-proton potential.

We would like to acknowledge our indebtedness to Professor Breit whose preliminary estimates first indicated the nature of the effects discussed in this paper and who helped with suggestions and discussion throughout the work.

APPENDIX

Remarks on the Use of Approximate Wave Functions in the First-Order Estimates by Eq. (2)

In (a), approximations (α) and (β) for F_0 at $r>r_0$ were used in the evaluation of Eq. (3). These approximations correspond to the replacing of the coulomb repulsion e^2/r in the differential equation for F_0 by a constant potential V_0. The solution for $V_0=E'$ is (α); for $V_0=0$ it is (β). A better approximation for the purpose of evaluating the right side of Eq. (3) would be obtained by letting V_0 have such a value that the effective kinetic energy $E'-V_0$ should approximate the average of the actual kinetic energy, in the region which matters for the integrals which occur in the perturbation formula Eq. (3). This V_0 will be referred to as $\langle e^2/r\rangle$ because $E'-e^2/r$ is the kinetic energy.

If $\delta D_0'(\alpha)$ and $\delta D_0'(\beta)$ are the values obtained by the use of approximations (α) and (β), respectively, a better approximation for $\delta D_0'$ is then obtained by taking their weighted average in the form

$$\delta D_0' \cong \frac{1}{E'}\{\langle e^2/r\rangle \delta D_0'(\alpha)+(E'-\langle e^2/r\rangle)\delta D_0'(\beta)\}.$$

Since about half of the integral from r_0 to ∞ in Eq. (3) is contributed by the region $r_0<r<r_0(1+1/\kappa)$, $e^2/[r_0(1+1/\kappa)]$ gives the right order of magnitude for $\langle e^2/r\rangle$. The values of $\delta D_0'$ given in Table I correspond to using this value. Since the differences $\delta D_0'(\alpha)-\delta D_0'(\beta)$ are no larger than the inaccuracy of the first-order perturbation method itself, the exact value of $\langle e^2/r\rangle$ to be used is not important. The uncertainties indicated in Table I are the smaller of the differences

$$|\delta D_0'-\delta D_0'(\alpha)| \quad \text{and} \quad |\delta D_0'-\delta D_0'(\beta)|$$

in each case.

In (b) and (c) two approximations were used for $\mathfrak{F}$ in the evaluation of $\delta K_0(r>3r_0)$ by Eq. (2): (1) approximate coulomb function, (2) approximate coulomb+"f-field" function.

Parabolic approximations were used, with the coefficient of ρ^2 determined in each case by taking an "average value" of the appropriate potential in the sense explained above. The exact nature of the approximations used is unimportant in this case, since $r^{-1}\exp(-\kappa r/r_0)$ is very small when $r-3r_0$ is sufficiently large for the differences between approximations (1) and (2) to become important.

The contributions to the total calculated phase shifts K_0^* of δK_0^* as compared to K_0^* ($r=3e^2/mc^2$) in Table II are:

E (Mev)	$K_0^*(r=3e^2/mc^2)$	δK_0^*
0.4	0.2068	0.0685 ± 0.0010
2.0	0.6069	0.0313 ± 0.0000

The values of δK_0^* given are the averages of the values obtained by using approximations (1) and (2). The indicated uncertainties are the differences between the averages and these values. They are seen to be negligible.

The Physical Significance of Birkhoff's Gravitational Equations

HERBERT E. IVES
Bell Telephone Laboratories, New York, New York

(Received December 11, 1946)

Birkhoff's gravitational equations are put in terms of dt in place of the local time ds used by him. The transformed equations show that Lorentzian mass has been used, and to the Newtonian attractive force is added a force normal to the direction of motion, v^2/c^2 times the component of the gravitational force normal to the motion.

1. INTRODUCTION

THE theory of gravitation proposed by the late G. D. Birkhoff was developed by him from a very general mathematical standpoint, and the physical significance of the theory is difficult to grasp in the form in which it has been presented. As indicated by the title of his most detailed presentation, "El Concepto Matematico de Tiempo y la Gravitacion,"[1] Birkhoff laid stress on the use of ds (local time) in place of dt (Newtonian time); the "forces" figuring in his development are Minkowski forces instead of physical (Lorentzian) forces. Yet his solution for a planetary orbit (which gives the correct advance of perihelion of Mercury) contains no terms in ds, raising the question whether this result does in fact depend on his adherence to this variable. Actuated by the desire to see what form his "force" equations would take if expressed in terms of dt and ordinary physical force (time rate of change of momentum), I have carried through the necessary transformations, with the results given below which exhibit some features of interest.

2. THEORY

Birkhoff's gravitational force, which is the third term of an expansion which he states[2] "it is natural to set" as typifying "all force vectors," gives, in his hands, for the motion of a particle moving in a plane in the gravitational field of a mass M,

$$\frac{d^2x}{ds^2}=-\frac{GMx}{r^3}-2\frac{GMx}{r^2c^2}\left[\left(\frac{dx}{ds}\right)^2+\left(\frac{dy}{ds}\right)^2\right]+\frac{GM}{r^2c^2}\frac{dx}{ds}\cdot\frac{dr}{ds}, \quad (1)$$

$$\frac{d^2y}{ds^2}=-\frac{GMy}{r^3}-2\frac{GMy}{r^2c^2}\left[\left(\frac{dx}{ds}\right)^2+\left(\frac{dy}{ds}\right)^2\right]+\frac{GM}{r^2c^2}\frac{dy}{ds}\cdot\frac{dr}{ds}, \quad (2)$$

It is these equations that we wish to put in terms of dt. To transform the right-hand side we use the relations

$$ds=dt(1-v^2/c^2)^{\frac{1}{2}}, \quad v^2=\dot{x}^2+\dot{y}^2,$$

where the dots indicate differentiation with respect to t. We note that the left-hand side is the Minkowski force,

$$F_L(1-v^2/c^2)^{-\frac{1}{2}}$$

in which F_L is the Lorentzian force, that is, the time variation of momentum where mass varies with velocity according to the relation

$$m=m_0(1-v^2/c^2)^{-\frac{1}{2}}.$$

We then have

$$(F_L)_x=[-(GMm_0x/r^3)(1+v^2/c^2)+(GMm_0\dot{x}\dot{r}/r^2c^2)](1-v^2/c^2)^{-\frac{1}{2}}, \quad (3)$$

$$(F_L)_y=[-(GMm_0y/r^3)(1+v^2/c^2)+(GMm_0\dot{y}\dot{r}/r^2c^2)](1-v^2/c^2)^{-\frac{1}{2}}. \quad (4)$$

Putting $r\dot{r}=x\dot{x}+y\dot{y}$ we get

$$(F_L)_x=-\frac{GMm_0}{r^2}\left[\frac{x}{r}+\dot{y}\frac{(\dot{y}x-\dot{x}y)}{rc^2}\right](1-v^2/c^2)^{-\frac{1}{2}}, \quad (5)$$

[1] G. D. Birkhoff, Boletin de la Sociedad Matematica Mexicana 1, 1 (1944).
[2] A. Barajas, G. D. Birkhoff, C. Graef and M. S. Vallarta, Phys. Rev. 66, 142 (1944).

$$(F_L)_y=-\frac{GMm_0}{r^2}\left[\frac{y}{r}-\dot{x}\frac{(\dot{y}x-\dot{x}y)}{rc^2}\right](1-v^2/c^2)^{-\frac{1}{2}}. \quad (6)$$

Comparing these with the Newtonian forces

$$F_x=-GMm_0x/r^3, \quad (7)$$

$$F_y=-GMm_0y/r^3, \quad (8)$$

it appears that the Birkhoff equations differ in the use of the Lorentzian mass, and the addition of terms in $(\dot{y}x-\dot{x}y)$.

It is instructive to put these equations in polar coordinates through the relations

$$\dot{y}x-\dot{x}y=r^2\dot{\theta}$$

and

$$F_R=(F_xx+F_yy)/r, \quad F_\theta=(-F_xy+F_yx)/r$$

used on the right-hand side, using on the left the statement of the Lorentzian force as given by Eddington,[3] yielding

$$m_0\Big\{(\ddot{r}-r\dot{\theta}^2)[1-(\dot{r}^2+r^2\dot{\theta}^2)/c^2]^{-\frac{1}{2}} +\dot{r}\frac{d}{dt}[1-(\dot{r}^2+r^2\dot{\theta}^2)/c^2]^{-\frac{1}{2}}\Big\} =-(GMm_0/r^2)(1+r^2\dot{\theta}^2/c^2) \times[1-(\dot{r}^2+r^2\dot{\theta}^2)/c^2]^{-\frac{1}{2}}, \quad (9)$$

$$m_0\Big\{(2\dot{r}\dot{\theta}+r\ddot{\theta})[1-(\dot{r}^2+r^2\dot{\theta}^2)/c^2]^{-\frac{1}{2}} +r\dot{\theta}\frac{d}{dt}[1-(\dot{r}^2+r^2\dot{\theta}^2)/c^2]^{-\frac{1}{2}}\Big\} =(GMm_0/r^2)(\dot{r}r\dot{\theta}/c^2) \times[1-(\dot{r}^2+r^2\dot{\theta}^2)/c^2]^{-\frac{1}{2}}. \quad (10)$$

These equations are solved by multiplying (9) by $\dot{r}$, and (10) by $r\dot{\theta}$, and adding, which gives

$$\frac{\frac{d}{dt}[1-(\dot{r}^2+r^2\dot{\theta}^2)/c^2]}{[1-(\dot{r}^2+r^2\dot{\theta}^2)/c^2]}=\frac{2GM\dot{r}}{r^2c^2} \quad (11)$$

from which

$$[1-(\dot{r}^2+r^2\dot{\theta}^2)/c^2]=\exp[-(2GM/rc^2)+k]. \quad (12)$$

[3] A. S. Eddington, Phil. Mag. [6] **34**, 321 (1917).

Using this result in (10) gives the areal constant

$$r^2\dot{\theta}=h\exp[-(2GM/rc^2)+k], \quad (13)$$

leading to the solution, replacing r by $1/u$

$$\frac{d^2u}{d\theta^2}+u=(c^2/h^2)[\exp(k+2GMu/c^2)-1] \times\exp(k+2GMu/c^2) \quad (14)$$

which is identically Birkhoff's expression, from which the advance of perihelion of Mercury is correctly indicated.

Equations (9) and (10) may be put in simpler, although less instructive form, by inserting the value of $[1-(\dot{r}^2+r^2\dot{\theta}^2)/c^2]^{\frac{1}{2}}$ from (12), giving

$$\ddot{r}-r\dot{\theta}^2=-\frac{GM}{r^2}\left[1-\frac{\dot{r}^2-r^2\dot{\theta}^2}{c^2}\right], \quad (15)$$

$$d(r^2\dot{\theta})/dt=2GM\dot{r}\dot{\theta}/c^2. \quad (16)$$

These are identically the expressions given by Fernández[4] who also puts his equations in terms of dt instead of ds, in discussing the problem of two bodies in Birkhoff's theory.

3. DISCUSSION

Examination of (9) and (10) shows that Birkhoff's equations for a planetary orbit are the equations which one would obtain by using Lorentzian masses throughout in place of the invariant masses of the simple Newtonian theory, *with the addition* of terms in $\dot{r}$, $r\dot{\theta}^2$, and c^2 on the gravitational side of the equations.

First consider the appearance of the Lorentzian masses. Birkhoff in his presentation lays great stress on the use of *local time*. The idea that a planet is controlled in its course by the time indicated on a clock carried on it lacks substantiality. Physically, forces act on masses. Actually the factor by which local time is distinguished from absolute time is the "contraction factor," $(1-v^2/c^2)^{\frac{1}{2}}$. Now this is also the factor, appropriately placed, by which *local mass* is distinguished from stationary mass. Our transformed equations are force equations in terms of Lorentzian local mass. Hence although Birkhoff

[4] C. G. Fernández, Boletin de la Sociedad Matematica Mexicana **1**, 25 (1944), especially p. 36.

talks of local time as the significant factor, he is really stressing the importance of the contraction factor,[5] and his development could just as well, but with real physical significance, be founded on local mass.

Next consider the added terms on the right in Eqs. (5) and (6). Their characteristic is that when multiplied respectively by $\dot{x}$ and $\dot{y}$ and added they cancel exactly, leaving us with the simple Lorentzian Eq. (11) which may be written

$$-\frac{1}{2}m_0\frac{\frac{d}{dt}(1-v^2/c^2)}{(1-v^2/c^2)^{\frac{1}{2}}}+\frac{GMm_0}{r^2c^2(1-v^2/c^2)^{\frac{1}{2}}}=0.$$

This equation states that the sum of the derivatives of kinetic and potential energies is zero which may be accepted as a fundamental requirement. An infinite number of such additional terms could be set down, which cancelling out, would leave the energy equation unchanged. Any term of this sort has, however, the result of changing the value of $r^2\dot{\theta}$, which is obtained by integration of the second of the equations in polar coordinates (10), alone. The *whole difference* between the Birkhoff solution (14) and the simple Lorentzian solution comes about from the value of $r^2\dot{\theta}$, the "areal constant," which occurs (squared) in the denominator of (14), the numerator having always the same fixed value determined by (12). The terms added by Birkhoff in his force equations change this from

$$r^2\dot{\theta}=h\exp[\tfrac{1}{2}k-GM/rc^2],$$

the Lorentzian value, to

$$r^2\dot{\theta}=h\exp[k-2GM/rc^2],$$

thereby changing the predicted advance of perihelion from $\frac{1}{3}$, the value obtained from the Newton-Lorentz solution, to the full observed value. The prediction of these particular added terms is, in the light of this analysis, the key contribution of Birkhoff's theory.

Let us study these added terms more in detail. They are completely described by the following

[5] The contraction factors are the coefficients of mass, length, and clock rate, which are demanded to insure the conservation of energy and momentum in radiation-matter interactions. Cf. H. E. Ives, Phil. Mag. [7] **36**, 392 (1945).

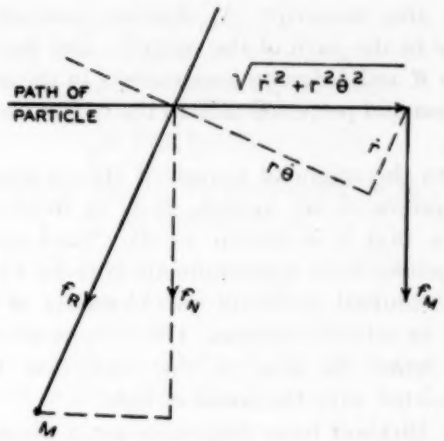

FIG. 1. Resolution of the force on a particle.

statement: *A particle in motion in a gravitational field experiences an additional force, normal to the direction of motion, of value v^2/c^2 times the component of the gravitational force normal to the direction of motion.*

The proof of this theorem is exhibited in the accompanying Fig. 1, in which

f_N = gravitational force normal to direction of motion—

$$f_R r\dot{\theta}(\dot{r}^2+r^2\dot{\theta}^2)^{-\frac{1}{2}};$$

f_M = force due to motion, normal to direction of motion—

$$f_N v^2/c^2=f_R(r\dot{\theta}/c^2)(\dot{r}^2+r^2\dot{\theta}^2)^{\frac{1}{2}}.$$

The component of added force in the radial direction is

$$f_M r\dot{\theta}(\dot{r}^2+r^2\dot{\theta}^2)^{-\frac{1}{2}}=f_R r^2\dot{\theta}^2/c^2,$$

and the component of added force in the direction normal to the radius is

$$-f_M\dot{r}(\dot{r}^2+r^2\dot{\theta}^2)^{-\frac{1}{2}}=-f_R\dot{r}r\dot{\theta}/c^2.$$

Putting $-(GMm_0/r^2)[1-(\dot{r}^2+r^2\dot{\theta}^2)/c^2]^{-\frac{1}{2}}$ for f_R we get the added terms in (9) and (10).

Denoting the Lorentzian forces (time variation of momentum, mass varying with velocity) by F_L, and the Newton-Lorentz gravitational force $-(GMm_0/r^2)[1-(\dot{r}^2+r^2\dot{\theta}^2)/c^2]^{-\frac{1}{2}}$ by G_L, the Birkhoff gravitational equations for a planetary orbit may be concisely expressed as follows

$$(F_L)_R=[G_L+(G_L)_N v^2/c^2]_R, \qquad (17)$$

$$(F_L)_\theta=[G_L+(G_L)_N v^2/c^2]_\theta, \qquad (18)$$

where the subscript N denotes components normal to the path of the particle, and the subscripts R and θ denote components in the radial direction and perpendicular to the radius, respectively.

As to the origin or nature of this transverse force produced by motion, it is of interest to observe that it is similar to the "fundamental law" proposed in a posthumous note by Gauss[6] for the mutual action of two elements of electricity in relative motion. The occurrence of c^2 stems from the idea of the attraction being transmitted with the speed of light.

The Birkhoff force equations for a planetary orbit can be summarized, according to this analysis, as follows: They are the equations one would obtain from a Newtonian attractive force acting on the Lorentzian local mass of the planet, with the addition of forces caused by motion, transverse to the path of the planet, which do not affect the conservation of energy but alter the areal constant. The precise value of these added forces and the method of obtaining them is thus of crucial importance. Apparently these forces are not introduced by Birkhoff with conscious resort to physical concepts, but they are present because of his choice for gravity of the third term[2] of a formal expansion in rational and integral components of a typical force function, in which successive terms are of increasing complexity and hence provide for additional force components. An independent physical derivation of these transverse forces would be welcome.

[6] C. F. Gauss, *Werke* (Göttingen, 1863–74), Vol. 5, p. 616.

PHYSICAL REVIEW VOLUME 72, NUMBER 3 AUGUST 1, 1947

Refraction of Plane Non-Uniform Electromagnetic Waves between Absorbing Media

L. PINCHERLE
King's College, University of London, London, England
(Received August 6, 1946)

When a plane non-uniform electromagnetic wave is refracted between two conducting media, there are two possible positions for the propagation vector in the second medium. Consideration of the energy flow shows that each solution holds within a certain range of values of the (complex) angle of incidence, the transition from one to the other occurring in a discontinuous way. The two cases of the electric vector perpendicular and parallel to the plane of incidence are discussed.

(1) INTRODUCTION

THE problem of the refraction of a plane non-uniform electromagnetic wave at the plane boundary between two conducting media is not generally fully discussed in textbooks where it is pointed out that, with the use of complex angles of incidence and refraction and of complex propagation vectors, the problem is formally identical to the usual one in which perfect dielectrics are involved.[1]

It is the purpose of this paper to complete this treatment discussing the new physical features which appear when both media are conducting, in particular, a discontinuity occurring in the (complex) propagation vector in the second medium at the (complex) angle of incidence for which there is no average flow of energy across the boundary.

[1] See, for instance, J. A. Stratton, *Electromagnetic Theory* (McGraw-Hill Book Company, Inc., New York, 1941), pp. 500–524.

(2) THE PROPAGATION VECTOR IN THE SECOND MEDIUM

Let the boundary be the plane $y-z$, and the plane of incidence the plane $x-z$, the x-axis being directed from the first medium into the second. Let any field component be represented by

$$Ee^{-\mathbf{k}_1\cdot\mathbf{r}+i\omega t} \tag{1}$$

with

$$\mathbf{k}_1=\mathbf{a}+i\mathbf{b}; \quad \mathbf{k}_2=\mathbf{A}+i\mathbf{B}, \tag{2}$$

E being a complex amplitude.

Given $\mathbf{k}_1$ and the constants of the second medium, $\mathbf{k}_2$ is determined by:

(a) The relations holding generally for non-uniform waves[2]

$$k_2^2 = A^2 - B^2 + 2i\mathbf{A}\cdot\mathbf{B} = \omega^2\mu\epsilon_2 + i\omega\mu\sigma_2, \quad (3)$$

where all letters have their usual meaning, and μ will be assumed to be the same for both media;

(b) The boundary conditions, which give (Snell's law):

$$k_1 \sin\theta_1 = k_2 \sin\theta_2, \quad (4)$$

θ_1, θ_2 being the (complex) angles of incidence and refraction. Equation (4) is equivalent to the two relations between real quantities:

$$a_z = A_z; \quad b_z = B_z: \quad (5)$$

a_z and b_z can be expressed as functions of the constants of the first medium and of θ_1; it is convenient in the following to consider them as the independent variables in terms of which to express the propagation vector in the second medium.

Conditions (3) and (5) are not sufficient to determine this vector in a unique way. In fact, if

$$2A_zB_z = 2a_zb_z > \omega\mu\sigma_2, \quad (6)$$

the product A_zB_z is negative, but, without consideration of the energy flow, we cannot immediately decide which of the two factors is negative. Only when A_zB_z is positive, physical reasons will immediately rule out the solution with both quantities negative. Even in the case of perfect dielectrics it is possible formally to construct a second solution for the field in the second medium, satisfying Maxwell's equations and the boundary conditions and corresponding to a "refracted wave" moving towards the boundary and on the same side of the normal as the incident wave: this solution is absurd from a physical point of view. It is an example of the striking way in which the presence of a conductivity in both media modifies these phenomena, that in our case a decision between the two possible solutions is not so immediate, and that, as we shall see, the requirement that the energy should flow from medium 1 to medium 2 leads to the necessity of choosing one solution within a certain range of the complex angle of incidence and the other within another range, the transition occurring in a discontinuous way.

[2] See, for instance, J. A. Stratton, reference 1, p. 341.

(3) THE ENERGY FLOW

(a) Electric vector Perpendicular to the Plane of Incidence ($E_\perp$)

If E, E', E'' are the complex amplitudes of the electric vector in the incident, reflected, and transmitted waves, respectively, the average flow of energy perpendicular to the boundary in the first medium is given by:

$$\langle S_x^{(1)}\rangle_{Av} = Re(\tfrac{1}{2}E_yH_z^*)$$
$$= (e^{-2a_zz}/2\mu\omega)[\,|E|^2b_xe^{-2a_xx} - |E'|^2b_xe^{2a_xx}$$
$$-2a_x|E||E'|\sin(2b_xx+\gamma)], \quad (x<0) \quad (7)$$

with

$$\gamma = \arg(E'/E). \quad (8)$$

The first two terms may be interpreted as the energy flow associated with the incident and reflected waves, respectively. The third term,[3] which vanishes for $\sigma_1 = 0$, is caused by interference between the incident and reflected waves: there is a local radiation from the maxima to the minima of the standing waves system.

The average flow of energy perpendicular to the boundary in the second medium is:

$$\langle S_x^{(2)}\rangle_{Av} = (1/2\mu\omega)e^{-2(A_xx+A_zz)}|E''|^2B_x, \quad (x>0) \quad (9)$$

so that the condition that S_x be continuous at $x=0$ is expressed by:

$$b_x[1-|E'/E|^2] - 2a_xIm(E'/E) = B_x|E''/E|^2. \quad (10)$$

This condition is automatically satisfied by the expressions for E' and E'', whatever the sign of B_x; however the physical conditions of our problem impose that the energy flow be directed from medium 1 to medium 2, therefore the additional relation for the unique determination of $\mathbf{k}_2$ is in this case

$$B_x \geqslant 0. \quad (11)$$

[3] M. Born and E. Ladenburg, Physik Zeits. 12, 198 (1911).

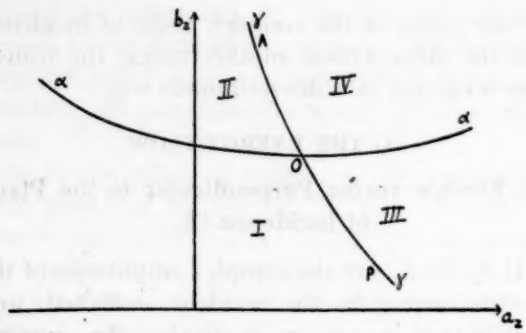

FIG. 1. E perpendicular to the plane of incidence. Discontinuity along AO.

(b) Electric Vector in the Plane of Incidence (E_{11})

In this case the condition of continuity of S_x at the boundary gives, if we indicate by H, H', H'', the amplitudes of the magnetic vector in the incident, reflected, and transmitted waves, respectively:

$$\frac{a_x\sigma_1+b_x\epsilon_1\omega}{\sigma_1^2+\epsilon_1^2\omega^2}(|H|^2+|H'|^2) +2\frac{b_x\sigma_1-a_x\epsilon_1\omega}{\sigma_1^2+\epsilon_1^2\omega^2}|H|\,|H'|\sin\gamma =\frac{A_x\sigma_2+B_x\epsilon_2\omega}{\sigma_2^2+\epsilon_2^2\omega^2}|H''|^2$$

$$\text{with} \qquad \gamma=\arg(H'/H), \tag{12}$$

and the condition that the energy must flow in the right direction is expressed by

$$A_x\sigma_2+B_x\omega\epsilon_2\geqslant 0. \tag{13}$$

(4) THE DISCONTINUITY FOR THE CASE $E_\perp$

Writing explicitly the equations determining A_x and B_x (see (3) and (5)):

$$B_x^2-A_x^2=\epsilon_2\mu\omega^2-b_x^2+a_x^2, \tag{14}$$

$$2A_xB_x=\sigma_2\mu\omega-2b_xa_x, \tag{15}$$

we see that either A_x or B_x is zero when

$$2a_xb_x=\sigma_2\mu\omega, \tag{16}$$

and that, when (16) is satisfied:

$$\begin{aligned} &B_x \text{ is zero if } b_x^2\geqslant\epsilon_2\mu\omega^2+a_x^2, \\ &A_x \text{ is zero if } b_x^2\leqslant\epsilon_2\mu\omega^2+a_x^2. \end{aligned} \tag{17}$$

In the case of small conductivities ($\sigma\ll\epsilon\omega$)

$$b_x\to(\epsilon_1\mu)^{\frac{1}{2}}\omega\sin\varphi_1, \tag{18}$$

φ_1 being the real angle of incidence, and $a_x\to 0$, so that Eq. (17) becomes

$$\sin\varphi_1\gtrless n, \quad \text{with} \quad n=(\epsilon_2/\epsilon_1)^{\frac{1}{2}}. \tag{19}$$

Although the notion of critical angle loses all meaning in the case of conducting media, we shall for brevity say that, when (16) is satisfied, B_x vanishes in the region of total reflection, and A_x in the region of ordinary refraction.

If now we plot the curves (Fig. 1)

$$b_x^2-a_x^2=\epsilon_2\mu\omega^2 \quad (\text{line } \alpha), \tag{20}$$

$$2a_xb_x=\mu\omega\sigma_2 \quad (\text{line } \gamma), \tag{21}$$

and divide the plane a_xb_x into four regions (no loss of generality is entailed in excluding negative values of b_x), B_x vanishes on the boundary between regions II and IV, and A_x on the boundary between I and III. The product A_xB_x is negative in regions III and IV. As B_x must always be positive (Eq. 11), and no change of sign of either factor occurs in crossing line α (Eq. 14), it follows that A_x is positive everywhere left and negative everywhere right of line γ. In the region of ordinary refraction the transition from positive to negative A_x occurs continuously, passing through $A_x=0$, but in the region of total reflection A_x does not vanish on line γ; therefore it must be there discontinuous. Indeed it jumps from the value $+(b_x^2-a_x^2-\epsilon_2\mu\omega^2]^{\frac{1}{2}}$ on the left to the value $-[b_x^2-a_x^2-\epsilon_2\mu\omega^2]^{\frac{1}{2}}$ on the right—namely, the planes of equal amplitude in the second medium, perpendicular to $\mathbf{A}$, have, on the two sides of the discontinuity, symmetrical positions with respect to the boundary.

To the two different orientations of $\mathbf{k}_2$ correspond different expressions for the field components, and also for these the transition from one set of values to the other occurs discontinuously when $B_x=0$. Experimental verification of these considerations could be better obtained by investigation of this last phenomenon.

A negative value of A_x means that the amplitude increases exponentially for $x\to\infty$; but in an actual case the cross section of the beam is not infinite, and then the amplitude decreases in penetrating into the second medium, as follows from $\mathbf{A}\cdot\mathbf{B}>0$.

A difficulty arises from the fact that at the discontinuity ($B_x=0$) there is no average flow

of energy across the boundary, and it is not apparent how the field in the second (dissipative) medium can be maintained. This difficulty is removed when a beam of finite cross section is considered, for then edge effects allow for some energy crossing the boundary even when $B_z=0$.[4]

(5) THE DISCONTINUITY FOR THE CASE $E_{\parallel}$

In this case the energy condition is:

$$(\sigma_2/\omega\epsilon_2)A_z+B_z\gtrless 0. \tag{22}$$

The presence of A_z in this expression is caused by the fact that, when the electric vector is in the plane of incidence, the Poynting vector, for a non-uniform wave, is not parallel to **B** (is not perpendicular to the planes of equal phase). In this case we have thus the possibility of B_z being negative, provided $\langle S_z^{(2)}\rangle_{Av}\gtrless 0$.

Taking the equality sign in (22), and eliminating A_z, B_z from (14), (15), (22), we obtain the pairs of values of a_z and b_z for which the flow of energy across the boundary vanishes, and for which we can consequently expect a transition from one solution for A_z, B_z to the other with reversed signs. We obtain:

$$b_z^2-a_z^2+\left[\frac{\sigma_2}{\omega\epsilon_2}-\frac{\omega\epsilon_2}{\sigma_2}\right]a_zb_z=\tfrac{1}{2}\epsilon_2\mu\omega^2\left[1+\frac{\sigma_2^2}{\epsilon_2^2\omega^2}\right]. \tag{23}$$

If $\sigma_2<\epsilon_2\omega$, Eq. (23), is represented by a line such as line β in Fig. 2, where lines α and γ are the same as in Fig. 1. As before, the product A_zB_z is negative only right of the line γ; thus, since the three hyperbolae meet at 0, the important part of curve β is only that in the region of total reflection; the remaining part corresponds to a spurious solution. A_z, as before, vanishes along OP, and is negative right of BOP. B_z vanishes along AO and now becomes negative in the region AOB. Along curve β, where the average flow of energy across the boundary vanishes, we must pass from one solution to the other; there is thus a discontinuous transition from (substituting (22) in (15)):

$$\begin{aligned} B_z&=[(\sigma_2/2\omega\epsilon_2)(2a_zb_z-\mu\omega\sigma_2)]^{\frac{1}{2}},\\ A_z&=-[(\omega\epsilon_2/2\sigma_2)(2a_zb_z-\mu\omega\sigma_2)]^{\frac{1}{2}} \end{aligned} \tag{24}$$

to the solution with opposite signs.

[4] J. Picht, Ann. d. Physik **3**, 433 (1929); F. Noether, Ann. d. Physik **11**, 141 (1931).

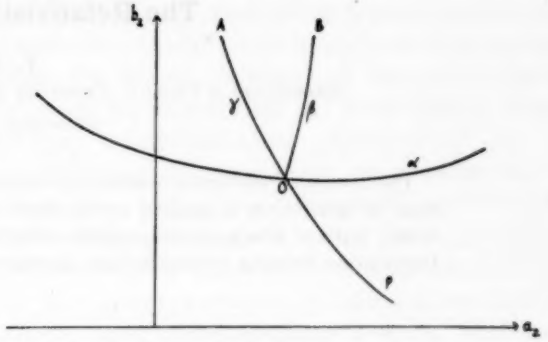

FIG. 2. E parallel to the plane of incidence. Discontinuity along BO.

Particular cases, and the relative position of the three hyperbolae for different values of the parameters, are easily discussed.

(6) USE OF THE REAL ANGLES OF INCIDENCE AS INDEPENDENT PARAMETERS

An alternative formulation of the above treatment may be given assuming as independent variables, instead of a_z and b_z, the real angles φ_1, ψ_1 that the normals to the planes of equal phase and of equal amplitude, respectively, make with the positive x-axis in the first medium. Formulae become then more expressive. Thus Eq. (21) representing the condition for the changing of sign of the product A_zB_z becomes

$$\cot\varphi_1\cot\psi_1=(\sigma_1/\sigma_2)-1, \tag{25}$$

and the condition for the polarizing angle, which makes $H'=0$ in the case $E_{\parallel}$ may be expressed as

$$\cot\varphi_1\cot\psi_2+\cot\varphi_2\cot\psi_1=2, \tag{26}$$

φ_2, ψ_2 being the angles corresponding to φ_1 and ψ_1 in the second medium.

An experimental arrangement for the verification of the above theory would consist of a prism (large with respect to the wave-length) made of the material of medium 1, and bounded on the second face by medium 2. By varying the angle of incidence on the first face, and the angle of the prism, all values of φ_1 and ψ_1 can be obtained. Such an experiment may provide a new method for the determination of conductivities.

The Relativistic Clock Problem

E. L. HILL
Department of Physics, University of Minnesota, Minneapolis, Minnesota
(Received April 18, 1947)

The theory of uniformly accelerated motions based on the conformal group of transformations in space-time is applied to the clock problem of relativity theory. Two solutions are found, both of which are at variance with the usual theory. The bearing of the problem on the relation between mechanics and electromagnetic theory is discussed briefly.

1. INTRODUCTION

ONE of the most interesting problems furnishing a link between the special and the general theory of relativity is the so-called *clock paradox*. This was first introduced into relativity theory by Einstein[1] and has since been discussed many times in the literature; for present purposes we may take the easily accessible treatment of Tolman[2] as standard. The interest in the problem centers around the fact that it leads to Einstein's important relation between gravitational potential and the rate of an ideal clock.

In the problem as ordinarily stated,[2] two identical clocks are initially in coincidence and at rest in the laboratory system, and it is assumed that their readings have been adjusted and their rates synchronized. One of the clocks, B, is then given a strong acceleration for a short time, which brings it quickly up to a velocity u with respect to clock A, while the latter remains at rest in the laboratory system. Clock B continues to move with this velocity for a long time, after which it is given a further strong acceleration which reverses its motion and returns it towards A with the velocity $-u$. Just before reaching the latter, B is decelerated in such a manner as to bring it into coincidence and relative rest with respect to A. The readings of the two clocks are then compared. According to the usual theory, the elapsed time intervals, as measured by the two clocks, are related by the equation

$$\Delta t_A = \Delta t_B(1+u^2/2c^2), \qquad (1)$$

to terms in $(u/c)^2$. The elapsed time, as read by the moving clock is thus *less* than that recorded by the stationary clock. The apparent paradox arising from taking the local-system of clock B as a standard of rest, in which A is then supposed to perform the contrary motion to that sketched above, is explained as an effect equivalent to that of the gravitational field which can be used to provide the apparent acceleration of clock A in the local-system of B.

A variant of the problem, in which the clocks are not required to be at relative rest when in coincidence, has been discussed by Møller.[3] Apart from the clock problem itself, for which he appears to concur in the result of the usual theory, Møller takes the occasion to discuss the problem of determining transformations between reference systems in uniform acceleration and, in fact, for even more general motions. We shall return to this aspect of Møller's discussion later in this paper.

Despite the fact that in its kinematical aspects the problem appears to be entirely symmetrical between the two clocks, Einstein's theory introduces a dissimilarity between them by the assumption that one of them is in an inertial system; the local-system of the other clock then cannot be an inertial system. However, the persistent difficulty is that there is no *a priori* way of making a decision as to which, if either, of the two clocks is in an inertial system. Its resolution in the relativistic argument appears to be quite as arbitrary as is the corresponding assumption in Newtonian mechanics.

It has been shown in previous work[4] that one can introduce uniformly accelerated reference systems into relativity theory by employing the conformal group of transformations C_4 in space-

[1] A. Einstein, Ann. d. Physik [4] 35, **898** (1911).
[2] R. C. Tolman, *Relativity, Thermodynamics and Cosmology* (Oxford University Press, New York, 1934), p. 192.
[3] C. Møller, Det. Kgl. Danske Videnskabernes Selskab, Matematisk-Fysiske Meddelelser, Bind XX, Nr. 19 (1943).
[4] E. L. Hill, Phys. Rev. **67**, 358 (1945); **72**, 143 (1947).

time, as a generalization of the Lorentz group L_4, which establishes transformations between systems in uniform relative motion. It is the purpose in the present paper to discuss the application of this theory to the clock problem; in this way we shall be able to lift one of the deficiencies of the current theory by establishing explicitly the transformations between the local-systems of the two clocks and so can make the kinematical treatment symmetrical between them. However, as the theory is kinematical in character, and makes no direct appeal to mechanical principles, we can draw no particular conclusions concerning the *causes* of the apparent motions of the clocks, nor can we infer any relationship to any particular type of force field such as gravitation.[5]

Our treatment will be limited to the case in which either of the clocks appears to perform a linear uniformly accelerated motion in the local-system of the other. If the clocks have *two* coincidences, they are then not at relative rest at either coincidence. An important point in the analysis must then be the method of establishing a comparison of the natural rates of the two clocks. We shall require that the rate at which either of the clocks appears to run in the local-system of the other, at the instant at which it comes to rest in that system, agrees with the rates of other neighboring clocks which are permanently at rest and synchronized in that system. The possibility of establishing extended covering times in the local-systems of *both* clocks, despite the inherent uncertainty as to whether either system is inertial in a mechanical sense, is founded on an appeal to the known form invariance of the electromagnetic field equations under C_4; if such a covering time can be established in *either* system by purely optical means, it can be established in *both*.

2. THE SUBGROUP OF THE CLOCK PROBLEM

Our first task is to abstract from the full group, C_4, that subgroup which describes the type of motion appropriate to our version of the problem. This can be built up from a translation, a uniform velocity, and a uniform acceleration along the x-axis. A study of the commutator table[4] of C_4 shows that we must adjoin three further transformations, representing (a) a translation of the time origin, (b) a dilatation in space-time, and (c) a "red-shift" transformation.[6] This gives us, in total, a 6-parameter subgroup of C_4. However, the two translations can be eliminated at once by taking as our fundamental particle representing a clock, that one which corresponds to the origin of coordinates in space-time; the moving clock will then cross the origin of coordinates at the zero of local-time, moving along the x-axis, and the clocks will be at the origins of space-coordinates in their respective local-systems. By including translations we should merely shift to other points representing the clocks.

The general transformation of this type has the subsidiary differential equations[7]

$$\begin{aligned} dx/d\mu &= -\tau\rho_1-\tfrac{1}{2}(\tau^2+x^2-y^2-z^2)\rho_2-x\tau\rho_3+x,\\ dy/d\mu &= y(-x\rho_2-\tau\rho_3+1),\\ dz/d\mu &= z(-x\rho_2-\tau\rho_3+1),\\ d\tau/d\mu &= -x\rho_1-x\tau\rho_2-\tfrac{1}{2}(\tau^2+x^2+y^2+z^2)\rho_3+\tau. \end{aligned} \tag{2}$$

For notation, we let (x_0, y_0, z_0, and τ_0) be the space-time coordinates in the local-system S_B of clock B, while (x, y, z, and τ) are those for the local-system S_A of A. We have now to establish the relationship between these sets of coordinates by integration of Eqs. (2), with adjustment of the constants to suit the conditions of the prescribed motion.

We start by considering only those points which move along the common x-axis of the two systems. On setting $y=z=0$ in Eqs. (2) we obtain

$$\begin{aligned} d(\tau+x)/d\mu &= (\tau+x)(1-\rho_1)-\tfrac{1}{2}(\tau+x)^2(\rho_2+\rho_3),\\ d(\tau-x)/d\mu &= (\tau-x)(1+\rho_1)+\tfrac{1}{2}(\tau-x)^2(\rho_2-\rho_3), \end{aligned}$$

[5] Even should one bring in considerations concerning an external force field, it does not appear mandatory that it be interpreted as a gravitational field; the invariance of the Maxwell-Lorentz field equations suggests a formal interpretation in terms of electromagnetic fields.

[6] E. L. Hill, Phys. Rev. **68**, 232L (1945).

[7] For comparison with the notation of reference 4, we have the correspondence

$$\rho_1\mu\rightarrow\alpha_8/c,\quad \rho_2\mu\rightarrow\alpha_{11}/c^2,\quad \rho_3\mu\rightarrow\alpha_{14}/c,\quad \mu\rightarrow\alpha_{15}.$$

The theory of the differential equations involved in the integration of a continuous group can be found in the books by J. E. Campbell, *Theory of Continuous Groups* (Oxford University Press, New York, 1903), p. 47; L. P. Eisenhart, *Continuous Groups of Transformations* (Princeton University Press, Princeton, New Jersey, 1933), Chapter 1.

and by integration we obtain the transformation equations for this class of points in the form

$$y=z=0,$$

$$\tau+x=\frac{(1-\rho_1)(\tau_0+x_0)}{(1-\rho_1)e^{-(1-\rho_1)\mu}+\frac{1}{2}(\rho_2+\rho_3)(\tau_0+x_0)[1-e^{-(1-\rho_1)\mu}]},$$

$$\tau-x=\frac{(1+\rho_1)(\tau_0-x_0)}{(1+\rho_1)e^{-(1+\rho_1)\mu}-\frac{1}{2}(\rho_2-\rho_3)(\tau_0-x_0)[1-e^{-(1+\rho_1)\mu}]}.$$

To find the trajectory of the point representing the moving clock, B, in the local-system of clock A, we set $x_0=0$ and eliminate τ_0. This yields the equation

$$(x+\omega^{-1}e^{\mu}\cosh\rho_1\mu)^2-(\tau-\omega^{-1}e^{\mu}\sinh\rho_1\mu)^2=(e^{\mu}/\omega)^2,$$

where

$$\omega=\frac{\rho_2-\rho_3}{2(1+\rho_1)}[1-e^{(1+\rho_1)\mu}]+\frac{\rho_2+\rho_3}{2(1-\rho_1)}[1-e^{(1-\rho_1)\mu}].$$

In order to synchronize the clocks we now require that for $x_0=0$

$$(d\tau_0/d\tau)=1 \quad \text{at} \quad (x,\tau)=(x_*,\tau_*),$$

where x_* and τ_* are, respectively, the point and the instant at which the moving clock, B, comes to rest in the local-system of clock A. They are given by the relations

$$x_*=\omega^{-1}e^{\mu}(1-\cosh\rho_1\mu), \quad \tau_*=\omega^{-1}e^{\mu}\sinh\rho_1\mu.$$

On writing out this condition in full, we find the relation

$$\begin{aligned}(\rho_2-\rho_3)(1-\rho_1)[&-\sigma+\sigma e^{(1+\rho_1)\mu}\\&+e^{\frac{1}{2}(1-\rho_1)\mu}-e^{\frac{1}{2}(3+\rho_1)\mu}]\\+(\rho_2+\rho_3)(1+\rho_1)[&-\sigma+\sigma e^{(1-\rho_1)\mu}\\&+e^{\frac{1}{2}(1+\rho_1)\mu}-e^{\frac{1}{2}(3-\rho_1)\mu}]=0\end{aligned}$$

with $\sigma=\pm1$.

Now when ρ_1 is considered to have an indeterminate numerical value, the exponentials in this expression are linearly independent functions of μ, so that this condition can be satisfied only by assuming

$$(\rho_2-\rho_3)(1-\rho_1)=0$$

and

$$(\rho_2+\rho_3)(1+\rho_1)=0. \tag{3}$$

These relations yield just two solutions, which we designate as

Case a: $\rho_1=+1, \quad \rho_2=-\rho_3=\rho_a,$
Case b: $\rho_1=-1, \quad \rho_2=+\rho_3=\rho_b.$

In the next two sections we shall examine the solutions for these cases separately.

3. SOLUTION FOR CASE a.

The differential Eqs. (2) reduce to the form

$$\begin{aligned}d(\tau+x)&=\rho_a(y^2+z^2)d\mu,\\d(\tau-x)&=(\tau-x)[2+\rho_a(\tau-x)]d\mu,\\dy&=y[1+\rho_a(\tau-x)]d\mu,\\dz&=z[1+\rho_a(\tau-x)]d\mu.\end{aligned} \tag{4}$$

By integration we find the transformation equations between the local-systems S_A and S_B of the two clocks to be

$$\begin{aligned}\tau+x&=(\tau_0+x_0)+\lambda_a\rho_a(y_0^2+z_0^2)\sinh\mu,\\\tau-x&=\lambda_a e^{\mu}(\tau_0-x_0),\\y&=\lambda_a y_0, \quad z=\lambda_a z_0\end{aligned} \tag{5}$$

with

$$\lambda_a=1/[e^{-\mu}-\rho_a(\tau_0-x_0)\sinh\mu].$$

The trajectory of the moving clock, B, in S_A is found by setting $x_0=y_0=z_0=0$ and eliminating τ_0. This gives us

$$(x-\rho_a^{-1}\coth\mu)^2-(\tau+\rho_a^{-1})^2=(1/\rho_a\sinh\mu)^2. \tag{6}$$

In the local-system of clock A, the moving clock, B, crosses the origin at time $\tau=0$, with a velocity $\beta_1=-\tanh\mu$, proceeds to the point $x_*=\rho_a^{-1}\tanh(\mu/2)$ on the x-axis, which it reaches at time $\tau_*=-1/\rho_a$, coming to rest at this point. On reversing its motion it again reaches the origin, at which clock A is fixed, at time $2\tau_*$, after which it continues its motion indefinitely along the x-axis, its speed approaching the value c asymptotically. By adjustment of the parameters one can cause the ultimate motion to take

place in either direction. The whole motion is symmetrical between the two clocks, since the transformation of Eqs. (5) is inverted by interchanging the coordinates and changing the sign of the group parameter μ.

The relation between the local-times of the two clocks is obtained directly from Eqs. (5) on setting $x_0=y_0=z_0=0$, which yields

$$\tau_0=\tau+x. \tag{7}$$

We see from this that $\tau_0=\tau$ for $x=0$, so that the readings of the two clock agree at *both* coincidences, in contrast with the result expressed in Eq. (1).

It follows also from Eq. (7) that $d\tau_0/d\tau$ is greater than or less than unity, according as $dx/d\tau$ is greater than, or less than, zero. This relation is peculiar in that it does not depend on the algebraic signs of ρ_a and of μ. There appears to be an absolute distinction between left and right directions along the x-axis; this may also be interpreted as an absolute distinction between past and future which is conditioned by the imposed temporal ordering of the coincidences as *first* and *second*.

It is of interest to note that we can arrive at a transformation corresponding to *uniform* relative motion of the two systems if we take the limiting case $\rho_a\to 0$, with $\beta_1=-\tanh\mu=$ const., with which we find

$$\begin{aligned} x&=(x_0+\beta_1\tau_0)/(1+\beta_1),\\ \tau&=(\tau_0+\beta_1 x_0)/(1+\beta_1),\\ \begin{Bmatrix} y\\ z\end{Bmatrix}&=\left[\frac{1-\beta_1}{1+\beta_1}\right]^{\frac{1}{2}}\begin{Bmatrix} y_0\\ z_0\end{Bmatrix}. \end{aligned} \tag{8}$$

The transformation of Eqs. (8) is formed by a homogeneous Lorentz transformation with the velocity parameter, β_1, followed by a dilatational transformation of all coordinates with a scale factor $[(1-\beta_1)/(1+\beta_1)]^{\frac{1}{2}}$. The complete group of transformations of this type is obtained by adjoining dilatations to the inhomogeneous Lorentz group, giving rise to an 11-parameter subgroup of C_4. From the point of view of physical interpretation this result throws new light on the meaning of the usual simple Lorentz transformation, which provides no mechanism for the synchronization of clocks in uniform relative motion.

We observe that our transformation does not satisfy the *a priori* requirement imposed by Møller[3] that it be of the form

$$x=f(x_0,\tau_0),\quad y=y_0,\quad z=z_0,\quad \tau=h(x_0,\tau_0).$$

There appears to be no reason to believe that transformations of this functional form have any wider validity than the Lorentz group.

4. SOLUTION FOR CASE b

It will not be necessary to give the calculational details for this case, since the work is similar to that of Section 3. The transformation equations are

$$\begin{aligned} \tau+x&=\lambda_b e^{\mu}(\tau_0+x_0),\\ \tau-x&=(\tau_0-x_0)-\lambda_0\rho_b(y_0^2+z_0^2)\sinh\mu,\\ y&=\lambda_b y_0,\quad z=\lambda_b z_0, \end{aligned} \tag{9}$$

with

$$\lambda_b=1/[e^{-\mu}+\rho_b(\tau_0+x_0)\sinh\mu].$$

This transformation can be obtained from that of Eqs. (5) by either of the formal substitutions

(a) $(x, y, z, \tau)\to(-x, y, z, \tau)$, $\rho_a\to-\rho_b$, $\mu\to\mu$,

(b) $(x, y, z, \tau)\to(x, y, z, -\tau)$, $\rho_a\to+\rho_b$, $\mu\to\mu$.

The remainder of the anaylsis proceeds exactly as in Section 3. The two clocks again appear to register the same time interval between coincidences. The moving clock appears to gain when it moves to the left and to lose when it moves to the right, which is just the reverse of the behavior found for case a.

5. DISCUSSION

The existence of two solutions of the clock problem shows that the conceptions of classical kinematical theory are not capable of characterizing the problem uniquely. Mathematically this arises from the circumstance that C_4 is a 15-parameter group, while the corresponding group of classical kinematical theory has but 13 parameters.[4] In order to see the nature of the influence of the enlarged character of C_4, let us examine the behavior of the particles which move along the x-axis. We find the formula for the trajectory of such a particle from Eqs. (5) and (9) on setting $y_0=z_0=0$ and eliminating τ_0. We obtain equations of the form

$$(x-x_0-\rho^{-1}\coth\mu)^2-(\tau\mp x_0\pm\rho^{-1})^2=(1/\rho\sinh\mu)^2.$$

For the apparent velocities of these particles we have

$$dx/d\tau = \pm(\tau \mp x_0 \pm \rho^{-1})/[(\tau \mp x_0 \pm \rho^{-1})^2 + (\rho \sinh\mu)^{-2}]^{\frac{1}{2}}.$$

If we now consider those particles at great distances in either direction along the axis, for any fixed time τ, we find that $|dx/d\tau| \to 1$ as $|x_0| \to \pm\infty$. In this way we are brought quite directly to a kinematical connection between the clock problem and the "expanding universe." This is, in fact, simply another apsect of the relationship between C_4 and cosmological theory, which has been discussed by Robertson[8] and by Infeld and Schild.[9]

To return to the comparison of the present analysis with the current relativistic theory, we observe that the divergence between the two mathematical procedures rests on the interpretation assigned to the "line-element" associated with the group C_4. The group is, in fact, characterized by a differential form of the type[4]

$$\lambda^2(x, y, z, \tau)(d\tau^2 - dx^2 - dy^2 - dz^2). \qquad (10)$$

In the relativistic theory an arbitrary assignment is made of the "inertial" system in which $\lambda = 1$. In the present theory we refrain from making a unique assignment of line-element to the local-systems of the clocks; our discussion leaves the line-element of any particular coordinate system indefinite to the extent indicated by the form (10). We are concerned only with relations *between* coordinate systems, but not with the absolute specification of either system. From the mathematical point of view the present procedure is more closely related to Weyl's theory[10] than to that of Einstein.

From the point of view of physical interpretation, this bifurcation is just that existing between mechanical and electrical theories, and it seems to the writer that by the apposition of the two procedures in the clock problem we are enabled to see the basic divergence between the two types of theory in a particularly elementary, but fundamental, light. The equations of mechanics are form invariant under transformations to systems moving with constant relative velocity, but the electromagnetic equations are insensitive to transformations involving uniform accelerations. The failure of the electromagnetic theory of mass seems to be a real measure of the incompatibility between the two theories. We seem here to be close to the root mathematical difficulties confronting the attempt to correlate quantum mechanics and the theory of relativity on any wider basis than that provided by the Lorentz group.

[8] H. P. Robertson, Phys. Rev. **49**, 755 (1936).
[9] L. Infeld and A. Schild, Phys. Rev. **68**, 250 (1945); *ibid.*, **70**, 410 (1946).
[10] H. Weyl, *Space-Time-Matter* (Methuen Press, London, 1922) Section 35.

Fine Structure of the Hydrogen Atom by a Microwave Method* **

WILLIS E. LAMB, JR. AND ROBERT C. RETHERFORD
Columbia Radiation Laboratory, Department of Physics, Columbia University, New York, New York
(Received June 18, 1947)

THE spectrum of the simplest atom, hydrogen, has a fine structure[1] which according to the Dirac wave equation for an electron moving in a Coulomb field is due to the combined effects of relativistic variation of mass with velocity and spin-orbit coupling. It has been considered one of the great triumphs of Dirac's theory that it gave the "right" fine structure of the energy levels. However, the experimental attempts to obtain a really detailed confirmation through a study of the Balmer lines have been frustrated by the large Doppler effect of the lines in comparison to the small splitting of the lower or $n=2$ states. The various spectroscopic workers have alternated between finding confirmation[2] of the theory and discrepancies[3] of as much as eight percent. More accurate information would clearly provide a delicate test of the form of the correct relativistic wave equation, as well as information on the possibility of line shifts due to coupling of the atom with the radiation field and clues to the nature of any non-Coulombic interaction between the elementary particles: electron and proton.

The calculated separation between the levels $2^2P_{\frac{1}{2}}$ and $2^2P_{3/2}$ is 0.365 cm^{-1} and corresponds to a wave-length of 2.74 cm. The great wartime advances in microwave techniques in the vicinity of three centimeters wave-length make possible the use of new physical tools for a study of the $n=2$ fine structure states of the hydrogen atom. A little consideration shows that it would be exceedingly difficult to detect the direct absorption of radiofrequency radiation by excited H atoms in a gas discharge because of their small population and the high background absorption due to electrons. Instead, we have found a method depending on a novel property of the $2^2S_{\frac{1}{2}}$ level. According to the Dirac theory, this state exactly coincides in energy with the $2^2P_{\frac{1}{2}}$ state which is the lower of the two P states. The S state in the absence of external electric fields is metastable. The radiative transition to the ground state $1^2S_{\frac{1}{2}}$ is forbidden by the selection rule $\Delta L=\pm 1$. Calculations of Breit and Teller[4] have shown that the most probable decay mechanism is double quantum emission with a lifetime of 1/7 second. This is to be contrasted with a lifetime of only 1.6×10^{-9} second for the non-metastable 2^2P states. The metastability is very much reduced in the presence of external electric fields[5] owing to Stark effect mixing of the S and P levels with resultant rapid decay of the combined state. If for any reason, the $2^2S_{\frac{1}{2}}$ level does not exactly coincide with the $2^2P_{\frac{1}{2}}$ level, the vulnerability of the state to external fields will be reduced. Such a removal of the accidental degeneracy may arise from any defect in the theory or may be brought about by the Zeeman splitting of the levels in an external magnetic field.

In brief, the experimental arrangement used is the following: Molecular hydrogen is thermally dissociated in a tungsten oven, and a jet of atoms emerges from a slit to be cross-bombarded by an electron stream. About one part in a hundred million of the atoms is thereby excited to the metastable $2^2S_{\frac{1}{2}}$ state. The metastable atoms (with a small recoil deflection) move on out of the bombardment region and are detected by the process of electron ejection from a metal target. The electron current is measured with an FP-54 electrometer tube and a sensitive galvanometer.

If the beam of metastable atoms is subjected to any perturbing fields which cause a transition to any of the 2^2P states, the atoms will decay while moving through a very small distance. As a result, the beam current will decrease, since the

* Publication assisted by the Ernest Kempton Adams Fund for Physical Research of Columbia University, New York.
** Work supported by the Signal Corps under contract number W 36-039 sc-32003.

[1] For a convenient account, see H. E. White, *Introduction to Atomic Spectra* (McGraw-Hill Book Company, New York, 1934), Chap. 8.
[2] J. W. Drinkwater, O. Richardson, and W. E. Williams, Proc. Roy. Soc. **174**, 164 (1940).
[3] W. V. Houston, Phys. Rev. **51**, 446 (1937); R. C. Williams, Phys. Rev. **54**, 558 (1938); S. Pasternack, Phys. Rev. **54**, 1113 (1938) has analyzed these results in terms of an upward shift of the S level by about 0.03 cm^{-1}.
[4] H. A. Bethe in *Handbuch der Physik*, Vol. 24/1, §43.
[5] G. Breit and E. Teller, Astrophys. J. **91**, 215 (1940).

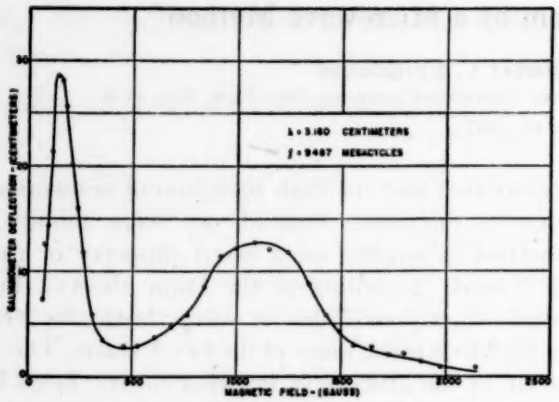

FIG. 1. A typical plot of galvanometer deflection due to interruption of the microwave radiation as a function of magnetic field. The magnetic field was calibrated with a flip coil and may be subject to some error which can be largely eliminated in a more refined apparatus. The width of the curves is probably due to the following causes: (1) the radiative line width of about 100 Mc/sec. of the ^2P states, (2) hyperfine splitting of the ^2S state which amounts to about 88 Mc/sec., (3) the use of an excessive intensity of radiation which gives increased absorption in the wings of the lines, and (4) inhomogeneity of the magnetic field. No transitions from the state $2^2S_{\frac{1}{2}}(m=-\frac{1}{2})$ have been observed, but atoms in this state may be quenched by stray electric fields because of the more nearly exact degeneracy with the Zeeman pattern of the ^2P states.

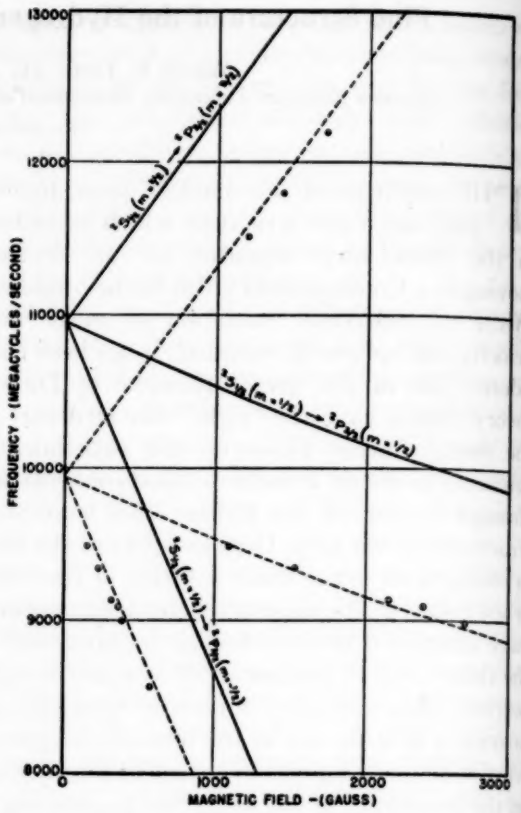

FIG. 2. Experimental values for resonance magnetic fields for various frequencies are shown by circles. The solid curves show three of the theoretically expected variations, and the broken curves are obtained by shifting these down by 1000 Mc/sec. This is done merely for the sake of comparison, and it is not implied that this would represent a "best fit." The plot covers only a small range of the frequency and magnetic field scale covered by our data, but a complete plot would not show up clearly on a small scale, and the shift indicated by the remainder of the data is quite compatible with a shift of 1000 Mc.

detector does not respond to atoms in the ground state. Such a transition may be induced by the application to the beam of a static electric field somewhere between source and detector. Transitions may also be induced by radiofrequency radiation for which $h\nu$ corresponds to the energy difference between one of the Zeeman components of $2^2S_{\frac{1}{2}}$ and any component of either $2^2P_{\frac{1}{2}}$ or $2^2P_{3/2}$. Such measurements provide a precise method for the location of the $2^2S_{\frac{1}{2}}$ state relative to the P states, as well as the distance between the latter states.

We have observed an electrometer current of the order of 10^{-14} ampere which must be ascribed to metastable hydrogen atoms. The strong quenching effect of static electric fields has been observed, and the voltage gradient necessary for this has a reasonable dependence on magnetic field strength.

We have also observed the decrease in the beam of metastable atoms caused by microwaves in the wave-length range 2.4 to 18.5 cm in various magnetic fields. In the measurements, the frequency of the r-f is fixed, and the change in the galvanometer current due to interruption of the r-f is determined as a function of magnetic field strength. A typical curve of quenching *versus* magnetic field is shown in Fig. 1. We have plotted in Fig. 2 the resonance magnetic fields for various frequencies in the vicinity of 10,000 Mc/sec. The theoretically calculated curves for the Zeeman effect are drawn as solid curves, while for comparison with the observed points, the calculated curves have been shifted downward by 1000 Mc/sec. (broken curves). The results indicate clearly that, contrary to theory but in essential agreement with Pasternack's hypothesis,[3] the $2^2S_{\frac{1}{2}}$ state is higher than the $2^2P_{\frac{1}{2}}$ by about 1000 Mc/sec. (0.033 cm^{-1} or about 9 percent of the spin relativity doublet separation. The lower frequency transitions $^2S_{\frac{1}{2}}(m=\frac{1}{2})\rightarrow {}^2P_{\frac{1}{2}}(m=\pm\frac{1}{2})$ have also been observed and agree

well with such a shift of the $^2S_{\frac{1}{2}}$ level. With the present precision, we have not yet detected any discrepancy between the Dirac theory and the doublet separation of the P levels. (According to most of the imaginable theoretical explanations of the shift, the doublet separation would not be affected as much as the relative location of the S and P states.) With proposed refinements in sensitivity, magnetic field homogeneity, and calibration, it is hoped to locate the S level with respect to each P level to an accuracy of at least ten Mc/sec. By addition of these frequencies and assumption of the theoretical formula $\Delta\nu=\frac{1}{16}\alpha^2R$ for the doublet separation, it should be possible to measure the square of the fine structure constant times the Rydberg frequency to an accuracy of 0.1 percent.

By a slight extension of the method, it is hoped to determine the hyperfine structure of the $2^2S_{\frac{1}{2}}$ state. All of these measurements will be repeated for deuterium and other hydrogen-like atoms.

A paper giving a fuller account of the experimental and theoretical details of the method is being prepared, and this will contain later and more accurate data.

The experiments described here were discussed at the Conference on the Foundations of Quantum Mechanics held at Shelter Island on June 1–3, 1947 which was sponsored by the National Academy of Sciences.

PHYSICAL REVIEW VOLUME 72, NUMBER 3 AUGUST 1, 1947

On Self-Quenching Halogen Counters

R. D. PRESENT*
University of Tennessee, Knoxville, Tennessee
(Received May 23, 1947)

SOME considerations relating the spectroscopic and photochemical properties of polyatomic gases with their use in Geiger-Mueller counters have been developed by the writer.[1] The self-quenching counter is able to operate without the usual large resistance because of the absence of secondary emission of electrons when the positive ion sheath reaches the cathode and is neutralized. The neutralization of the ions (at about 10^{-7} cm from the wall) results in neutral atoms or molecules having an excitation energy of $(I-\varphi)$ approximately, where I is the ionization energy and φ the photoelectric work function of the surface. In the case of a monatomic or diatomic (non-quenching) gas this excitation energy is transferred to the metal in about 10^{-12} sec. and secondary electrons are liberated if $I>2\varphi$. In the case of most polyatomic gases (with four or more atoms), the neutralized molecules will predissociate (in about 10^{-13} sec.) before they can make an inelastic collision with the wall, and the emission of secondary electrons will be negligible. In order to determine whether a given gas will show self-quenching action, it is sufficient to examine its absorption spectrum at wave-lengths corresponding to an excitation energy of $(I-\varphi)$. Continuous absorption, or a line broadening corresponding to a predissociation lifetime of 10^{-13} sec., indicate that the molecule undergoes primary photo-decomposition. Such a gas will make a self-quenching counter. If a mixture of quenching and non-quenching gases is used, the counter will show self-quenching action only if the ionization potential of the non-quenching gas exceeds that of the quenching gas. Under these circumstances electron transfer changes the composition of the positive ion sheath so that, when it reaches the cathode, there is a negligible number of non-quenching ions. A more detailed discussion will be found in reference 1.

We should like to point out here that the mechanism of secondary-emission quenching is compatible, under special circumstances, with the

* Also consultant at Clinton Laboratories, Oak Ridge, Tennessee.

[1] S. A. Korff and R. D. Present, Phys. Rev. **65**, 274 (1944). The theoretical considerations in this paper were mainly developed by R. D. Present; the experimental work and its interpretation were done mainly by S. A. Korff.

quenching gas being diatomic. The halogens Cl_2, Br_2, and I_2 are examples of diatomic gases which would be expected to show self-quenching action.[2] The absorption spectra of these gases have been investigated into the far ultraviolet. The ionization potentials are respectively 13.2, 12.8, and 9.7 volts. If the cathode surface is carbon[3] (photoelectric work function ≈ 5 volts) the values of $(I-\varphi)$ correspond to wave-lengths of 1500, 1600, and 2600A for the three gases, respectively. In this region of the spectrum both Cl_2 and Br_2 show continuous absorption corresponding to primary photo-decomposition.[4] One should expect that these gases would give rise to no secondary emission. The ultraviolet absorption spectrum of I_2 shows several bands in the region from 2760 to 1750A.[5] Several of these bands are sharp and are accompanied by fluorescence, indicating the absence of predissociation except as induced by collisions.[6] Decomposition of the neutralized I_2 molecules at the cathode surface is not indicated as in the case of the other halogens. Nevertheless, if the cathode surface be of carbon,[3] secondary emission cannot occur because the ionization potential is less than twice the work function. The work function of carbon is 4.7 volts for ordinary contamination; however, halogen contamination generally raises the work function by several tenths of a volt.[7] For all surfaces for which $I<2\varphi$ the secondary emission by positive ions is quenched.

The possible effects of electron attachment cannot be neglected when the halogens are used in appreciable concentrations. After the initial ionizing event there will evidently be a small number of negative ions moving in toward the center wire from the outer regions of the counter. When a negative ion reaches the high field region near the wire, an electron will detach itself and initiate a new avalanche unless the field is below the counting threshold. As the positive ion sheath moves outward, in a fast counter the field near the wire increases; the threshold field is reached when the positive ions have traveled the critical distance (about half the distance to the wall[8]). The negative ions in a fast halogen counter must all have been neutralized before the positive ion sheath reaches the critical distance. The reason for this is found partly in the greater mobility of the negative compared to the positive ions.[9] Furthermore, the negative ions may be neutralized in crossing the positive ion sheath (the electron affinities of the halogen atoms are less than the ionization potentials of the molecules). If the partial pressure of halogen gas is not too large, it appears likely that the performance of these counters should be unimpaired by multiple pulses and spurious counts arising from negative ions. However, the concentration of halogen must be large enough to quench metastable rare-gas atoms.[2] Finally, just as in the case of oxygen counters,[10] attachment of the electrons formed in the initial ionizing event can cause a mean time lag of as much as 10^{-4} sec. between the passage of the ionizing particle and the initiation of the discharge (unless the concentration of halogen is only a few percent). This would make the halogen counter unsuitable for coincidence experiments in which the efficiency must be high and the resolving time low.

[2] S. H. Liebson, Bull. Am. Phys. Soc. **22**, 2 (1947), has recently reported that counters filled with suitable mixtures of halogen and noble gases show self-quenching (fast) counter action.

[3] The inner surfaces of the cathodes used in reference 2 were coated with Aquadag (graphite).

[4] Both the Cl_2 and Br_2 continuous absorption regions in the ultraviolet extend down to 1560A (limit of observations) and the maximum of the Cl_2 absorption appears to be near this value. H. Cordes and H. Sponer, Zeits. f. Physik **63**, 334 (1930).

[5] O. Oldenberg, Zeits. f. Physik **25**, 136 (1924); P. Pringsheim and B. Rosen, Zeits. f. Physik **50**, 1 (1928); D. T. Warren, Phys. Rev. **47**, 1 (1935).

[6] Predissociation induced by gas collisions would be ineffective in preventing secondary emission since the neutralized molecule would make an inelastic collision with the wall before it could collide with another molecule. The van der Waals field at the surface has a sufficient range to induce predissociation of the neutralized molecule but the interaction is insufficient to reduce the lifetime to less than 10^{-11} sec.

[7] C. Ouellet and E. K. Rideal, J. Chem. Phys. **3**, 150 (1935).

[8] H. G. Stever, Phys. Rev. **61**, 38 (1942).

[9] Immediately after electron attachment the halogen molecule ion dissociates into an atomic ion and a neutral atom. Because of its smaller mass and effective cross section the negative atomic ion should have a greater mobility than the positive molecular ion. The discharge terminates before the mobilities can be affected by impurities.

[10] M. E. Rose and W. E. Ramsey, Phys. Rev. **59**, 616 (1941).

Letters to the Editor

PUBLICATION of brief reports of important discoveries in physics may be secured by addressing them to this department. The closing date for this department is five weeks prior to the date of issue. No proof will be sent to the authors. The Board of Editors does not hold itself responsible for the opinions expressed by the correspondents. Communications should not exceed 600 words in length.

A Low Temperature Transformation in Lithium*

CHARLES S. BARRETT
Institute for the Study of Metals, University of Chicago, Chicago, Illinois
June 12, 1947

LITHIUM has been reported as having a body-centered cubic structure in the range from ordinary temperatures to liquid air temperature.[1,2] X-ray diffraction at low temperatures now reveals, however, that a transformation can be induced in the metal if it is plastically deformed at temperatures in the vicinity of −196°C.

Analysis of the Geiger-counter spectrometer record of the diffraction pattern shows that the new phase produced by this treatment is face-centered cubic in structure with the lattice constant $a_0=4.41$A at −196°C. The body-centered cubic phase in the same sample at this temperature has $a_0=3.50$A. There is an expansion of atomic radius accompanying the increase of coordination number from 8 to 12, as would be expected, and because this expansion has the value 2.8 percent it follows that the calculated densities of the two phases are identical within experimental error. The calculated density is 0.534.

The transformation to the face-centered cubic form is accompanied by a series of audible clicks, as in the twinning of tin or magnesium and the formation of martensite. By analogy with these processes it may be concluded that the transformation goes by abrupt shear movement in small isolated regions. The constraints imposed by the material around these transforming regions can account for the fact that we have been unable to transform much more than half of any of the polycrystalline samples by any type of straining we have tried. Presumably then, proper straining of a single crystal might lead to complete transformation. The face-centered phase disappears fairly rapidly when heated above about −117°C.

We were led to search for low temperature transformations in various metals by C. Zener's theory of the susceptibility of body-centered cubic phases to instability at low temperatures,[3,4] which may be summarized as follows. A homogeneous shear of 0.35 in a body-centered cubic structure along the (110) plane and the $[1\bar{1}0]$ direction will produce an atomic arrangement that is very nearly face-centered cubic. Consider the relative free energy of the two phases. The free energy of the body-centered cubic phase increases as the temperature is lowered, and increases more rapidly than would the free energy of a face-centered cubic phase, provided the thermal vibrations of the atoms in some direction of the body-centered structure are abnormally large. In metals and alloys of body-centered cubic structure that have filled inner shells of electrons, the shear constant $(C_{11}-C_{12})/2$ should be small and is, in fact, very small; as this constant applies to shear in the (110) plane in the $[1\bar{1}0]$ direction, the thermal vibration amplitudes in this direction should be large, and since the entropy is proportional to the logarithm of the amplitude it follows then that the entropy should be large. The free energy of a phase with large entropy rapidly increases as the temperature is lowered, since $F=U-TS$ and $\partial F/\partial T=-S$, where F is the free energy, U the internal energy, T the temperature, and S the entropy; it is not unlikely that F for the body-centered phase in such cases will exceed that for the face-centered phase and make a transformation possible, as in some compositions of beta-brass, where $(C_{11}-C_{12})/2$ is twice as large in the face-centered form as in the body-centered. Such transformations should be aided by shear in the direction for which the shear modulus is low, both because it reduces the sluggishness of the transformation by aiding the atoms in surmounting the potential barrier in this direction and because this is the direction required for the shear movement of the transformation.

A more detailed account of the investigation of this metal and others will be published elsewhere.

* This work was supported by the Office of Research and Inventions, U.S.N. (Contract No. N-6ori-20-IV).
[1] F. Simon and E. Vohsen, Zeits. f. physik. Chemie **133**, 165–187 (1928).
[2] E. Posnjak, J. Phys. Chem. **32**, 354–359 (1928).
[3] C. Zener, Phys. Rev. **71**, 846 (1947).
[4] C. Zener, *Elasticity and Anelasticity of Metals* (University of Chicago Press, Chicago, to be published).

On the Hyperfine Structure of the Ground State of H and D Atoms

OTTO HALPERN
Columbia University, New York, New York
June 16, 1947

RECENTLY[1] measurements of the hyperfine structure of H and D atoms have been carried out which are extremely interesting from a theoretical as well as an experimental point of view.

According to the latest precision measurements, not only the absolute values of the hyperfine structure splittings ν_H, ν_D differ from the theoretical value by about one part in 400, but also the ratio of these quantities differs from the theoretical value by about 1 part in 1700, the calculated value always being smaller than the observed. The theoretical evaluation was carried out with the aid of the well-known Fermi formula

$$\nu=\frac{8\pi}{3h}\frac{2I+1}{I}\mu_N\mu_0|\psi(0)|^2, \qquad (1)$$

in which the nuclear spin is denoted by I; μ_N is the magnetic moment of the nucleus, μ_0 is Bohr's magneton, and $\psi(0)$ the Schroedinger wave function at the origin. Through $|\psi(0)|^2$, the Bohr radius of the ground state enters into

the expression of the hyperfine structure splitting, $|\psi(0)|^2$ being proportional to a^{-3}. It is customary to eliminate the Bohr radius by introducing the Rydberg constant for infinite mass, together with the reduced mass of the electron. It then turns out that the hyperfine structure splitting is given by the expression

$$\nu = C\frac{2I+1}{I}\mu_N\left(\frac{m_r}{m_0}\right)^3. \quad (2)$$

Here C contains universal constants and numbers, while m_r stands for the reduced mass of H or D, respectively. m_0 denotes the electronic mass. The ratio ν_H/ν_D is then given by

$$\nu_H/\nu_D = (4/3)(\mu_H/\mu_D)(m_H/m_D)^3,$$

and the numerical value for ν_H/ν_D as observed, is 4.3416 compared with a computed value of 4.3393.

Equation (1) is derived by neglecting the small components of the Dirac equation and replacing the large components by Schroedinger functions.

The discrepancy observed which, if the accuracy of observation is sufficient, in the case of the ratio at least, cannot be ascribed to inaccurate values of the universal constants, makes it advisable to re-examine the derivation of (1).

We have obtained a value for ν by consistently using Dirac's equation, retaining all four components through the perturbation calculation and using the rigorous Dirac functions in the evaluation of the matrix element for the perturbed energy. The hyperfine structure splitting apart from numerical factors is now given by

$$\nu = C'\frac{e\mu_N}{(h/mc)^3}[1-(E/mc^2)^2]^{\frac{1}{2}} = C'\frac{e\mu_N}{(h/mc)^3}(2R/mc^2)^{\frac{1}{2}}. \quad (3)$$

The second equation in (3) is obtained by the somewhat arbitrary insertion of the empirical Rydberg constant in place of R_∞ which would, of course, follow from the Dirac equation.

This calculation leads, within the accuracy aimed at, to the same value as given by (2), with the one difference that the ratio of reduced to electronic mass appears in the three-halves rather than in the third power. This correction diminishes the discrepancies between the observed and calculated values of ν_H and ν_D, as follows. For H, the discrepancy is reduced to one part in 600; for D, to one part in 500; both deviations are obviously still large if one believes in the presently accepted values of the universal constants.

The ratio ν_H/ν_D, on the other hand, now differs from its calculated value by only one part in 8000; this is much smaller than the accuracy claimed for the earlier determinations of μ_H/μ_D, which enters as a factor into (3) and is assumed to be known to about 1 part in 3000.

In interpreting this result, several points must be kept in mind: The accuracy of the experimental determination of μ_H/μ_D and the calculated value which contains it as its most uncertain element, are not yet sufficiently good to exclude a different dependence on the ratio of the reduced masses.

The theory here used is obviously not consistent; we have carried out all calculations with the one-body Dirac equation and taken into account the two-body nature of the problem by the empirical introduction of R_H and R_D. This point will need further theoretical study.

We have also investigated the question of how the electronic magnetic moment may be expected to depend on the nuclear mass and have found different results depending on the physical interpretation given to the coordinates which enter into the Dirac equation.

A detailed paper will follow shortly.

[1] J. E. Nafe, E. B. Nelson, and I. I. Rabi, Phys. Rev. 71, 914 (1947). I am greatly indebted to the authors for telling me about their results before publication.

Nuclear Capture of Mesons and the Meson Decay

B. PONTECORVO
National Research Council, Chalk River Laboratory, Chalk River, Ontario, Canada
June 21, 1947

THE experiment of Conversi, Pancini, and Piccioni[1] indicates that the probability of capture of a meson by nuclei is much smaller than would be expected on the basis of the Yukawa theory.[2,3] Gamow[4] has suggested that the nuclear forces are due exclusively to the exchange of neutral mesons, the processes involving charged mesons and the β-processes having probabilities which are smaller by a factor of about 10^{12}.

We notice that the probability ($\sim 10^6$ sec.$^{-1}$) of capture of a bound negative meson is of the order of the probability of ordinary K-capture processes, when allowance is made for the difference in the disintegration energy and the difference in the volumes of the K-shell and of the meson orbit. We assume that this is significant and wish to discuss the possibility of a fundamental analogy between β-processes and processes of emission or absorption of charged mesons.

An immediate consequence of the experiments of the Rome group[1] is that the usual interpretation of the β-process as a "two-step" process ("probable" production of virtual meson and subsequent β-decay of the meson) completely loses its validity, since it would predict too long β-lifetimes: the meson is no longer the particle responsible for nuclear β-processes, which are to be described according to the original Fermi picture (without mesons). Consequently there is no need to assume that charged mesons have integral spin, as the Yukawa explanation of β-processes required. Once we believe that the ordinary β-process is not connected in any way with the meson, it is difficult to see strong reasons for the usual assumption that the meson decays with emission of a β-particle and a neutrino. We shall consider then the hypothesis that the meson has spin $\frac{1}{2}\hbar$ and that its instability is not a β-process, in the sense that it does not involve the emission of one neutrino. The meson decay must then be described in a different way: it might consist of the emission of an electron and a photon or of an electron and 2 neutrinos[5] or some other process.

In the hypothesis that the meson decay is not a β-process (meson of spin $\frac{1}{2}$) *the process of nuclear absorption or production of a single meson would be accompanied by the emission of a neutrino.* This analogy between β-particles and mesons suggests, in addition, that just as the production of single β-particles is extremely unlikely, while the production of electron pairs is a very likely phenomenon, so the production of a single charged meson would be very unlikely, while the production of pairs of mesons would be quite probable. The experimental evidence is, in fact,[6] that most, if not all, of the meson showers are created in connection with large Auger showers.

The assumption that the emission or absorption of one meson is accompanied by the emission of a neutrino would explain in a natural way a somewhat puzzling experimental result. Among the few pictures of a meson stopping in the gas of a cloud chamber, no "star" has been observed at the end of the meson track.[7] The absence of a star must be due to a process leaving the capturing nucleus in a not too excited state: the mechanism proposed here would explain that the capture of a negative meson from a nucleus Z results in a nucleus $Z-1$ close to its ground level, since the excess energy could be carried away by the neutrino. Actually, in such a process we should expect that the emission of a neutrino of high energy with consequent production of the nucleus $Z-1$ in a state of low excitation would be more likely than the emission of a neutrino of low energy with the production of the nucleus $Z-1$ in a state of high excitation (cf. K-capture process).

The hypothesis that the meson decay is not a β-process, while the meson absorption is a β-process, does not require that hypothetical particles such as neutral mesons are invoked to account for nuclear forces. In fact, a heavy electron *pair* theory of nuclear forces was successfully developed by Marshak.[8] Moreover, a pair theory is capable of accounting, at least in principle, for the existence of processes in which several pairs of mesons are produced in a single act, as suggested by Heisenberg in connection with a different problem.[9]

Returning to the actual decay of the meson, an experiment suggests itself which might answer the following question: Is the electron emitted by the meson with a mean life of about 2.2 microseconds accompanied by a photon of about 50 Mev? This experiment is being attempted at the present time, since it is felt that the available analysis[10] of the soft component in equilibrium with its primary meson component is probably insufficient to decide definitely whether the meson decays into either an electron plus neutral particle(s) or electron plus photon.

[1] M. Conversi, E. Pancini, and O. Piccioni, Phys. Rev. **71**, 209 (1947). See also T. Sigurgeirson and A. Yamakawa, Phys. Rev. **71**, 319 (1947).
[2] E. Fermi, E. Teller, and V. Weisskopf, Phys. Rev. **71**, 314 (1947).
[3] J. A. Wheeler, Phys. Rev. **71**, 320 (1947).
[4] G. Gamow, Phys. Rev. **71**, 550 (1947). See also G. Gamow and E. Teller, Phys. Rev. **51**, 289 (1937).
[5] W. Nordheim, Phys. Rev. **59**, 544 (1941).
[6] G. Cocconi, A. Loveredo, and V. Tongiorgi, Phys. Rev. **70**, 852 (1946).
[7] See for a critical survey: T. H. Johnson and R. P. Shutt, Phys. Rev. **61**, 380 (1942).
[8] R. E. Marshak, Phys. Rev. **57**, 1101 (1940).
[9] References can be found in *Cosmic Radiation*, edited by W. Heisenberg (Dover Publications, New York, 1946), p. 127.
[10] See reference 9, pp. 84–97.

An On-Orbit Injector for Betatrons and Synchrotrons

DAVID C. DEPACKH AND ANDREW V. HAEFF
Naval Research Laboratory, Washington, D. C.
May 29, 1947

ONE of the primary limitations on the yield from present electron accelerators of the betatron and synchrotron type lies in the injection process. The injector must lie off the orbit in which the acceleration is supposed to occur in order not to interfere with the acceleration process, and this necessarily implies radial oscillations of the injected electrons of an amplitude at least equal to the distance between the stable orbit and the injector. The frequency of these radial oscillations is approximately $\nu_0(1-n)^{\frac{1}{2}}$, where ν_0 is the rotation frequency of the electrons, and n is the exponent in the expression $H=H_0(r/r_0)^{-n}$ law of decrease of the magnetic field with radius. If n has a nominal value of 0.5, it is seen that the oscillation frequency is 0.71 of the electron frequency and that as a consequence we cannot expect any appreciable damping of this oscillation by increasing magnetic field in a time comparable to several cycles of this oscillation. Moreover, the beneficial effect of such damping is further reduced if, as is the practice, the injection is performed at high voltage, since in a given time interval the relative change of field is less with a large field than a small one for a field increasing approximately linearly with the time. The net result of these conditions is that although injected electrons may clear the injector on the first transit because of the difference between ν_0 and $\nu_0(1-n)^{\frac{1}{2}}$, nevertheless a great many of them will strike it on subsequent transits and thus be lost.

In order to circumvent this difficulty, it is proposed to employ an injector which surrounds the stable orbit so that electrons rotating in the stable orbit may pass through the injector structure without interference. Thus in substance the injector (see Fig. 1) consists of an annular

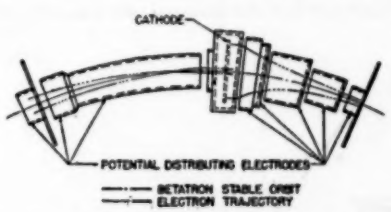

FIG. 1. Schematic drawing of on-orbit injector. The magnetic field is normal to the paper.

cathode and a series of electron lenses which narrow and collimate the electron beam, so that as it emerges from the injector it appears ideally as a cylindrical tube the axis of which is the stable orbit. One can design the lens system to make the diameter of this tube of such a size that oscillation within the beam is of no importance. The part of the injector behind the cathode can be designed so that electrons, passing through the injector on subsequent transits and having been defocused because of space charge or for some other reason, can be refocused as they pass through the low potential region near the center of the

cathode ring. Since the electron velocity during the injection pulse falls as the electron enters the injector, goes through a minimum as it passes through the cathode ring, and rises to its initial value as the electron leaves the gun, it is necessary to supply a compensating magnetic field in the neighborhood of the injector during the injection pulse.

An injector of this type has been designed at the Naval Research Laboratory and is under development.

The Beta-Ray Spectrum of C^{14}[1]

PAUL W. LEVY
Clinton Laboratories, Oak Ridge, Tennessee
June 9, 1947

A 180° beta-ray spectrometer of 10-cm radius, using a Geiger-Mueller tube as the detecting device, has been used to investigate the continuous beta-ray spectrum of the 4700-year C^{14} activity. It was necessary to use a very thick source because of the long half-life and low concentration of C^{14} in the available material. The spectrum obtained with this source appears simple, that is, it has only one component and has a maximum energy of 0.154 Mev. As is to be expected from the fact that no gamma-rays have been detected accompanying the decay of C^{14}, no conversion electron lines appear.

The maximum energy of the beta-ray spectrum was determined from the Kurie plot, Fig. 1, which was constructed from that part of the spectrum high enough in energy so that absorption in the window of the detecting G. M. tube is negligible. One cannot say, however, that this part of the spectrum is entirely free from the effects of self-absorption and back scattering due to the thickness of the source. These effects might possibly combine in a way that introduces an undetermined error in the 0.154-Mev end point and, therefore, one cannot claim the 2 percent inherent accuracy of the spectrometer at this energy. Yet it is surprising that the Kurie plot is straight, and, if it were not for the unusual thickness of the source, one would interpret this as evidence that the spectrum was free from large disturbing effects.

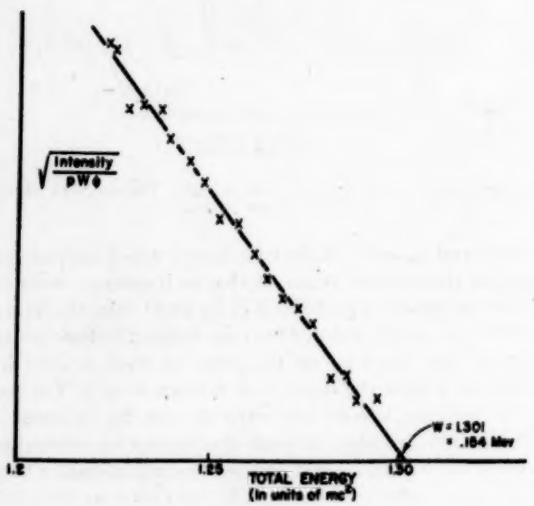

FIG. 1. Kurie plot of C^{14} beta-ray spectrum.

The author wishes to express his thanks to L. D. Norris for preparing the C^{14} source.

This work was done under the auspices of Manhattan District Contract W 7405-eng. 39.

[1] A detailed description of this work and the spectrometer used is contained in Plutonium Project Report CP-3702 which is to be published as a contribution to the Plutonium Project Record volume on nuclear physics.

On the Change of the Mean Life of Negative Mesotrons

HAROLD K. TICHO AND MARCEL SCHEIN
Department of Physics, University of Chicago, Chicago, Illinois
June 23, 1947

RECENT experiments[1,2] have demonstrated that negative mesotrons, stopping in solid materials of low atomic number, do disintegrate; this result is in contradiction with the calculations of Tomonaga and Araki[3] who predicted that mesotrons carrying a negative charge should be captured by the nuclei of solid absorbers, whatever their atomic number. Subsequently, Fermi, Teller, and Weisskopf,[4] and also Wheeler[5] investigated the energy loss of mesotrons after they have stopped ionizing and concluded that negative mesotrons should fall into the (mesotron) K-shell within 10^{-12} second. From the K-orbit, mesotrons can either be captured by the atomic nucleus or disintegrate spontaneously. Their decay constant should therefore be $\lambda+\Lambda$, where $1/\lambda=\tau_0$ is the mean life for disintegration and Λ the probability per second for capture. The fact that the disintegration of negative mesotrons is observed in light absorbers indicates that Λ is not much larger than λ; hence, $\Lambda\sim 5\times 10^5$ sec.$^{-1}$, which is in strong disagreement with meson theories which yield $\Lambda\sim 10^{13}$ sec.$^{-1}$. According to Wheeler[5] Λ should increase roughly as Z^4.

If it is true that the capture probability is considerably smaller than that calculated on the basis of meson theories of nuclear forces, then the disintegration electrons arising from the decay of negative mesotrons should also follow a disintegration curve with the modified decay constant $\lambda+\Lambda$. The number of negative mesotrons dN_d^-, *disintegrating* in the time interval dt, is equal to the original number of negative mesotrons N_0^- times the probability that they have neither disintegrated nor been captured before t, $\exp(-\lambda t-\Lambda t)$, times λdt. The integration of this expression yields

$$N_d^- = N_0^-[\lambda/(\lambda+\Lambda)]\exp[-(\lambda+\Lambda)t].$$

The capture constant Λ could, therefore, be measured by determining the mean life $1/(\lambda+\Lambda)$ of negative mesotrons alone. In such a determination one should use $\tau_0=2.15\times 10^{-6}$ second for $1/\lambda$. This value of τ_0 was obtained by Nereson and Rossi[6] chiefly in lead, where negative mesotrons do not disintegrate.

If the experiment is carried out in the usual way, i.e., without differentiating between positive and negative mesotrons, a small change of the disintegration constant

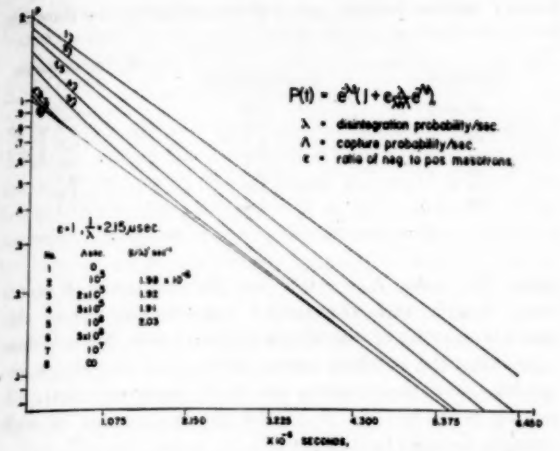

FIG. 1. The integral-disintegration curves which should be obtained if negative mesotrons both disintegrate and get captured. The values $(1/\lambda)'$ are the "mean-life" value calculated from the average slope of these curves.

should still be observable in materials of suitable atomic number. This change of the disintegration constant is due to the fact that the experimental data obtained really represent a superposition of two decay curves, one produced by positive mesotrons with a mean life $1/\lambda$ and one produced by negative mesotrons with a mean life $1/(\lambda+\Lambda)$. Hence, the total disintegration curve is represented by the following expression:

$$N_d = N_0^+ \exp(-\lambda t) + N_0^- [\lambda/(\lambda+\Lambda)] \exp[-(\lambda+\Lambda)t].$$

Disintegration curves of this kind for values of Λ between 0 and ∞, and assuming an equal number of positive and negative mesotrons, are shown in Fig. 1. The quantities $(1/\lambda)'$ are the "changed" values of the mean life obtained by determining the average slope of the curves for a time interval from 1×10^{-6} to 4.5×10^{-6} sec. This "change" may be as large as 11 percent. From the curves, however, it is clear that in such an investigation particular attention must be paid to very short decay times, especially if the capture constant is large. This consideration applies also to experiments where the ratio of disintegration electrons to stopped mesotrons is measured.

[1] M. Conversi, E. Pancini, and O. Piccioni, Phys. Rev. **71**, 209 (1947).
[2] T. Sigurgeirsson and A. Yamakawa, Phys. Rev. **71**, 319 (1947).
[3] S. Tomonaga and G. Araki, Phys. Rev. **58**, 90 (1940).
[4] E. Fermi, E. Teller, and V. Weisskopf, Phys. Rev. **71**, 314 (1947).
[5] John A. Wheeler, Phys. Rev. **71**, 320 (1947).
[6] N. Nereson and B. Rossi, Phys. Rev. **64**, 199 (1943).

Analysis of the Hyperfine Structure in the Microwave Spectrum of the Symmetric Top Molecule CH_3I*

WALTER GORDY, A. G. SMITH, AND JAMES W. SIMMONS
Department of Physics, Duke University, Durham, North Carolina

June 7, 1947

THE preliminary measurements[1] of the $J=1$ to $J=2$ rotational transition of CH_3I have been repeated at a lower temperature, $-70°C$. As a result of the increased absorption at the lower temperature, additional lines have been observed and a more accurate estimate of relative intensities has been made.[1] The measurements at low temperature revealed that none of the observed lines arises from molecules in excited vibrational states.

A complete analysis of the hyperfine structure resulting from the nuclear quadrupole moment of iodine has now been made. In Fig. 1 the theoretically predicted structure is compared with that experimentally observed.[2] The particular formula used to calculate the positions of the CH_3I lines is that used by Coles and Good[3] to calculate the quadrupole effects in NH_3:

$$T_F = [eQ\partial^2 V/\partial z^2]\cdot[3K^2/2J(J+1)-\tfrac{1}{2}] \cdot[3C(C+1)-4J(J+1)I(I+1)/(2J-1)(2J+3)(2I-1)(2I+3)], \quad (1)$$

where

T_F represents the hyperfine splitting of the rotational energy levels,
$C=F(F+1)-I(I+1)-J(J+1)$,
$F=J+I, J+I-1, \cdots J-I$ (or to $I-J$ when $I\geqq J$),
$I=5/2$, the nuclear spin of iodine, and
$eQ(\partial^2 V/\partial z^2)$ represents the quadrupole coupling coefficient, Q being the quadrupole moment of iodine, V, the molecular potential at the iodine nucleus, and z, the coordinate axis along the C−I bond.

Because of the nuclear effects the K-levels, associated with a given J-level, which otherwise would be degenerate for low J-values, are well separated. This allows two hyperfine patterns for the $J=1$ to $J=2$ transition corresponding to the transitions $0\rightarrow0$ and $1\rightarrow1$ for K. The relative intensities of the lines of a given K-transition can be determined from the intensity rules for atomic fine structure. To determine the relative intensities of the two

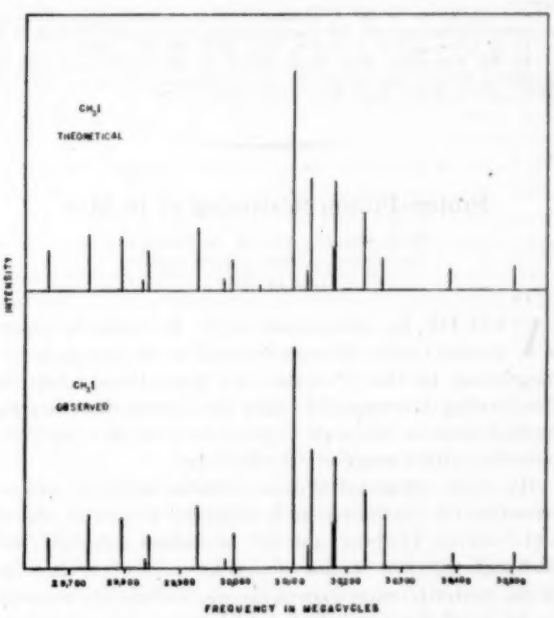

FIG. 1. Theoretical and observed hyperfine structure of the CH_3I spectrum for the rotational transition $J=1$ to $J=2$.

patterns arising from different K-transitions we have applied the theory of Dennison:[4]

$$\frac{\text{Intensity of terms for } K \text{ divisible by 3}}{\text{Intensity of terms for } K \text{ not divisible by 3}} = \frac{4I^2+4I+3}{4I^2+4I}, \quad (2)$$

where I is the nuclear spin of the 3 identical nuclei. Here I is $\frac{1}{2}$ the spin of H; and the intensity ratio is 2:1.

It is apparent from the above analysis that the microwave spectra of symmetric top molecules can be used in two different ways to ascertain nuclear spins. From formula (1) the spin of iodine is determined as 5/2. Formula (2) allows a determination of the spins of the 3 identical atoms on the corners of the tetrahedron.

The quadrupole moment of the iodine nucleus is negative, in agreement with the accompanying ICN measurements. The value of the coupling coefficient $eQ(\partial^2 V/\partial z^2)$, 1520 ± 15[mc], for CH_3I is different from the ICN value, 2070 ± 20 mc. Since Q is the same, this means that the $\partial^2 V/\partial z^2$ factor is significantly different for the two cases and that the C−I bonds in the two molecules are not equivalent. The difference in bonding is also revealed by the widely differing C−I interatomic distances, 2.00A for ICN and 2.13A for CH_3I.

The moment of inertia, I_B, for the ground vibrational state determined from the hypothetical frequency corresponding to no quadrupole-moment splitting of the energy levels is 111.4×10^{-40} g cm.[2] The C−I interatomic distance remains 1.13A, as determined in the previous paper.

* The research described in this report was supported by Contract No. W-28-099-ac-125 with the Army Air Forces, Watson Laboratories, Air Materiel Command.

[1] Walter Gordy, A. G. Smith, and James W. Simmons, Phys. Rev. 71, 917(L) (1947), in the preliminary report a rather large error was made in the estimated intensity of one of the lines. This is corrected in Fig. 1.

[2] For references to the development of the theory of quadrupole-moment interactions see the accompanying note on BrCN and ICN.

[3] D. K. Coles and W. E. Good, Phys. Rev. 70, 979 (1946).

[4] D. M. Dennison, Rev. Mod. Phys. 3, 280 (1931); see also G. Herzberg, *Infrared and Raman Spectra of Polyatomic Molecules*, (D. Van Nostrand Company, Inc., New York, 1945), p. 28.

Proton-Proton Scattering at 10 Mev

R. E. Peierls and M. A. Preston
The University, Birmingham, England
June 19, 1947

A STUDY has been made of R. R. Wilson's experimental results[1] in order to analyze the proton-proton interaction in the ^3P state. We have found that the P-scattering is compatible with the assumption that the nuclear force in this state is given by a 10-Mev repulsive potential with a range of 2.5×10^{-13} cm.

We have compared Wilson's results with the general formulae for scattering with arbitrary phases of the S- and P-waves. The best value for the S-phase is $K_0=52°\ 30'$. Although the cross sections found for angles less than 30° in the center of mass system are not sufficiently accurate to be used for numerical calculations, they definitely show that the P-phase is negative, implying a repulsive force. The value $K_1=-0.8°$ fits the experimental points best, though with the stated experimental errors this figure is an order of magnitude estimate only. Since Wilson states that the absolute values of the cross section are less reliable than their ratios, we have confirmed that, adjusting both K_0 and K_1, a 10 percent change in scale changes K_1 only by about 0.2°.

TABLE I. Relation between P-wave phases and interaction potentials.

Potential	K_1 (calculated)	K_1 (perturbation theory)
−30 Mev	5.6°	2.7°
−20	3.0	1.8
−10	1.3	0.9
0	0.0	0.0
10	−0.8	−0.9
20	−1.3	−1.8
30	−1.8	−2.7

From the S-phase it is possible to calculate for each energy the "relative slope" of the wave function (ratio of the derivative to the function itself) at the limit of the range of the nuclear forces. The derivative of this quantity with respect to energy is directly related to the mean range of forces, without any hypothesis about the shape of the well, and combining the results of Wilson and Creutz at 8 Mev[2] with those at 10 Mev and with previous values at smaller energies, we have obtained for the range of forces the value $2.4_8\times10^{-13}$ cm.

Assuming this range, one can calculate the P-phase shift as a function of the depth of a rectangular potential well (added to the Coulomb potential). The results are given in the second column of Table I.

Since the experimental value of K_1 is −0.8°, we see that the proton-proton interaction in the ^3P state is represented by a repulsive potential of about 10 Mev. The measurements of scattering at 14.5 Mev[4] do not disagree with this result.

Since this conclusion is at variance with the theoretical curve given in the graph in Wilson's note,[1] which indicates a P-phase of about −2.1° for a 10.5-Mev potential, we have checked our calculation by means of perturbation theory using Eq. (8.1) in the paper of Breit, Condon, and Present.[3] This leads to the values in the third column of the table, which all seem to agree with the second column for small potential.

This result is quite compatible with current ideas about nuclear forces. If we assume, as is customary, that the forces are charge-independent and are mainly of the "Majorana" and "Heisenberg" type, we can estimate the depth of well for these two forces from the ^3S and the virtual ^1S level of the deuteron. With the value of the range used above, this leads to a repulsive potential of about 12 Mev for the ^3P state, in quite satisfactory agreement with the present data. However, it is evidently quite possible to admit a certain amount of "Wigner" or "Bartlett" force and some tensor force.

[1] R. R. Wilson, Phys. Rev. 71, 384 (1947).
[2] R. R. Wilson and E. C. Creutz, Phys. Rev. 71, 339 (1947).
[3] G. Breit, E. U. Condon, and R. D. Present, Phys. Rev. 50, 825 (1936).
[4] R. R. Wilson, E. J. Lofgren, J. R. Richardson, B. T. Wright, and R. S. Shankland, Phys. Rev. 71, 560 (1947).

Meson Production

W. HORNING AND M. WEINSTEIN
Department of Physics, University of California, Berkeley, California
June 9, 1947

McMILLAN and Teller[1] have treated the production of mesons by the collision of heavy particles with heavy nuclei. With the essential assumption that the collision time is small compared to nuclear periods, they have used the Fermi-Thomas model to calculate the effect of the presence of many nucleons in depressing the threshold. In obtaining the cross section near threshold, however, they have extrapolated from higher energies, and so overestimated the effect because of the rapid departure of the cross section from a simple power law. On the same theoretical basis, a better estimate can be obtained by carrying through the perturbation calculation near threshold.

The process is third order in the meson field interaction. The heavy particles transfer momentum by exchanging a meson; the final meson is emitted before, during, or after the exchange. In the symmetric scalar theory the matrix elements do not vary appreciably near threshold, and the integral over final states reduces to the volume in phase space in which energy and momentum are conserved and the exclusion principle[1] satisfied. The cross section is

$$\sigma_{\text{scalar}}=0.7(g^2/\hbar c)^3 V(\mu c/\hbar)(\Delta E/\mu c^2)^{7/2}\ \text{cm}^2,$$

where V is the volume of the nucleus, μ the mass of the meson, and ΔE the excess of incident energy over threshold. The result depends strongly on the coupling constant, which is usually taken to be $(g^2/\hbar c)=\frac{1}{10}$.

In the symmetric scalar theory there is considerable contribution to the integral from terms in which the final meson is produced during the exchange of a virtual meson. If the mechanism for heavy particle momentum transfer were a potential interaction, these terms would not be present. The importance of these terms arises directly from the finiteness of the ratio of the meson mass to the mass of the heavy particle. Also, using a potential interaction, the contribution from terms in which scattering precedes meson emission is, at threshold, equal and opposite in sign to that in which scattering follows meson emission. This equality is destroyed if exchange of positive, negative, and neutral mesons scatters the heavy particles. These properties of the meson field distinguish it from the more familiar case of the electromagnetic field, for which a potential description of the interaction is valid.

The energies now available on the Berkeley cyclotron make especially interesting the case of bombardment with neutrons obtained by stripping an energetically homogeneous beam of deuterons. The energy distribution of a beam of neutrons so prepared is governed largely by the distribution in momentum of the neutron relative to the center of gravity of the deuteron and so can be calculated by Fourier analysis of the deuteron wave function assuming an exponential well. In the symmetric scalar theory, for velocities of the center of gravity of the deuteron between 0.8 and 1 times the threshold velocity for the neutron, the total cross section varies from 0.014 to 2.1×10^{-30} cm^2. When the center of gravity moves with threshold velocity, the cross section is that for neutrons at 16 Mev above threshold.

These results, of course, share the large uncertainty in all present meson theories.

We wish to thank Professor J. R. Oppenheimer for guidance in this problem.

[1] W. G. McMillan and E. Teller, Phys. Rev. **72**, 1 (1947).

The Disintegration Scheme of Sc^{46}*

CHARLES PEACOCK AND ROGER G. WILKINSON
Indiana University, Bloomington, Indiana
June 21, 1947

A SMALL 180° beta-ray spectrometer, having good resolution, has been used to study the radiations from Sc^{46}. Samples were produced by bombarding Sc_2O_3 with the external cyclotron deuteron beam. For beta-ray measurements, sources were prepared by precipitating chemically purified Sc_2O_3 on thin mica backing; for gamma-ray determinations, the photoelectrons ejected from a thin lead radiator were studied. Our results indicate that there are two groups of beta-rays of maximum energies 0.36 ± 0.01 Mev and 1.49 ± 0.01 Mev, as well as two gamma-rays of energies 0.88 ± 0.02 Mev and 1.12 ± 0.02 Mev. A comparison of the relative number of particles emitted in each beta-group shows that about 6 percent of the beta-rays belong to the higher energy group. A straight line Fermi plot is obtained for the 0.36-Mev group but not for the less intense, higher energy group, indicating a transition of the forbidden type.

Coincidence absorption experiments were carried out by Mr. Edward T. Jurney and Miss Margaret Ramsey to ascertain the mode of decay. Beta-gamma and gamma-gamma coincidences show conclusively that each beta-ray of the 0.36-Mev group is followed by the cascade emission of the two gamma-rays. Definite results have not yet been obtained from coincidence measurements for the very weak 1.49-Mev group, but it is quite likely from energy considerations that a beta-ray emission of this group is followed by the emission of a 0.88-Mev gamma-ray. A study of the photoelectron lines bears this out to some extent. By using Gray's[3] empirical curve for the variation of the photoelectric absorption coefficient with energy, it is found that the 0.88-Mev gamma is roughly 5 percent more abundant than the 1.12-Mev gamma. It is concluded, therefore, that the decay scheme is that shown in Fig. 1. This has been substantiated in part by Miller and Deutsch.[2]

Further investigation reveals the presence of a weak conversion line at 0.86 Mev. This suggests strongly that the 0.88-Mev gamma-ray is internally converted. Assuming this to be the case, one finds for the conversion coefficient a value of 0.0001. However, a careful check on the decay of the line, and further chemical separation are necessary to verify this conclusion.

It is to be noted that the values of the energies given here differ somewhat from those of Walke[3] and Meitner,[4] who have previously reported a 0.26-Mev beta-ray and a 1.5-Mev gamma-ray. In addition, Walke suggested a 1.5-

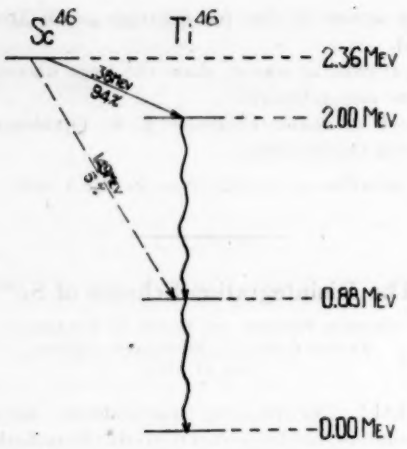

FIG. 1.

Mev beta-ray and a 1.25-Mev gamma-ray. Meitner was unable to find a beta-group with a 1.5-Mev end point and attributed Walke's result to scattering. Careful study has convinced us that the 1.49-Mev group cannot be due to scattering inherent in the geometry of our instrument or to secondary electrons from the source or backing. Further confirmation of this group is found in the fact that it decays with the same half-life as the 0.36-Mev group. The decay has been followed for about one half-life and is found to be approximately 85 days as reported by Walke.

* This research was supported by a grant from the Office of Naval Research.

[1] L. H. Gray, Proc. Camb. Phil. Soc. **27**, 103 (1931).
[2] A. Miller and M. Deutsch, paper presented at Montreal meeting of American Physical Society, abstract to be published in *Physical Review*.
[3] H. Walke, Phys. Rev. **57**, 163 (1940).
[4] L. Meitner, Arkiv f. Mat. Astron., och Fysik, **32A**, No. 6.

The $(4n+1)$ Radioactive Series: The Decay Products of U^{233}

F. HAGEMANN, L. I. KATZIN, M. H. STUDIER,* A. GHIORSO,** AND G. T. SEABORG**
Argonne National Laboratory, Chicago,† Illinois
June 19, 1947

DURING 1944–1946 we studied the chain of decay products of U^{233}, the new isotope of uranium which was first separated and examined (1941–1942) by Seaborg, Gofman, and Stoughton.[1] These decay products, which constitute a substantial fraction of the entire missing, $4n+1$, radioactive series are listed, together with their radioactive properties, in Table I.

The radioactivity of the Tl^{209} has not yet actually been observed, its existence in the chain is inferred from the partial alpha-decay of Bi^{213}. The isotope Pb^{209} has been previously reported, as a result of its production by the (d, p),[2] (n, γ),[3] and (n, p)[3] reactions.

A number of the preceding members of this $(4n+1)$ radioactive series have been previously reported as follows:

$$_{94}Pu^{241} \xrightarrow{\beta^-} {}_{95}Am^{241} \xrightarrow{\alpha} {}_{93}Np^{237} \xrightarrow{\alpha} {}_{91}Pa^{233} \xrightarrow{\beta^-} U^{233}.$$

TABLE I.

Isotope	Type of radiation	Half-life	Energy of radiation (Mev)
$_{90}Th^{229}$	α	7×10^3 yr.	4.85
$_{88}Ra^{225}$	β^-	14.8 days	~0.2
$_{89}Ac^{225}$	α	10.0 days	5.80
$_{87}Fr^{221}$	α	4.8 min.	6.30
$_{85}At^{217}$	α	0.018 sec.	7.00
$_{83}Bi^{213}$	β^- (96%) α (4%)	47 min.	~1.2 (β^-) 6.0 (α)
$_{84}Po^{213}$	α	very short	8.30
($_{81}Tl^{209}$)	(β^-)	?	?
$_{82}Pb^{209}$	β^-	3.3 hr.	0.7
$_{83}Bi^{209}$	stable		

The 27.4-day Pa^{233} was first reported by Meitner, Strassmann, and Hahn,[4] and the doubts as to this isotopic assignment which later arose as a result of the discovery of fission were cleared up by the work of v. Grosse, Booth, and Dunning[5] and Seaborg, Gofman, and Kennedy.[6] The 2.25×10^6 year Np^{237} was first identified by Wahl and Seaborg,[7] while Pu^{241} and 500-year Am^{241} were first reported by Seaborg, James, and Morgan.[8] Also of interest are two previously reported beta-emitting radioactive isotopes, 23-minute Th^{233} [9] from the reaction Th^{232} (n, γ) and 7-day U^{237} [10,11] from the reaction U^{238} $(n, 2n)$, which may be referred to as "collateral" members of the series.

As the name for the $(4n+1)$ radioactive decay family we suggest "neptunium" series or family; thus the longest-lived member would give its name to the family in a manner similar to the naming of the uranium and thorium decay series.

Another independent study of the decay products of U^{233} was carried on simultaneously by A. C. English, T. E. Cranshaw, P. Demers, J. A. Harvey, E. P. Hincks, J. V. Jelley, and A. N. May of the Division of Atomic Energy of the National Research Council of Canada, which has resulted in essentially similar findings.[12]

* Present address, Institute of Nuclear Studies, University of Chicago, Chicago, Illinois.
** Present address, Radiation Laboratory, University of California, Berkeley, California.
† Work performed under auspices of Manhattan District, Contract Number W-7401-eng-37.
[1] G. T. Seaborg, J. W. Gofman, and R. W. Stoughton, Phys. Rev. **71**, 378 (1947).
[2] R. L. Thornton and J. M. Cork, Phys. Rev. **51**, 383 (1937).
[3] W. Maurer and W. Ramm, Zeits. f. Physik **119**, 602 (1942).
[4] L. Meitner, F. Strassmann, and O. Hahn, Zeits. f. Physik **109**, 538 (1938).
[5] A. v. Grosse, E. T. Booth, and J. R. Dunning, Phys. Rev. **59**, 322 (1941).
[6] G. T. Seaborg, J. W. Gofman, and R. W. Stoughton, Phys. Rev. **59**, 321 (1941).
[7] A. C. Wahl and G. T. Seaborg, reported in Chem. Eng. News **23**, 2190 (1945).
[8] G. T. Seaborg, R. A. James, and L. O. Morgan, reported in Science **104**, 379 (1946) and Chem. Eng. News **25**, 358 (1947).
[9] E. Fermi, E. Amaldi, O. D'Agostino, F. Rasetti, and E. Segrè, Proc. Roy. Soc. **A146**, 483 (1934).
[10] Y. Nishina, T. Yasaki, H. Ezoe, K. Kimura, and M. Ikawa, Phys. Rev. **57**, 1182 (1940).
[11] E. M. McMillan, Phys. Rev. **58**, 178 (1940).
[12] English, Cranshaw, Demers, Harvey, Hincks, Jelley, and May, Phys. Rev. **72**, 253 (1947).

The $(4n+1)$ Radioactive Series*

A. C. ENGLISH, T. E. CRANSHAW, P. DEMERS, J. A. HARVEY, E. P. HINCKS, J. V. JELLEY, AND A. N. MAY
Division of Atomic Energy, National Research Council of Canada, Chalk River, Ontario, Canada
June 20, 1947

THE three radioactive series known to occur naturally are characterized by members whose mass numbers are represented by the integers $4n$ (thorium series), $(4n+2)$ (uranium series), and $(4n+3)$ (actinium series). While the existence of a fourth series comprising the "missing" radioactive $(4n+1)$-isotopes has been postulated at various times,[1-4] early searches which were made for its members in natural minerals gave negative results.[2,3] More recently Wahl[5] has reported the observation of a line at mass 237 in mass spectrograms from certain minerals, and attributes it to a member of the new series. Since 1935 α- and β-active $(4n+1)$-species have been produced by artificial transmutation, and among the heavy elements almost a dozen have been reported in the literature. (See for example Seaborg's Table of Isotopes[6] and his recent review.[7]) In 1942 Seaborg, Gofman, and Stoughton[8] discovered and investigated the properties of U^{233}, the long-lived α-emitting product of the β-decay of Pa^{233} and the third member of a $(4n+1)$-chain which starts with Th^{233}.

The investigation of the ensuing route taken by the chain which was undertaken by the authors started with a search for the decay products of milligram amounts of U^{233}. A chemical extraction of radium resulted in an α-activity which decayed in a complex manner with periods of the order of days. Direct evidence for a chain including at least four α-emitters was first provided by the observation of 4-track stars in a photographic emulsion which had been soaked in the radium solution. Subsequent measurement of decay periods and α-particle energies showed that these formed part of a new disintegration series, distinct from the thorium, the uranium, and the actinium series. Making use of both chemical and physical evidence it has been possible to deduce the main route of the series, which, after the α-decay of U^{233}, passes through seven new nuclear species, and ends with the known[9] 3.3-hr. β-decay of Pb^{209} to stable Bi^{209}.

The path of the series which passes through isotopes of the type $(4n+1)$ is shown in Fig. 1. Both U^{233} and its daughter Th^{229} are fairly long-lived, and, as far as this work was concerned, it has been convenient to treat the former as the parent of the series. Since the radium isotope is β-active, the main chain does not include an emanation followed by the usual "A" and "B" products. Instead, the main α-sequence starts with Ac^{225}, and the series thus includes isotopes of the recently named elements, francium $(Z=87)$ and astatine $(Z=85)$. The end product is Bi^{209} and not a lead isotope as in the case of the other three series. (It is interesting to note that the route is almost exactly that predicted by Turner[4] in 1940.) A 2 percent α-branching of Bi^{213} was detected, but the disintegration of Tl^{209} could not be investigated because of the low activity. A search was made for α-branching of Ra^{225} but none could be found. it is probably less than one percent.

The disintegration properties of the members of the

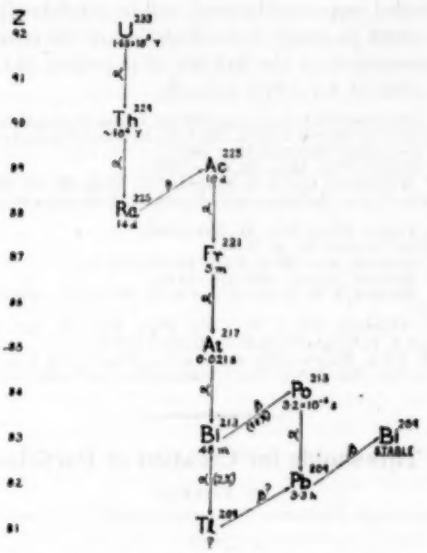

FIG. 1. The path of the $(4n+1)$-series following U^{233}.

series are summarized in Table I. Previously published data included for completeness are shown in light-faced type, while results obtained by the authors are in heavy type. The α-particle energies were measured with a grid-type ionization chamber, biased amplifier, and pulse analyzer. The 21-millisecond half-life of At^{217} was measured by photographing pulses on an oscilloscope with a triggered time base, and the 3.2-microsecond half-life of Po^{213} by a coincidence experiment using a variable resolving time.

The α-emitters of the series are found to lie on a good straight line in a Geiger-Nuttall plot (logarithm of disintegration constant against logarithm of α-particle energy), with the exception of Po^{213} which falls well below the line in the manner of the very short-lived C' bodies. This line lies between and is parallel to those representing the $4n$ and $(4n+3)$-series.

The authors feel that the name "Neptunium Series," after the longest-lived known $(4n+1)$-member, Np^{237},[7] should be adopted.

We wish to thank those members of the Montreal Laboratory who gave us assistance during the above investigation, and especially Professor F. A. Paneth and Dr. B. L. Goldschmidt whose interest and advice were invaluable.

TABLE I. The $(4n+1)$ radioactive series.

Species	Type of radiation	Half-life	Energy of particles in Mev α	Energy of particles in Mev β
$_{92}U^{233}$	α[10]	1.63×10^5 y[10]	4.825 ±0.003	
$_{90}Th^{229}$	α	$\{5\times10^3$ y[10]; ~10^4 y$\}$	~5	
$_{88}Ra^{225}$	β	14 d		<0.05
$_{89}Ac^{225}$	α	10 d	5.801 ±0.010	
$_{87}Fr^{221}$	α	5 m	6.31 ±0.02	
$_{85}At^{217}$	α	2.1×10^{-2} s	7.023 ±0.010	
$_{83}Bi^{213}$	α(2%), β(98%)	46 m	5.86 ±0.03	~1.3
$_{84}Po^{213}$	α	3.2×10^{-6} s	8.336 ±0.005	
$_{82}Pb^{209}$	β[9]	3.3 h[9]		0.70[9]
$_{83}Bi^{209}$	stable			

A detailed report of the work will be published later.

Note added in proof: A recalculation of the results from the measurement of the half-life of polonium 213 gives a better value of 4.4×10^{-6} seconds.

* The work reported here was carried out in the Montreal Laboratory of the Division of Atomic Energy, National Research Council of Canada, between November 1944 and May 1946.

[1] A. S. Russell, Phil. Mag. 46, 642 (1923).
[2] W. P. Widdowson and A. S. Russell, Phil. Mag. 48, 293 (1924).
[3] I. Curie, H. von Halban, and P. Preiswerk, J. de phys. et rad. 6, 361 (1935).
[4] L. A. Turner, Phys. Rev. 57, 950 (1940).
[5] W. Wahl, Science 93, 16 (1941).
[6] G. T. Seaborg, Rev. Mod. Phys. 16, 1 (1944).
[7] G. T. Seaborg, Science 104, 379 (1946).
[8] G. T. Seaborg, J. W. Gofman, and R. W. Stoughton, Phys. Rev. 71, 378 (1947).
[9] R. L. Thornton and J. M. Cork, Phys. Rev. 51, 383 (1937); K Fajans and A. F. Voigt, Phys. Rev. 60, 619 (1941).
[10] J. M. Cork, *Radioactivity and Nuclear Physics* (D. Van Nostrand Company, Inc., New York, 1947), information attributed to G. T. Seaborg.

Thresholds for Creation of Particles

H. FESHBACH
Massachusetts Institute of Technology, Cambridge, Massachusetts
AND
L. I. SCHIFF*
University of Pennsylvania, Philadelphia, Pennsylvania
June 9, 1947

IN the design of very high energy particle accelerators, it is of interest to know the smallest energy that a bombarding particle need have in order that a given combination of particles can be created in a collision. The calculation of such a threshold on the basis of purely energetic considerations, under the assumption that a mechanism of creation exists, was pointed out by Dr. M. S. Livingston to be a straightforward application of relativistic dynamics. This note presents the pertinent formulas, and discusses some limitations on their application.

We consider a collision in which a particle of rest mass, m_1, and kinetic energy, E, collides with an initially stationary particle of rest mass, m_2, and new particles of aggregate rest mass M (in addition to m_1 and m_2) are created. E is smallest when all particles are at rest after the collision in the center of mass-coordinate system (in which the center of mass of m_1 and m_2 is at rest before the collision). Application to this problem of the relativistic relation between energy and momentum leads to an expression for the threshold kinetic energy:

$$E=Mc^2(m_1+m_2+\tfrac{1}{2}M)/m_2. \qquad (1)$$

Equation (1) can be solved for Mc^2, which is the energy that is available in the center of mass system for particle creation, reactions, etc.:

$$Mc^2=[2m_2c^2E+(m_1+m_2)^2c^4]^{\frac{1}{2}}-(m_1+m_2)c^2.$$

In the non-relativistic limit ($E\ll m_1c^2$ and m_2c^2), this reduces to the usual expression $m_2E/(m_1+m_2)$.

If the colliding particles are protons ($m_1=m_2\equiv m$) and a pair of neutrons or a positive and negative proton are created ($M=2m$), Eq. (1) shows that the threshold energy is 6 $mc^2\leqq5.6$ Bev. If an electron or a photon ($m_1\leqq0$) collides with a proton, the threshold for nucleon-pair production is 4 $mc^2\leqq3.7$ Bev. The corresponding thresholds for meson-pair production are higher than would be expected from non-relativistic theory by about 5 percent in the case of protons and about 10 percent in the case of electrons or photons.

Equation (1) indicates that a considerable reduction in the thresholds for nucleon-pair production would occur if the target particle were a heavy nucleus rather than a proton. This is actually true only if the target nucleus remains intact after the collision. We now show that the transfer of a large amount of momentum to the nucleus is very likely to break it up. The recoil momentum q of m_2 is given by:

$$(q/c)^2=\frac{2M(m_1+\frac{1}{2}M)(m_2+\frac{1}{2}M)(m_1+m_2+\frac{1}{2}M)}{(m_1+m_2+M)^2}.$$

In the case of a heavy nucleus ($m_2\ll m_1$, $m_2\ll M$), $q\sim mc$ for nucleon production either by protons or electrons. The region in which the creation process takes place has dimensions of the order of $\hbar/mc\sim10^{-14}$ cm. This is so small that only one of the constituent nucleons of the target nucleus is likely to be involved. Thus the nucleus remains intact only if this nucleon transfers the momentum q to the remainder of the nucleus.

The fraction of the events in which this occurs is of the order of the fraction of all collisions between a nucleon of momentum q, and a nucleus in which the nucleon is scattered at a large angle and the nucleus absorbs most of the momentum. Such a scattering process can be treated by the Born approximation. The cross section for back scattering is roughly equal to

$$(m^2/\hbar^4)\left|\int e^{i\mathbf{k}\cdot\mathbf{r}}V(\mathbf{r})d\mathbf{r}\right|^2, \quad \text{where} \quad k\sim(q/\hbar), \qquad (2)$$

and the total scattering cross section is approximately the geometrical nuclear cross section R^2, where R is the nuclear radius; here, $V(\mathbf{r})$ is the interaction potential between nucleon and nucleus. Equation (2) is roughly equal to $(m\bar{V}/\hbar^2)^2(\hbar/q)^6\sim(1/R_0^4)(\hbar/q)^6$, where $\bar{V}$ is the average nuclear potential, and R_0 is the range of nuclear forces. We are thus led to expect that the target nucleus remains intact in about $(\hbar/qR_0)^4(\hbar/qR)^2\sim10^{-7}$ of those collisions in which nucleon creation occurs, and is energetically possible with a proton target (the corresponding fraction for meson creation is considerably larger). This indicates that the effect is extremely improbable, and especially difficult to observe since newly created neutrons (although perhaps not negative protons) would tend to be masked by fragments of nuclei broken up by ordinary collisions.

McMillan and Teller[1] have pointed out that the kinetic energy of the nucleons inside a nucleus lowers the threshold. If this energy is assumed to be not greater than 30 Mev, it can be shown that the thresholds for nucleon-pair production are reduced to 4.1 Bev for protons and 2.6 Bev for electrons or photons. Since very few of the nucleons have the maximum kinetic energy, the cross section will be small just above the threshold. A simple estimate based on the Thomas-Fermi model indicates that the effective threshold is half-way between the figures given here and those given in the third paragraph. However, the difficulty of observing the effect in the presence of a background of nuclear fragments might make it worth while to work with a hydrogen target at the higher thresholds.

* Now at Stanford University.

[1] W. G. McMillan and E. Teller, Phys. Rev. 72, 155(A) (1947).

The Mean Life of Mesotrons at an Altitude of 11,500 Ft.

HAROLD K. TICHO
Department of Physics, University of Chicago, Chicago, Illinois
June 23, 1947

IN 1943 Nereson and Rossi[1] described an experiment for determining the mean life of cosmic-ray mesotrons at sea-level in various solid absorbers. The purpose of this letter is to report on a measurement of the mean life which was carried out at Climax, Colorado (11,500 ft. above sea-level) to determine whether the mean life is altitude-dependent. The method consisted of a direct comparison of the lifetime of each individual mesotron, stopping in a 10-cm Al absorber with the period of vibration of an accurately calibrated quartz crystal.[2] Figure 1 shows the counter-tube assembly, and the integral-decay curve obtained by this method. The upper set of points between 0.05 and 0.5 μsec. represents the total number of delays observed with the Al absorber in its place, whereas the lower set was obtained by subtracting all delays occuring with the Al absorber removed. When delays of this kind (produced by natural delays in the counters accompanying a simultaneous event) are subtracted, the curve remains a true exponential to time delays as small as 0.05 μsec. This fact indicates that if any contribution to the decay curve of delays arising from the disintegration of of short-life ($\tau_0 < 10^{-8}$ sec.) mesotrons should exist, it must be quite negligible for time intervals larger than 0.05 μsec.

The data in Fig. 1 were analyzed according to the statistical method of Peierls[3] which permits an evaluation of the mean life and its standard deviation from a set of individual lifetime determinations. The value obtained by this method for the mean life of mesotrons at rest is $\tau_0 = 1.78 \pm 0.10$ μsec. For the calculation of the standard deviation the points between 0.05 and 0.5 μsec. were omitted because of the natural delays which occur occasionally in the G. M. counters in that interval. Assuming that the mean range of the disintegration electrons, having an energy of 50 Mev, is 7 cm in Al, the ratio of disintegration electrons to mesotrons stopped in the absorber is calculated to be 0.50 ± 0.06.

The value for the mean life determined at Climax is not in complete agreement with that obtained by Nereson and Rossi[1] at sea-level. These authors compiled their best value

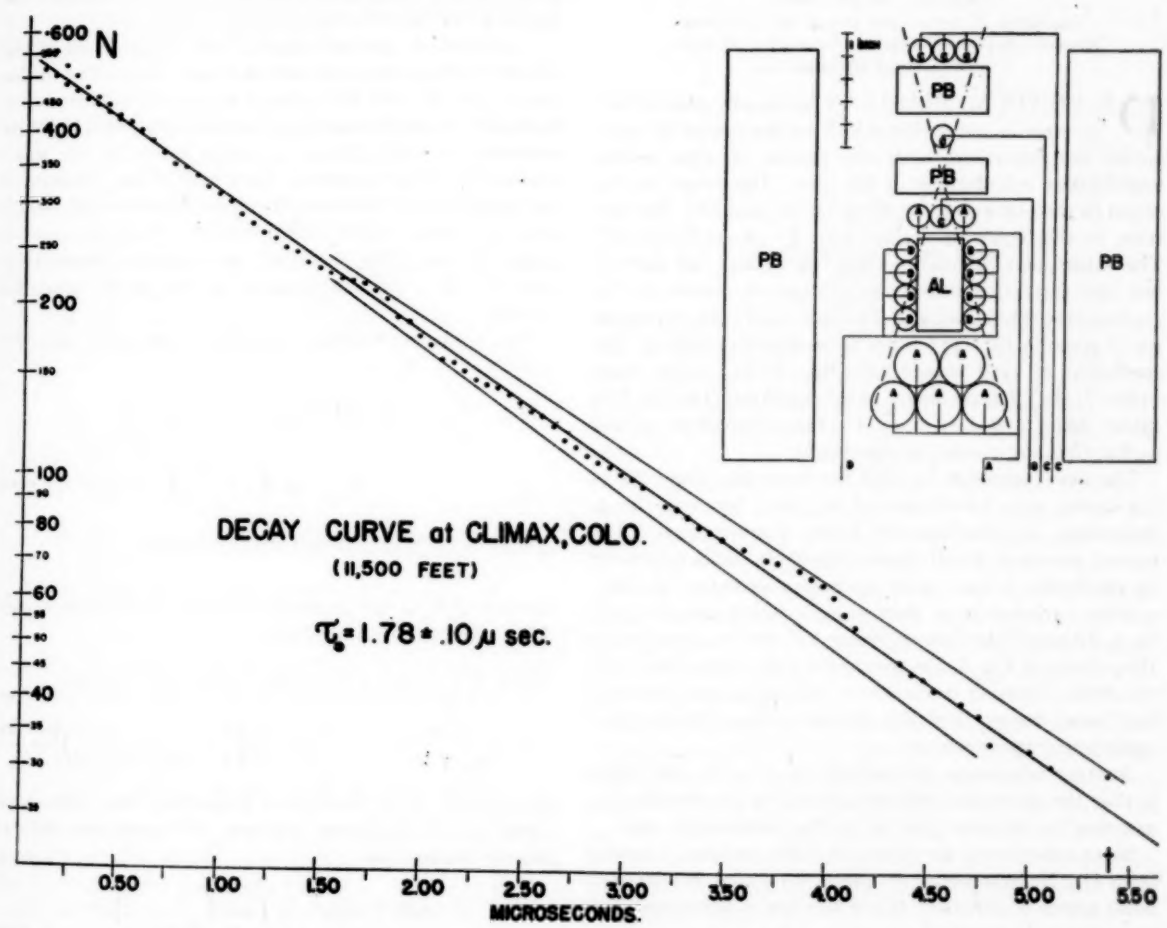

FIG. 1. The counter-tube assembly and the integral-disintegration curve obtained at Climax, Colorado. The upper set of points in the time interval from 0.05 to 0.5 μsec. is due to counter-pulse delays accompanying simultaneous events.

for the mean life $\tau_0 = 2.15 \pm 0.07$ μsec. by adding all their data collected in various materials. It seems difficult to explain the difference between the two values by a systematic error in the experimental method since the disintegration curve appears linear, and hence the error would have to increase *linearly* with the time interval which has actually been recorded. A shortening of the mean life, however, may be due to a contribution by negative mesotrons decaying in the absorber. The following letter explains why such a contribution might result in an apparent change of the mean life.

The author wishes to express his gratitude to Dr. Walter O. Roberts of the Fremont Pass Station of the Harvard College Observatory at Climax, and to the Climax Molybdenum Company for making available the facilities required for carrying out this investigation.

[1] N. Nereson and B. Rossi, Phys. Rev. **64**, 199 (1943).
[2] H. Ticho, Rev. Sci. Inst. **18**, 271 (1947).
[3] R. Peierls, Proc. Roy. Soc. **149**, 467 (1935).

Errata: The Double Focusing Beta-Ray Spectrometer

[Phys. Rev. **71**, 681 (1947)]

FRANKLIN B. SHULL AND DAVID M. DENNISON
Randall Laboratory of Physics, University of Michigan, Ann Arbor, Michigan

DR. EDWIN M. McMILLAN has kindly pointed out an error in our article which he discovered by comparing our equations with the results of some earlier unpublished calculations of his own. The error has its origin in the expression for H_z given on page 682. The last term in this equation should read $[-(\beta-\alpha/2)z^2H_0/a^2]$. The subsequent calculations are, we believe, all correct, but this correction introduces changes in certain of the coefficients in the equations. The final result, the expression for r^* given in Eq. (25), must be modified as follows. The coefficient of $(\delta z)^2$ should be $[(4\beta-3)/3a]$ rather than $[(4\beta-2)/3a]$. The coefficient of ϕ_z^2 should be $[(16\beta/3-2)a]$ rather than $[(16\beta/3-2/3)a]$. The remaining terms, as well as Eq. (26), are correct as they stand.

The new expression for r^* is less favorable, since the ϕ_r defocusing may be eliminated for $\beta=\frac{1}{4}$ but not the ϕ_z defocusing. To eliminate the latter, β must equal $\frac{3}{8}$. The correct choice of β will depend upon the baffle system to be employed. It may often be more convenient to allow a wider variation in ϕ_r than in ϕ_z in which case β should be $\frac{1}{4}$. Although the focused image will not be as perfect as that shown in Fig. 1, the conclusion still stands that, with the double focusing spectrometer, the image may be made both more intense and also sharper than with the usual semicircular spectrometer.

Another advantage pointed out to us by Dr. McMillan is that the dispersion ($p\delta r/r\delta p$ where p is the electron momentum) is twice as great as in the semicircular case.

Since submitting our paper we have received a reprint from Dr. N. Svartholm[1] in which the image formed by a point source is discussed. His results are in agreement with our corrected equations.

[1] N. Svartholm, Ark. f. Mat. Astron. och Fys. **33A** [24] (1946).

On the Magnetic Exchange Moment for H^3 and He^3

FELIX VILLARS
Swiss Federal Institute of Technology, Zurich, Switzerland
June 23, 1947

RECENT experiments of Bloch and others[1] on the magnetic moment of H^3 gave the value 1.0666 for the ratio of the magnetic moments of H^3 and proton. Assuming a value of 2.789 n.m. for $\mu(p)$, we find $\mu(H^3)=2.975=\mu(p)+0.186$ n.m. This result seemed to be in contradiction to the results of theoretical investigations of Sachs and Schwinger,[2] which require $\mu(H^3)\leqslant\mu(p)$, unless very artificial assumptions on the ^2P and ^4P admixtures to the S-component of the ground-state eigenfunction are made.[3]

However, Schwinger's ansatz[4] for the nuclear Hamiltonian does not allow for taking into account the charge-exchange phenomena connected with the interaction of nucleons. On the other hand, it is well known that these phenomena give rise to exchange moments.[5] Whereas the magnetic exchange dipole moment vanishes in the case of the deuteron (on account of the symmetry properties of the de-eigenfunction), this is not the case for H^3 and He^3, provided that the quantum number T of the total isotopic spin is $\frac{1}{2}$. (It vanishes for $T=\frac{3}{2}$.)

A calculation has been carried out on the basis of the symmetrical pseudoscalar meson theory. According to this theory, the H^3 and He^3 ground states are doublet states both with respect to spin and isotopic spin ($S=T=\frac{1}{2}$) and symmetrical with respect to permutations of the space coordinates of the particles, if we neglect the influence of the tensor force. The latter is responsible for small admixtures of higher states, the influence of which may be neglected here, since there is a non-vanishing expectation value of the exchange moment in the above described S state.

The exchange moment operator is given by $M=M^{(1)}+M^{(2)}$:

$$M^{(1)}=-\frac{ef^2}{2}\mu\sum_{A<B}(\tau^A\times\tau^B)_z\Big\{z^{AB}(z^{AB}\cdot\sigma^A\times\sigma^B)\Big/ r_{AB}^2\cdot\Big(1+\frac{1}{\mu r_{AB}}\Big)-(\sigma^A\times\sigma^B)\Big\}e^{-\mu r_{AB}},$$

$$M^{(2)}=+\frac{ef^2}{2}\mu^2\sum_{A<B}(\tau^A\times\tau^B)_z\cdot(z^A\times z^B)\cdot V(AB),$$

where $V(AB)$ is the interaction energy of the nucleon pair AB in the pseudoscalar theory:

$$V(AB)=\Big\{\tfrac{1}{3}(\sigma^A\sigma^B)+(3(\sigma^Az^{AB})(\sigma^Bz^{AB})/r_{AB}^2-(\sigma^A\sigma^B))\times\Big(\frac{1}{3}+\frac{1}{\mu r_{AB}}+\frac{1}{(\mu r_{AB})^2}\Big)\Big\}\frac{e^{-\mu r_{AB}}}{r_{AB}}.$$

On account of its symmetry properties, the expectation value of $M^{(2)}$ vanishes, whereas $M^{(1)}$ gives, in units of nuclear magnetons

$$M^{(1)}=(8/3)\gamma(f\mu)^2\cdot T_z\int dv\varphi^2\Big(\frac{1}{\mu r_{AB}}-2\Big)e^{-\mu r_{AB}}.$$

(γ is the ratio of the masses of proton and meson: $\gamma\leqq10$,

$T_3+\frac{1}{2}$ is the charge of the nucleus, φ the orbital part of the ground state eigenfunction, $z^{AB}=z^A-z^B$, $r_{AB}=|z^{AB}|$, $(f\mu)$ the dimensionless coupling constant of the meson field: $(f\mu)^2\cong\frac{1}{16}$, and $\mu=Mc/\hbar$.) A rough evaluation of $M^{(1)}$ has been made with the help of gauss functions $\varphi\sim\exp(-\alpha r^2)$, $r^2=\frac{1}{2}(r_{12}^2+r_{13}^2+r_{23}^2)$, with the following result (J is the volume integral in M).

μ^2/α	1.0	1.5	2.0	2.5	0.75
J	−0.14	−0.21	−0.23	−0.23	−0.058
M	+0.18	+0.28	+0.31	+0.31	+0.077

Thus, with reasonable values of γ, $(f\mu)$, and μ^2/α we obtain both the right sign and right order of magnitude of the correction to be added.

It should be noted that for He^3 the correction is equal in magnitude but opposite in sign. We would, therefore, expect for He^3 a total magnetic moment $\mu\cong\mu(N)-M\cong-2.1$ n.m. Experimental evidence would be very interesting.

[1] F. Bloch, A. C. Graves, M. Packard, and R. W. Spence, Phys. Rev. **71**, 373 and 551 (1947); H. L. Anderson and A. Novick, Phys. Rev. **71**, 372 (1947).
[2] R. G. Sachs and J. Schwinger, Phys. Rev. **70**, 41 (1946).
[3] R. G. Sachs, Phys. Rev. **71**, 457 (1947).
[4] E. Gerjuoy and J. Schwinger, Phys. Rev. **61**, 138 (1942).
[5] S. T. Ma and F. C. Yu, Phys. Rev. **62**, 118 (1942); C. Møller and L. Rosenfeld, Kungl. Danske Vidensk. Selsk. **20**, No. 12 (1943); W. Pauli and S. Kusaka, Phys. Rev. **63**, 400 (1943).

Errata: Theory of Dipole Interaction in Crystals

[Phys. Rev. **70**, 954 (1946)]

J. M. Luttinger and Laszo Tisza
Research Laboratory of Electronics, Massachusetts Institute of Technology, Cambridge, Massachusetts

SEVERAL misprints have been noticed in the above paper. These are the following:

P. 956, line 7 should read p_x^ν, p_y^ν, p_z^ν, $\nu=1, \cdots, 8$.

P. 956, Eq. 7 should read

$$U=-\tfrac{1}{16}\sum_{\mu,\nu=1}^{8}\sum_{xy}F_{\mu\nu}{}^{xy}p_x{}^\mu p_y{}^\nu. \qquad (7)$$

P. 957, Eq. 12 should read

$$Z_i=(-)^{\alpha_i l_1+\beta_i l_2+\gamma_i l_3}\quad i=1, \cdots, 8. \qquad (12)$$

P. 960, last equation. The denominator should be raised to the 5/2 power.

P. 960, Table II, first line should read

$$f_2=-\tfrac{1}{2}[S_x(0, \tfrac{1}{2}, \tfrac{1}{2})-S_x(\tfrac{1}{2}, 0, 0)].$$

P. 960. The small table under Table II contains several inversions and a sign error. It is correctly given by:

$S_x(\frac{1}{2}$	0	$0)=-15.040$		$S_y(0$	$\frac{1}{2}$	$\frac{1}{2})=31.521$	
$S_x(0$	$\frac{1}{2}$	$\frac{1}{2})=$	4.334	$S_y(\frac{1}{2}$	$\frac{1}{2}$	$\frac{1}{2})=$	2.599
$S_y(\frac{1}{2}$	$\frac{1}{2}$	$\frac{1}{2})=$	10.620	$S_z(0$	$\frac{1}{2}$	$\frac{1}{2})=12.329$	

Lastly, in Table V, p. 963, lines 4 and 5 should be exchanged (which moves a minus sign down one line), and line 12 should read $-2X_8-Y_8+Z_8$.

The authors would like to thank Professor L. W. McKeehan for having pointed out several of the above misprints.

Burst Production by Penetrating Cosmic-Ray Particles*

Herbert Bridge, Bruno Rossi, and Robert Williams
Laboratory for Nuclear Science and Engineering, Massachusetts Institute of Technology, Cambridge, Massachusetts

May 23, 1947

A TRAY of Geiger-Mueller tubes, G, and an ionization chamber, C, were arranged, respectively, above and below a lead block 6 in. thick, as shown in Fig. 1. The

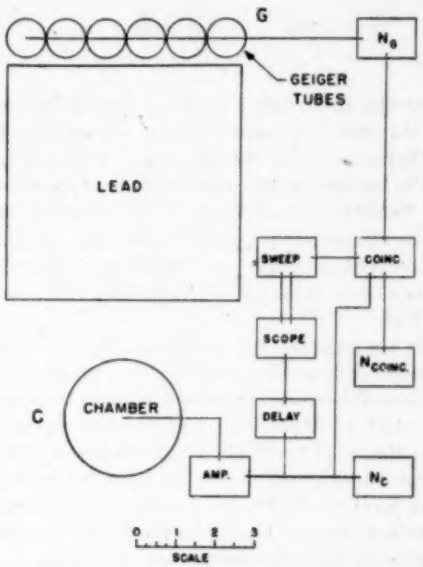

FIG. 1. Schematic arrangement of equipment.

Geiger-Mueller tubes were connected in parallel. Each was 1 in. in diameter and 20 in. long. The chamber was cylindrical in shape, 3 in. in diameter, 20 in. long, and was filled to 7.3 atmospheres with highly purified argon so that "fast" electron pulses would be recorded quantitatively. The pulses of the ion chamber were applied to the vertical deflecting plates of a cathode-ray oscilloscope through a linear amplifier and a delay line. The oscilloscope was provided with a fast horizontal sweep (5 microseconds per inch) which was triggered by the coincidences between the (undelayed) pulses of the ionization chamber and the pulses of the Geiger-Mueller tubes. The oscilloscope screen was photographed on a moving film. The individual counting rates of the chamber (N_c) and of the Geiger-Mueller tubes (N_g) were also recorded.

A polonium source of α-particles was placed on the wall of the chamber for the purpose of calibration. The resolving time $(\tau_1+\tau_2)$ for the selection of coincident pulses was determined both by direct observation of the pulses on the oscilloscope screen and by counting chance coincidences between pulses in the Geiger-Mueller tubes and α-particle pulses in the ionization chamber. Its value was found to be 50 microseconds.

For the main experiments, the circuits were adjusted so as to record only pulses greater than 1.1 times a Po

α-particle pulse. (The α-particle pulse corresponds to about 35 fast particles incident on the chamber from the vertical direction.) Measurements were taken at sea level in a light wooden building, and at 30,000 feet in the rear cabin of a B-29. The results are as shown in Table I.

TABLE I. Results of measurements.

Altitude (feet)	Time of observation (hours)	N_s (Counts in the chamber, per hour)	N_g (Counts in the G. M. counter tray, per hour)	Coincidence (per hour)	Chance coincidence (per hour) $N_s N_g(\tau_1+\tau_2)$
0	292	1.94	0.72×10^5	0.25	0.002
30,000	1.6	500	14.7×10^5	96	10

At both elevations only a small fraction of the coincident records obtained is accounted for by chance coincidences. We also believe that air showers have a negligible effect on our results because of the small number of showers with a particle density high enough to be recorded in these measurements, and thus conclude that most of the coincidences observed are caused by ionizing particles capable of producing a burst in the ionization chamber after traversing 6 in. of lead.

It does not seem possible to assume that these particles are electrons since an electron capable of producing a sufficiently large shower under 6 in. of lead must have an energy in excess of 10^{12} ev. Hence they must be of the "penetrating" type. On the other hand, the total number of penetrating cosmic-ray particles only increases by a factor of about 6 from sea level to 30,000 feet, while the observed effect increases by a factor of several hundreds. We are thus led to the conclusion that the penetrating component at 30,000 feet contains particles which are much more effective in producing bursts than are ordinary mesons.

As has been shown by one of us,[1] the shape of the pulse from an ionization chamber enables one to decide in most cases whether the pulse is caused by heavily ionizing particles from a disintegration or by an electron shower. Classification of our records according to pulse shape gives the results shown in Table II.

TABLE II. Classification of records according to pulse shape.

Altitude (feet)	Percent of pulses from: Showers	Heavily ionizing particles	Uncertain origin
0	78	—	22
30,000	57	30	13

It is likely that most of the showers observed at sea level are initiated by collision or radiation processes of ordinary mesons. These processes can only account for a very small fraction of the showers observed at 30,000 feet. It is natural to assume that the majority of the showers at this altitude are produced by electrons or photons generated by primary cosmic-ray particles (protons?) either directly or through the intermediary of short-lived mesons.

At 30,000 feet our data show evidence for nuclear disintegrations produced by penetrating ionizing rays. It is likely that most of the particles responsible for this effect are also primary "protons" (even though some of them may be negative mesons undergoing nuclear capture after being brought to rest).

The shower production by primary cosmic-ray particles, for which evidence is found in the present experiments, may account for that part of the soft component which cannot be explained by the disintegration of ordinary mesons.[2]

* The research described in this letter was supported partially by Contract N5 ORI-78, U. S. Navy Department, Office of Naval Research. The B-29 used for the measurements at high altitude was provided by the U. S. Army Air Force.

[1] H. Bridge, Phys. Rev. 72, 172(A) (1947).
[2] H. Bridge and B. Rossi, Phys. Rev. 71, 379 (1947).

Erratum: The Band Theory of Graphite

[Phys. Rev. 71, 622 (1947)]

P. R. WALLACE
National Research Council of Canada, Chalk River Laboratory, Chalk River, Ontario

Figure 13, the plot of the trend of $\rho\perp/\rho\parallel$ (ratio of resistivity *across* graphite planes to that *in* the planes),

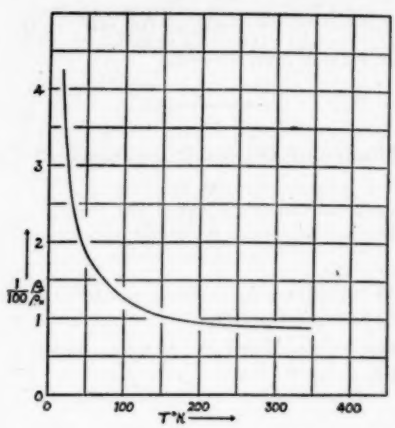

FIG. 1.

appeared in the paper in incorrect form. The corrected graph is as follows:

Nuclear Moments of the Bromine Isotopes*

S. B. BRODY, W. A. NIERENBERG, AND N. F. RAMSEY
Columbia University, New York, New York

June 13, 1947

THE molecular beam[1] resonance method has been used to study the radiofrequency spectrum[2] of Br^{79} and Br^{81} in CsBr and LiBr. Typical results are shown in Fig. 1.

The positions of the resonance minima are the same in CsBr and LiBr, indicating that the minima are due to the bromine isotopes. The positions of the resonance minima shift proportionately to the magnetic field. This is the usual criterion[1] for assuming that the observed resonance frequency is at the Larmor frequency of the nucleus in the external magnetic field, which gives for the gyromagnetic

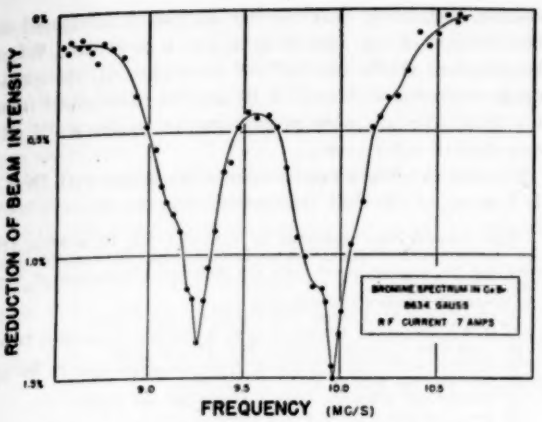

FIG. 1. Reduction in beam intensity as a function of oscillator frequency.

ratio

$$g_I = h\nu/\mu_N H, \qquad (1)$$

where μ_N is the nuclear magneton.

As will be discussed in a later paper by one of us (N.F.R.), there are certain special circumstances in the case of very large nuclear electrical quadrupole-moment interactions when the frequency of an observed resonance minimum may be double that of Eq. (1). This possibility is excluded in the present experiments by comparison with optical fine-structure experiments of Tolansky[3] interpreted by Schmidt[4] which indicate a value of 2.6 nuclear magnetons for bromine in fair agreement with our observed values using Eq. (1) and in marked disagreement if values of the frequency double that given in (1) are used. Furthermore, the integrated intensity of the resonance minima in Fig. 1 is greater than would be expected for a resonance of double the frequency of Eq. (1) and is approximately correct for a normal resonance.

With (1) being used to determine the gyromagnetic ratios and with the spins of the bromine isotopes taken to be[4,5] $\frac{3}{2}$, the magnetic moments of the bromine isotopes are 2.110 ± 0.021 and 2.271 ± 0.023 nuclear magnetons. Since each isotope is present in about 50 percent abundance, it is impossible from the present experiments to assign specific isotopes to the different observed moments.

Although the resonance minima are quite broad they do not possess the characteristic shape for a nuclear electrical quadrupole interaction with spin[2,6] $\frac{3}{2}$. This is somewhat surprising in view of the large quadrupole interaction of Br in BrCN found by Townes.[5] The spectra correspond more nearly to those of an arbitrarily assumed $\mathbf{I}\cdot\mathbf{J}$ interaction which has been found useful in accounting for some other resonance-minima curves. Further studies of the shape and interpretation of the bromine resonance are being made.

* Publication assisted by the Ernest Kempton Adams Fund for Physical Research of Columbia University.

[1] I. I. Rabi, S. Millman, P. Kusch, and J. R. Zacharias, Phys. Rev. **55**, 526 (1939).
[2] W. A. Nierenberg, N. F. Ramsey, and S. B. Brody, Phys. Rev. **70**, 773 (1946).
[3] Tolansky, Proc. Roy. Soc. **A136**, 585 (1932).
[4] T. Schmidt, Zeits. f. Physik **108**, 408 (1938).
[5] C. H. Townes, A. N. Holden, J. Bardeen, and F. R. Merritt, Phys. Rev. **71**, 644 (1947).
[6] B. T. Feld and W. E. Lamb, Jr., Phys. Rev. **67**, 15 (1945).

Millimeter-Wave Spectra: Hyperfine Structure of BrCN and ICN*

WALTER GORDY, WILLIAM V. SMITH, A. G. SMITH, AND HAROLD RING**
Department of Physics, Duke University, Durham, North Carolina
June 7, 1947

USING the method prevously described,[1] we have examined the $J=3$ to $J=4$ transition of BrCN and the $J=4$ to $J=5$ transition of ICN, both of which occur in the region of 9 mm. As was discovered by Townes[2] in the $J=2$ to $J=3$ transition of BrCN, Br has a rather large quadrupole moment which splits the pure rotational lines into a number of components. In our laboratory the quadrupole moment of the iodine nucleus has been observed through the splitting of the rotational lines of methyl iodide[3] as well as through the hyperfine structure of ICN reported here.

The quadrupole-moment effects were first noticed in atomic spectra, and the interaction was shown by Schuler and Schmidt[4] to be proportional to the square of the cosine of the angle between the angular momentum vector of the orbital electron and the nuclear spin vector. Casimer,[5] and also Bethe[6] have derived a theory for the quadrupole effects in atomic spectra. This theory as well as the intensity rules derived for atomic fine structure[7] has been adapted to the analysis of the molecular hyperfine structure reported here.

In Figs. 1 and 2 are shown the calculated and observed hyperfine spectra for BrCN and ICN. The calculated lines are given for the ground vibrational states only, although in both these molecules lines caused by excited vibrational states were observed. These are indicated in the experimental diagrams by lighter lines. The lines on the low frequency side are caused by the vibration which corre-

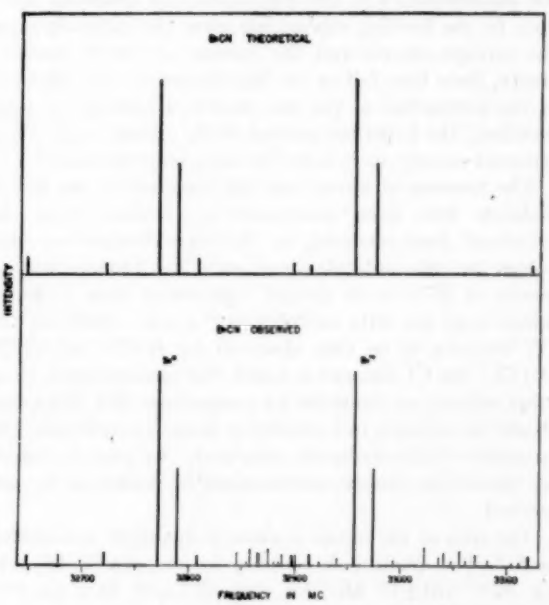

FIG. 1. Theoretical and observed hyperfine structure of the BrCN spectrum for the rotational transition $J=3$ to $J=4$. The heavy lines are for the ground vibrational state; the light ones in the observed spectrum are due to excited vibrational states.

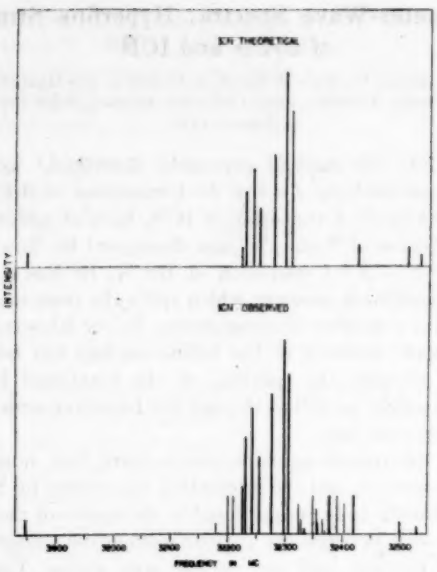

FIG. 2. Theoretical and observed hyperfine structure of the ICN spectrum for the rotational transition $J=4$ to $J=5$. The heavy lines are for the ground vibrational state; the light ones in the observed spectrum are due to excited vibrational states.

sponds to the stretching of the carbon-halogen bond, and in each case the stronger lines in the ground state are repeated with identical spacing in the excited vibrational state. From the separation of these groups it is possible to calculate the increase in the average bond length in the excited state over that for the ground state. They are: for BrC 0.0029A (0.17 percent increase); for IC 0.0037A (0.18 percent increase). This increase in length is due to the anharmonicity of the bond-stretching potential function. In the bending vibrational state the molecule is on the average shorter and the moment of inertia smaller. Hence, these lines fall on the high frequency side. Because of the interaction of the two modes of bending (L-type doubling) the hyperfine pattern of the ground state is not repeated exactly, as it is for the stretching vibration.

The moment of inertia and the structure of the BrCN molecule have been determined by Townes[2] from the rotational lines occurring at the lower frequencies. Our values for this molecule agree with his. The moment of inertia of ICN in its ground vibrational state is determined from our data as 260×10^{-40} g cm^2. Assuming the CN distance to be that observed for BrCN and ClCN (1.15A), the CI distance is 2.00A. No measurements from other sources are available for comparison, but this value should be accurate to 1 percent at least. To determine the structure of this molecule completely, we plan to search for the carbon isotope which should be detectable by our method.

The spin of the iodine nucleus is definitely established as 5/2. The quadrupole coupling factors, $eQ\partial^2V/\partial z^2$, are: for Br^{79}, 670±15 Mc; for Br^{81}, 567±15 Mc; for I^{127}, 2070±20 Mc. The quadrupole moment of I is negative, indicating that the iodine nucleus is flattened in the direction of the spin axis, i.e., it is oblate. That of Br is positive, indicating that the Br nucleus is elongated in the direction of the axis of spin, i.e., it is prolate. When the coupling coefficient $\partial V^2/\partial z^2$ is evaluated, the quadrupole moments of I and of Br can be determined from this data. We are now attempting to evaluate $\partial^2V/\partial z^2$ from data of other types.

We wish to acknowledge a helpful discussion with Dr. C. H. Townes, of the Bell Telephone Laboratories.

* This research was supported by Contract No. W-28-099-ac-125 with the Army Air Forces, Watson Laboratories, Air Materiel Command and by a grant-in-aid from the Research Corporation of New York.
** Frederick Gardner Cottrell Fellow.
[1] W. Gordy and M. Kessler, Phys. Rev. 71, 640 (1947).
[2] C. H. Townes, A. N. Holden, and F. R. Merritt, Phys. Rev. 71, 64 (1947); and with J. Bardeen, Phys. Rev. 71, 664 (1947).
[3] W. Gordy, A. G. Smith, and J. W. Simmons, Phys. Rev. 71, 917(L) (1947); see also the note on CH_3I in this issue.
[4] H. Schuler and Schmidt, Zeits. f. Physik 94, 457 (1935).
[5] H. von Casimer, Physica 2, 719 (1935).
[6] H. Bethe and R. F. Bacher, Rev. Mod. Phys. 8, 82 (1936).
[7] H. E. White and A. Y. Eliason, Phys. Rev. 44, 753 (1933).

On the Inelastic Scattering of Neutrons in Crystals*

OTTO HALPERN
Columbia University, New York, New York
June 20, 1947

THE inelastic scattering of a monochromatic neutron beam by crystal powders has been studied extensively by C. G. Shull and E. O. Wollan[1]; the experimental technique followed closely the well-known procedure in x-ray experiments. The very remarkable results obtained by these authors with a variety of scatterers seem to be in quantitative, and even qualitative disagreement with the presently accepted theories. It is, therefore, perhaps of interest to indicate an experimental approach to this problem which has no analogy in x-ray technique and promises to give valuable independent information. We suggest the study of the transmission of monochromatic neutron beams through single crystals of iron in a transverse magnetic field. Theory[2] then predicts very precisely that (apart from special angles of incidence here left out of consideration) no coherent scattering will occur. The weakening of the beam is due to incoherent nuclear scattering, inelastic lattice scattering, isotope disorder effects, and capture. Of these effects only inelastic lattice scattering will be influenced by a magnetic field. This special polarization effect has its origin in the fact that the incoherence of the inelastic scattering is due to energy exchange with the lattice while no element of incoherence enters into the interaction with the individual atom. Here the amplitudes of the wave scattered by the nucleus and by the magnetically active electron shell, superpose in the same way as we know them to interfere in the well-studied polarization effects obtained with polycrystalline iron.

In the present experiment the difference in transmission in the unmagnetized and saturated state of the scatterer is measured. This difference, $\Delta I/I$, will again be given in the customary approximation by the well-known formula

$$\Delta I/I=\tfrac{1}{2}p'^2d^2. \qquad (1)$$

In (1) p' denotes the excess cross section arising from the

interference term of nuclear and magnetic scattering in the inelastic process; d is the thickness of the crystal. The corresponding quantity p for coherent scattering has been assumed to be, and most likely is, much larger than p'; for this reason an arrangement eliminating coherent effects is here described.

Any observed "single transmission effect" is, therefore, determined by the inelastic scattering and can in turn be used to obtain quantitative information about its magnitude. One advantage of the arrangement here described lies in the replacement of a scattering by a transmission experiment. It is furthermore not difficult to obtain good saturation of the single crystal provided the magnetizing field is parallel to an easy axis of magnetization. Thus depolarization effects[3] can here be eliminated more easily than in previous experiments.

The presently accepted theoretical estimates[4] would lead to moderate but easily measurable effects; if, on the other hand, as suggested by the experiments quoted,[1] inelastic scattering should be much larger than expected, the "inelastic single-transmission effect" would become quite large. The isolation of the inelastic scattering would permit one to test the theory[4] rather precisely.

* Publication assisted by the Ernest Kempton Adams Fund for Physical Research of Columbia University.

[1] C. G. Shull and E. O. Wollan, Phys. Rev. **72**, 168(A) (1947).
[2] O. Halpern *et al*, Phys. Rev. **59**, 981 (1941).
[3] O. Halpern and T. Holstein, Phys. Rev. **59**, 960 (1941).
[4] R. Weinstock, Phys. Rev. **65**, 1 (1944).